Enhancing the Modeling and Efficiency of Photovoltaic Systems

by
Yousef Mahmoud

A thesis
presented to the University of Waterloo
in fulfillment of the
thesis requirement for the degree of
Doctor of Philosophy
in
Electrical and Computer Engineering

Waterloo, Ontario, Canada, 2016

AUTHOR'S DECLARATION

I hereby declare that I am the sole author of this thesis. This is a true copy of the thesis, including any required final revisions, as accepted by my examiners.

I understand that my thesis may be made electronically available to the public.

Abstract

Solar energy is a strong contender among the sustainable alternatives that offer practical potential for replacing increasingly depleted fossil fuels and supplying the world's growing energy demands. However, despite its sustainability, the spread of its use has been limited due to the high costs arising from its inadequate efficiency.

With this challenge as motivation, the goal of the research presented in this thesis was to contribute to the expansion of the utilization of photovoltaic (PV) systems. To achieve this goal, the work was approached from two perspectives: 1) facilitation of research into PV systems through the enhancement of existing PV models and simulation tools, which are highly complex and necessitate substantial computational effort, and 2) improvement of the efficiency of PV systems through the development of new techniques that mitigate power losses in PV systems.

With respect to the first perspective, two innovative modeling approaches are introduced. The first, a new circuit model for PV systems, features accuracy comparable to that of existing models but with a reduced computational requirement. The proposed model mimics the accuracy of existing models without their dependency on a transcendental implicit equation, thus providing a shorter computational time without sacrifying the accuracy.

The second modeling approach, which was developed for use in model-based online applications, involved the creation of a fast tool for estimating the power peaks of the power-voltage curves for partially shaded PV systems. Utilizing a PV circuit model for estimating the power peaks in large PV systems through the simulation of their entire power curve consumes extensive computational time, which is unacceptable for online applications even with the use of the proposed circuit model mentioned above. Rather than employing a PV circuit model to find the power peaks, the proposed tool relies on simple rules that govern the formation of power peaks in a partially shaded PV system as a means of establishing the power peaks directly, thus significantly reducing the time required.

The second perspective led to the development of three methods for reducing different types of power losses prevalent in PV systems. The first is an MPPT technique for use with partially shaded PV systems that exhibit multiple power peaks in their output power curves. The proposed MPPT is uniquely distinguishable because of its ability to eliminate misleading power losses in PV systems. Rather than searching and scanning heuristically for the GMPP, it employs the fast modeling tool mentioned above to calculate the location of the GMPP deterministically, thus avoiding the need for curve scanning. The

irradiance values required by the modeling tool are estimated innovatively using captured images of the PV modules obtained by an optical camera.

The objective of the second was to reduce the mismatch power losses common in partially shaded PV systems through the development of an improved PV reconfiguration method. The reconfiguration proposed in this thesis is produced by a simple algorithm that establishes a better configuration and requires only negligible computational time for ensuring the minimization of mismatch power losses.

The third is an enhanced maximum power point tracker (MPPT) for reducing tracking power losses in PV systems that operate under rapidly changing irradiance levels. The proposed method combines model-based and heuristic techniques in order to accelerate the tracking speed and thus decrease this type of loss. In the proposed MPPT, the temperature measurements typically necessary in any model-based PV application have been eliminated through reliance on a new set of equations capable of estimating the temperature through the utilization of current and voltage measurements.

Acknowledgements

Although I am indeed the sole author of this thesis, as declared earlier, I am surely not the sole contributor! Many people have contributed to my thesis, to my education, and to my life, and it is my great pleasure to take this opportunity to acknowledge them.

First, I would like to express my sincere gratitude to my advisor Professor Ehab El-Saadany for the continuous guidance, patience, revisions of my work, and invaluable comments throughout the period of this research. I am indebted for what I have learnt from him and the opportunity he has provided me to pursue my own research interests. I also gratefully acknowledge his financial support for my study at University of Waterloo and the research presented in this dissertation.

My appreciation and thanks are also extended to my Ph.D. committee members: Professor Claudio Canizares, Professor David Clausi, Professor Mohamed Elhawari and Professor Magdy Salama for their time and insight.

It is my pleasure to express my sincere appreciation to my M.Sc. advisor Professor Weidong Xiao and my M.Sc. co-advisor Professor Hatem Zeineldin for all their help and support which have not ended till now. You were the first teachers who introduced me to research and taught me, consciously and unconsciously, how good research is done.

I would like to thank all my past and present colleagues in Smart Distribution System lab for making it such a friendly place to work. A special thank goes to my friend Dr. Azhar Ulhaq for the nice company, entertainment and countless hours of discussions. Although your stay in University of Waterloo was not long, it was the most pleasant period in my Ph.D. years.

My most genuine and deepest thanks go to my mom and dad for their immense love, support, unforgettable inspiration and encouragement. You have always believed in me and encouraged me to keep pushing and to never give up. Whatever I am today is because of both of you, and your endless sacrifice. My strive to make you proud has been an inspiration to excel in everything that I do. No amount of thanks will be enough for the way you have supported and encouraged me to follow my dreams.

Dedication

This thesis is dedicated to my mom and dad.

TABLE OF CONTENTS

LIST OF FIGURES

LIST OF TABLES

NOMENCLATURE

Acronyms

GMPP	Global maximum power peak
MPP	Maximum power point
MPPT	Maximum power point tracking
P&O	Perturb and observe
PV	Photovoltaic
RTS	Real time simulator
STC	Standard test conditions

Variables

A	Ideality factor of diode
B	Voltage temperature coefficient
C_i	Current temperature coefficient
F	Scale factor of reflectance
G	Irradiance
G_o	Irradiance at standard test conditions
G_{co}	Irradiance of the reference PV cell
I	Output current
I_m	Current at max power point
I_{ph}	Photon current

I_{pho}	Photon current at standard test conditions
I_s	Saturation current
I_{so}	Saturation current at standard test conditions
I_{sc}	Short circuit current
K	Boltzmann constant
M	Digital image
N_s	Number of series connected cells
n_d	Number of diode-bypassed photovoltaic units
n_f	Number of fixed modules
n_p	Number of parallel photovoltaic units
n_r	Number of reconfigurable modules
n_s	Number of series connected photovoltaic units
q	Electron charge
r	Number of rows
R_s	Series resistance
R_{sh}	Shunt resistance
T	Temperature of a photovoltaic module
Δt	Exposure duration
T_{co}	Temperature of the reference photovoltaic cell
V	Terminal Voltage
V_m	Voltage at max power point
V_{oc}	Open circuit voltage

Z_j	Integer modeling the effect of a bypass diode
α_0	First polynomial coefficient
α_1	Second polynomial coefficient
α_2	Third polynomial coefficient
α_3	Fourth polynomial coefficient

Chapter 1 INTRODUCTION

Despite their harsh and polluting effects on the environment, fossil fuels are still the most economical option, so they remain the world's primary source of energy supply [1]. More than 70 % of global generated electricity is supplied by fossil fuels such as natural gas, coal, and petroleum [2]. Unfortunately, the available supply of these resources is shrinking and will inevitably run out [3]. On the other hand, worldwide energy demands are increasing exponentially, with a resultant urgent need for new alternative energy resources to replace the disappearing fossil fuels [4]. One sustainable energy source that has a practical potential to replace fossil fuels and meet growing energy demands is solar power [5], which is also viewed as beneficial with respect to climate change and public health considerations.

The most predominant method of converting solar energy into electrical energy is the use of photovoltaic (PV) systems consisting of thousands of small solar cells [6]. The efficiency of the first solar cell developed was only 1 %, making it impractical for power generation [7]. Fortunately, the work conducted by PV material researchers has led to efficiency levels as high as 21.7 % in today's commercial solar cells, an improvement also accompanied by declining costs [8]. These advances have contributed to exponential growth in the use of PV power systems over the past two decades. As shown in Figure 1-1, the cumulative capacity of installed PV power plants has increased from less than 10 GW in 2006 to almost 180 GW in 2014 [9], with a projected capacity of 540 GW by 2019, which corresponds to a five-year projection of more than triple the installed capacity. The International Energy Agency has predicted that by 2050, solar energy will be the world's largest source of electricity [6].

1.1. Research Motivation

In spite of continuous improvements in the efficiency and cost-effectiveness of PV systems, their spread nonetheless continues to be restricted due to the relatively high costs arising from their still comparatively low efficiency [10, 11]. The primary goal of PV system research therefore remains further enhancement of efficiency. In addition to the efforts of PV material scholars, power systems researchers also contribute to the achievement of this goal by endeavoring to increase the overall efficiency of PV systems through the mitigation of their losses. They are also working on facilitating the investigation of a variety of aspects of PV systems through the enhancement of existing PV models and simulation tools, which are characterized by significant complexity and entail major computational effort.

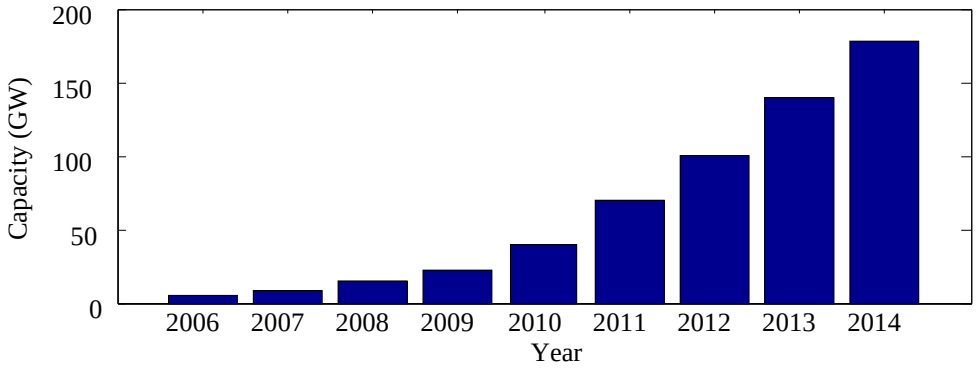

Figure 1-1: The global capacity of installed PV systems.

1.1.1. Power Losses in PV Systems

As illustrated in Figure 1-2, PV systems are subject to numerous types of power losses, including tracking power losses, misleading power losses, and mismatch power losses. Tracking power losses occur in homogeneous PV systems that receive the same irradiance level across all of their modules. These losses are caused by the inability of maximum power point tracking (MPPT) algorithms to track the maximum power of PV systems quickly in a rapidly changing irradiance environment.

Figure 1-3 illustrates the operation of an MPPT algorithm based on the power curve of a PV system. As can be seen, the power curve has a power peak at a specific voltage, termed the maximum power point (MPP) voltage. The location of this voltage changes with variations in the irradiance throughout the day. To extract the maximum available power, an MPPT algorithm is therefore implemented as a means of ensuring that the system operates at this varying MPP voltage [12]. The algorithm typically relies on a hill-climbing principle whereby the operating voltage is incremented or decremented in order to achieve increases in the power generated. The process begins with an increment/decrement in the voltage, followed by the measurement of the corresponding amount of power generated. If the generated power increases, the algorithm continues to change the voltage in the same direction. However, if the generated power decreases, the algorithm causes changes in the opposite direction. This procedure continues until the voltage reaches and oscillates around the MPP voltage and thus generates peak power. It is important to mention that these changes in PV voltage has no effect on the load voltage because PV systems are isolated by DC-DC converters which keep the output voltage regulated at a fixed load voltage.

As noted above, before reaching the MPP voltage, the system operates at non-maximum power points (represented by the black circles in Figure 1-3) and thus loses some of the available power. These

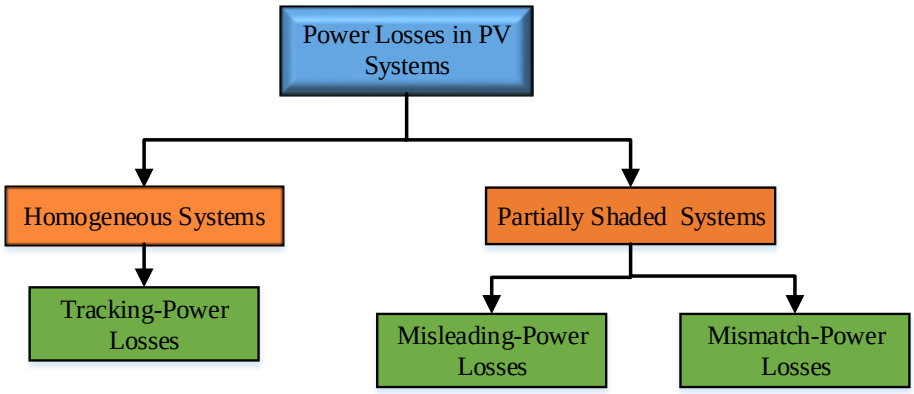

Figure 1-2: Categories of the most common power losses in PV systems.

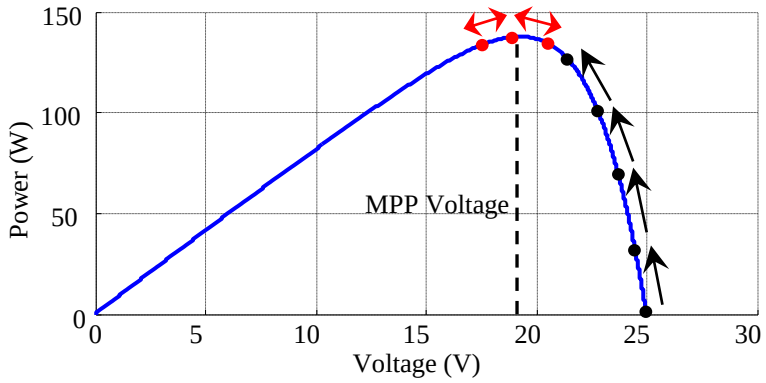

Figure 1-3: Conceptual operation of the hill-climbing MPPT.

losses are called tracking power losses [13] and are more predominant in systems that operate under rapidly varying irradiance levels, which cause a continual shifting of the location of the MPP voltage.

Many MPPT methods have been developed for improving the operation of PV systems and reducing their tracking power losses. The most recent and effective methods are dependent on mathematical PV modeling as a means of reducing the heuristic nature of the tracking and accelerating its speed. The determinism of the model shortens the time needed for searching for the MPP voltage, which in turn decreases tracking power losses. However, these methods have not been commonly sought after or implemented because the precise temperature measurement required increases the complexity and cost of their implementation.

Other types of power losses in PV systems are caused by partial shading, which occurs when some modules of a PV system are shaded by passing clouds, trees, adjacent objects, etc., while the rest of the

Figure 1-4: An example of a partially shaded PV system.

system is fully illuminated, as represented in Figure 1-4. Under these conditions, not only is the power of the shaded modules reduced, but some of the power of the unshaded modules is also lost [14, 15]. These power losses in unshaded modules appear in two forms: misleading and mismatch power losses, as indicated in Figure 1-2.

An examination of the power curve for the partially shaded PV system shown in Figure 1-5 can provide an understanding of misleading power losses. As can be seen, multiple power peaks appear in the power curve of partially shaded PV systems as opposed to the single power peaks that appear in the curves of homogeneous PV systems [16]. Multiple power peaks make tracking the MPP challenging because MPPT algorithms can become trapped in one of the local maximum peaks rather than continuing on to identify the global maximum power peak (GMPP) [17]. In this case, the difference between the available global power and the local power extracted is called a misleading power loss.

Biological optimization is a method that has been recently applied for solving this problem and tracking the global power peak in partially shaded PV systems [18, 19]. In spite of its accurate convergence to the GMPP, this technique requires periodic scanning of the power curve, during which the system is forced to operate with non-maximum power points, which induces power losses. The periodicity of the scanning can also prevent the system from working on the true GMPP if the shading profile changes between two successive scans, because the system continues to function with the previous GMPP until the next scan. Therefore, optimization-based MPPTs are incapable of eliminating misleading power losses.

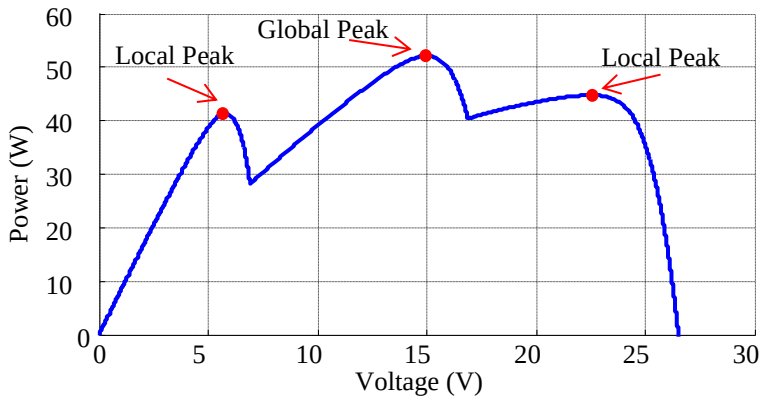

Figure 1-5: The power curve of a partially shaded PV system.

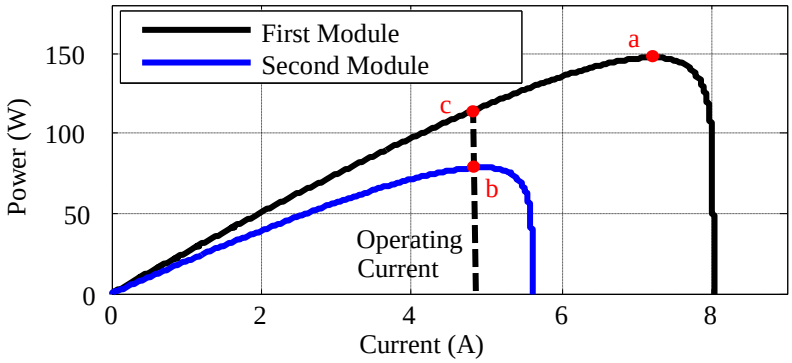

Figure 1-6: The power curves of two series connected PV modules.

Mismatch power losses, which occur in partially shaded series-connected PV modules, are the second form of partial shading losses. An example of this type of loss is illustrated in Figure 1-6, which shows the power curves of two series-connected PV modules: one shaded and the other fully illuminated. Although the operating current passing through both modules (represented by a dashed line in the figure) can harvest the maximum power from the second PV module (point b), it cannot extract the maximum power from the first module (point a). The difference between the extracted power (point c) and the maximum available power (point a) of the first module is referred to as a mismatch power loss.

PV reconfiguration has been reported as an effective method for reducing mismatch power losses in partially shaded PV systems [20, 21]. This technique is based on the fact that the mismatch power losses in a system can be minimized through appropriate changes in the configuration of the system. The PV system modules are therefore connected through switches, permitting them to be reconfigured during the operation of the system in order to minimize mismatch power losses. The optimal configuration that

results in minimum mismatch power losses is first determined, and the PV modules are then reconfigured accordingly. However, the main deficiency associated with the available reconfiguration methods is the long delay required for establishing the optimal configuration, during which time the system does not operate based on the optimal configuration and the mismatch power losses are hence not minimized. For this reason, despite their effectiveness in cases involving slowly moving shadows such as those from trees and adjacent objects, existing methods are ineffective in the presence of faster-moving shadows, such as those caused by shifting clouds.

1.1.2. Limitations of Existing PV Models

The accurate PV models described in the literature are complex due to their dependency on a transcendental implicit equation [22]. This feature poses no problem for studies of PV systems that receive homogeneous irradiance because of the feasibility of quickly modeling an arbitrary number of PV units using only one aggregated PV model. However, it creates challenges with respect to investigating PV systems that receive nonhomogeneous irradiance [23]. Since each PV unit might be subjected to a different irradiance level, such systems require the simultaneous simulation of connected PV models, resulting in a lengthy computational time.

Such excessive computational time, which might reach hours or days for the modeling of large partially shaded PV systems, is accompanied by two challenges. The first is that it impedes the ability of PV system designers and researchers to conduct simulation studies easily in a reasonable amount of time. Second, it hinders the feasibility of developing model-based MPPT algorithms for partially shaded PV systems, thereby limiting the exploration of potential further improvements in the efficiency of PV systems [24]. This is because model-based MPPTs are online applications that require PV systems to be modeled in a few seconds, which is unfortunately impossible using currently available PV models [24]. In spite of the demonstrated advantages of existing model-based MPPTs with respect to reducing tracking power losses in homogeneous PV systems, no model-based MPPT methods have yet been developed for use with partially shaded systems.

1.2. Research Objectives

Driven by these motivations, the goal of the work presented in this thesis was to mitigate the different types of power losses that occur in PV systems as a means of improving system efficiency, and to develop enhanced modeling and simulation tools for use with PV systems. The following specific objectives were targeted:

1. Facilitate PV system research and enable PV designers and researchers to conduct simulation studies easily in reasonable amounts of time by developing a new PV circuit model that requires shorter computational time than that associated with existing PV models.

2. Develop a fast modeling tool for partially shaded PV systems that provides computational speed suitable for model-based online applications, thus enabling the practical creation of model-based MPPT algorithms for partially shaded PV systems, which have the potential to improve the PV system efficiency,

3. Develop an enhanced MPPT method that accelerates tracking for PV systems, thereby offering a means of reducing tracking power losses in homogeneous PV systems that operate under rapidly changing irradiance conditions.

4. Eliminate misleading power losses in partially shaded PV systems through the removal of the periodic curve scanning required in existing optimization-based MPPT approaches.

5. Minimize mismatch power losses in partially shaded PV systems affected by rapidly moving shadows through the development of an improved reconfiguration method that entails only a negligible time delay.

1.3. Thesis Outline

This thesis is divided into two main parts: the next two chapters, which are concentrated on the modeling of PV systems, and the subsequent three chapters, which are focused on the mitigation of the three types of power losses common in PV systems. The individual chapters are organized as follows.

Chapter 2 explains the challenges facing PV system researchers and designers with respect to modeling PV systems. It describes the complexity of the available accurate models and the extensive computational time needed for correctly modeling large PV systems. To address these issues, a new PV circuit model is proposed that reduces computational time while maintaining accuracy.

Chapter 3 reveals the gap in the literature with respect to the investigation of model-based MPPTs for partially shaded PV systems, which have not yet been developed, in spite of their potential to improve dynamic and steady-state tracking performance, which is adversely affected by the computational time needed for existing models. A fast modeling tool capable of performing the modeling required in model-based MPPTs in just a few seconds is then proposed. Rather than using a PV circuit model for simulating the entire power curve in order to estimate its peaks, a time-consuming process even with the PV model proposed in Chapter 2, the proposed approach

calculates the power peaks of partially shaded PV systems directly based on simple rules, without the need for simulating the entire curve.

Chapter 4 highlights the drawbacks associated with the model-based MPPTs recently reported in the literature as methods of accelerating the MPP tracking speed for PV systems and of reducing tracking power losses. These techniques require accurate temperature measurements that increase the cost and complexity of their implementation compared to that of non-model-based MPPTs. A method for eliminating the need for temperature measurements in model-based MPPTs is then suggested.

Chapter 5 reveals the weakness inherent in optimization-based MPPTs and discusses their inability to eliminate misleading power losses in partially shaded PV systems, despite their effectiveness in mitigating them. An interdisciplinary solution is proposed for eliminating these losses by employing, for the first time, an imaging device for the MPPT of PV systems.

Chapter 6 demonstrates the failure of existing PV reconfiguration methods to minimize mismatch power losses in PV systems that are subject to rapidly moving shadows. It points out that the time delay associated with their response to changes in shadowing has a negative impact on the reduction of power losses. A more effective reconfiguration method based on the newly developed algorithm is proposed; it offers a negligible time delay that enhances the mitigation of power losses.

Chapter 7 concludes the thesis, highlights the research contributions, and suggests topics for future investigation.

Chapter 2 A PHOTOVOLTAIC MODEL WITH REDUCED COMPUTATIONAL TIME

A reliable and accurate photovoltaic model is essential in PV system studies. It can be used for simulating the electrical characteristics and dynamics of PV power plants under various metrological conditions, or for estimating the operating temperature and efficiency of a solar plant in a specific location [25]. In addition, PV models help designers optimize the design and sizing of PV power plants [26] and are also used to verify and test the performance of newly developed MPPT algorithms [27], control schemes [28], and designs of PV power electronic converters [29].

Various versions of PV models were developed in the past, as depicted in Figure 2-1. The practical model consists of a voltage-dependent current source, a diode, a series, and shunt resistances, as shown in Figure 2-1(a). Despite parameterization difficulties [30], this model has been widely used in the literature because it strikes a good compromise between complexity and accuracy [31]. The practical model is selected in [32] to simulate and verify the newly developed hybrid power generation system. As well, it is exploited to test new supervisory algorithms [33] and analyze novel PV power electronic converters [34]. It is generally preferred in studies where accuracy is important [35].

For simplification, the shunt resistance is neglected in the simplified series model portrayed in (b). This model has mostly been used to test newly developed MPPT algorithms, as in [36]. In addition to the shunt resistance, the series resistance is also neglected in the ideal PV model as depicted in Figure 2-1(c). It is the simplest model available [37] and consists only of a voltage-dependent current source and a diode.

More advanced PV models are the double diode [38] and triple diode models [39], shown in Figure 2-1(d) and Figure 2-1(e), respectively. Both of these models feature high accuracy because they take the recombination of carrier into consideration [40]. On the other hand, they are rarely used due to their complexity, high computational cost, and inability to be parameterized based solely on datasheet information [41].

The previously mentioned models (practical, simplified, double diode, and triple diode) suffer from high computational time due to their dependency on complex transcendental implicit equations [22]. The only model that exhibits significantly lower computational time is the ideal model, which relies on a simple non-transcendental equation [22]. However, its accuracy is not guaranteed because it has only three degrees of freedom (corresponding to the three parameters), which are insufficient to reproduce the information provided by manufacturing datasheets [42].

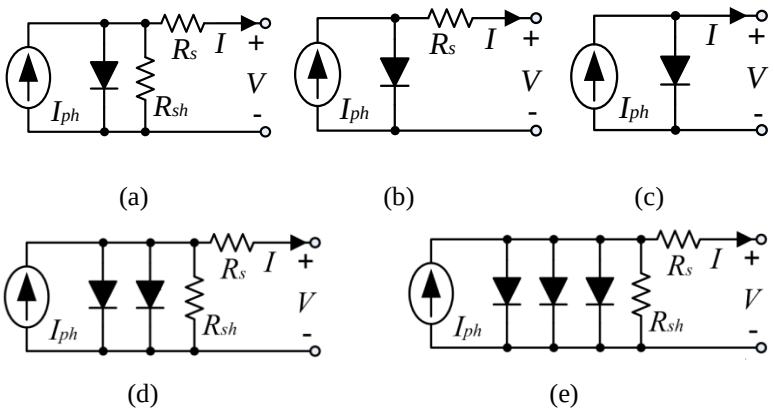

Figure 2-1: Existing circuit PV models: (a) practical model; (b) simplified series model; (c) ideal model; (d) double diode model; and (e) triple diode model.

Lambert W function based PV model is also available in the literature. It expresses the PV voltage as an explicit function of the PV current [43]. Similar to the ideal PV model, there is no dependency on complex transcendental implicit equation in this model as it relies on a simple non-transcendental equation. On the other hand, executing Lambert *W* function is not straightforward and requires nontrivial calculations.

In studies of PV systems which receive homogeneous irradiance, it is possible to model an arbitrary number of PV units using only one aggregated PV model because they receive the same irradiance. This leads to quick computational time modeling as in [44]. On the other hand, studies considering the partial shading impact require simulating numerous connected PV modules simultaneously, as each PV unit might be subjected to a different irradiance level [45]. This results in a high computational time which impedes the ability of PV researchers and designers of conducting simulation studies easily in reasonable amount of time. Unfortunately, there is still no available PV model desirable for modeling large partially shaded, which requires low computational time and high accuracy.

This chapter proposes an accurate and low computational time model based on the practical PV model. It reduces the computational time by replacing the series resistance of the model with a voltage-dependent voltage source. The voltage source is a third-degree polynomial function of the terminal voltage to mimic the characteristics of the practical model. The model does not have an implicit dependency and thus decreases the simulation effort. The proposed model, with added dependent voltage source, has five degrees of freedom, which is sufficient to accurately align the *I*-*V* and *P*-*V* curves with the information provided by manufacturer datasheets, yet at a lower computational time. Moreover, the model is parameterized based on manufacturing datasheets without a need for extra measured points. The

effectiveness of the model is verified and compared at different atmospheric conditions to measurements of various PV materials available commercially, such as mono-crystalline, poly-crystalline, and thin film.

The chapter is organized as follows: it starts with an outline of the limitations of the most commonly used practical PV model, after which the proposed model is presented, derived, and implemented to model various commercial PV modules. The proposed model is then adjusted to take the effect of temperature and irradiance variations into consideration, and a new factor is introduced to improve the accuracy of the model at low irradiance levels. Next, a comprehensive model evaluation is conducted in which the accuracy of the model is verified by comparing it to the measured curves provided by manufacturers of mono-crystalline, poly-crystalline and thin film PV technologies. Finally, the computational time of the model is measured and compared to that of other available models, and a case study of a partial-shaded PV system is conducted to test and compare the effectiveness of the proposed model under certain conditions.

2.1. Proposed PV Model

As stated in the Introduction, the available models in the literature are either inaccurate or suffer from high computational time. The following equation of the practical model shown in Figure 2-1 (a) [46] is the *I-V* characteristic equation that relates the terminal voltage *V* to the output current *I* [47]:

$$I = I_{ph} - I_s[e^{\frac{q(V+IR_s)}{N_sKTA}} - 1] - \frac{V + IR_s}{R_{sh}} \tag{2-1}$$

where q, K, T and N_s are the electron charge ($1.60217657 \times 10^{-19}$), Boltzmann constant ($1.3806488 \times 10^{-23}$), module temperature and number of series connected cells, respectively. The five parameters I_{ph}, I_s, A, R_s and R_{sh} are the photon current, saturation current, ideality factor of diode, series and shunt resistances, respectively. These parameters are determined such that the corresponding *I-V* curve precisely passes through the datasheet information [40]. However, (2-1) is a transcendental nonlinear equation and cannot be solved for one variable, either the voltage *V* or the current *I*, in terms of the other. Solving such an equation is complicated, time-consuming and requires a numerical iterative solver, since it cannot be solved analytically, as Figure 2-2(a) illustrates.

2.1.1. Equivalent Circuit

The proposed PV model relies on the practical PV model and reduces the computational time by replacing its series resistance with a voltage-dependent voltage source. The proposed model, depicted in Figure 2-3, consists of a current source, diode, shunt resistant and polynomial voltage-dependent voltage

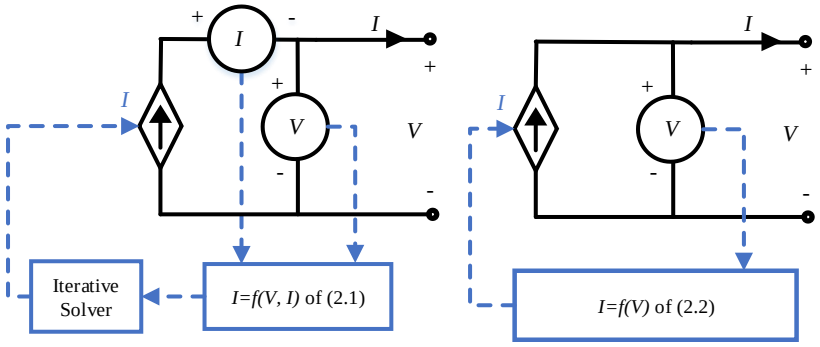

Figure 2-2: Simulation model implementation: (a) practical model where *I=f(V,I)*; (b) proposed model where *I=f(V)*.

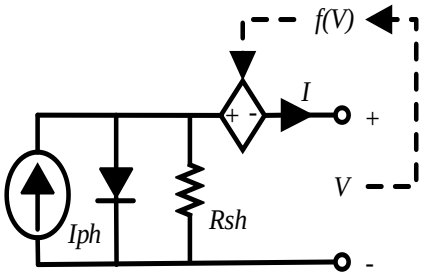

Figure 2-3: Proposed equivalent PV circuit model.

source. The voltage source dependency on the terminal voltage V is a third-degree polynomial that possesses four degrees of freedom. The polynomial function is chosen as a third order because it has four parameters capable to pass through the four points given by PV manufacturers.

Equation (2-2) describes the relation between the terminal voltage V and current I of the proposed model shown in Figure 2-3:

$$I = I_{ph} - I_s\left[e^{\frac{q(\alpha_o+\alpha_1 V+\alpha_2 V^2+\alpha_3 V^3)}{N_s KTA}} - 1\right] - \frac{\alpha_o + \alpha_1 V + \alpha_2 V^2 + \alpha_3 V^3}{R_{sh}} \quad (2\text{-}2)$$

where α_0, α_1, α_2 and α_3 are the polynomial coefficients determined such that the model analogously follows the behavior of the practical PV model. It is important to emphasize that (2-2) is a non-transcendental equation that is easily simulated by direct substitution, without a need for a numerical solver, as shown in Figure 2-2(b). This feature reduces the computational time of the proposed model without affecting its accuracy. The model would be advantageous in studies of PV systems operating under partial shading conditions, as demonstrated later in this chapter.

2.1.2. Model Parameterization

There are two sets of parameters which need to be determined for the proposed PV model. The first set is the parameters corresponded to the practical model which are I_{ph}, I_s, A, R_s and R_{sh}. The second set is the polynomial coefficients α_0, α_1, α_2 and α_3. All the model parameters at standard test conditions STC (where temperature and irradiance are equal to 25°C and 1 KW/m^2) are determined based on the information provided by all manufacturing datasheets, without a need for additional measurements. The manufacturers provide the following information at STC: short-circuit current point (0, I_{sc}), open circuit voltage point (V_{oc}, 0), voltage and current at max power point (V_m, I_m), and the implicit information that the slope of power curve equals zero at voltage V_m ($dP/dV = 0$ at $V=V_m$) [48].

The first set of parameters is determined similar to the standard parameterization approach available in the literature for the practical PV model such as in [49]. Starting with the short-circuit current point and substituting (0, I_{sc}) in (2-1) results in:

$$I_{ph} = I_{sc} + I_{so}[e^{\frac{qI_{sc}R_s}{N_sKTA}} - 1] + \frac{I_{sc}R_s}{R_{sh}} \tag{2-3}$$

where I_{pho} and I_{so} are the photon current and saturation current both at STC. Similarly, substituting an open circuit voltage (V_{oc}, 0) point in (2-1) produces:

$$I_{ph} - I_{so}[e^{\frac{qV_{oc}}{N_sKTA}} - 1] - \frac{V_{oc}}{R_{sh}} = 0 \tag{2-4}$$

Substituting (2-3) in (2-4) and rearranging results in:

$$I_{so} = [(V_{oc} - I_{sc}R_s)/R_{sh} - I_{sc}]/(e^{\frac{qI_{sc}R_s}{N_sKTA}} - e^{\frac{qV_{oc}}{N_sKTA}}) \tag{2-5}$$

Substituting the max current and voltage point (V_m, I_m) in (2-1) results in:

$$I_m - I_{pho} + I_{so}[e^{\frac{q(V_m+I_mR_s)}{N_sKTA}} - 1] + \frac{V_m + I_mR_s}{R_{sh}} = 0 \tag{2-6}$$

Finally, applying ($dP/dV = 0$) and substituting voltage and current at maximum power (V_m, I_m) results in:

$$I_{pho} - I_{so}[(1 + \frac{q(V_m + I_mR_s)}{N_sKTA})e^{\frac{q(V_m+I_mR_s)}{N_sKTA}} - 1] - \frac{2V_m}{R_{sh}} = 0 \tag{2-7}$$

Equations (2-3), (2-5), (2-6) and (2-7) are the four equations which can be written from the information provided by manufacturer datasheets. Because there are five parameters to be estimated for the practical model, while there are only four information provided by manufacturer datasheets, an additional equation or assumption needs to be introduced to find the fifth parameter. In [40], one

predefined parameter, the ideality factor, was assumed arbitrary and then the rest four parameters are derived accordingly. Similarly, the parameterization in [50] approximates that one parameter, the shunt resistance R_{sh}, equals to inverse of the slope at short-circuit point, and then derives the rest four parameters accordingly. The parameterization in [49] finds empirically the value of the ideality factor that results in minimum deviation between the simulated and measured *I-V* curves and then the rest of the parameters are derived. Here the parameterization provided in [49] is followed. The parameterizing procedure is summarized in the flowchart shown in Figure 2-4.

The flowchart starts by determining the value of the ideality factor of the diode 'A'. It is worth mentioning here that any assumed value for the ideality factor guarantees the passing of the model through the information provided in the manufacturer datasheet. However, choosing an appropriate value for 'A' improves the accuracy at the rest of the points of the *I-V* curve. Following the parameterization in [49], different values of 'A' in the range of [1-2] are substituted and the value that results in minimum deviation between the modeled and measured curve is chosen.

After determining 'A', the constants *K*, *q* and datasheet parameters V_m, I_m, I_{sc} and V_{oc} are substituted in (2-3), (2-5), (2-6) and (2-7) to find the four parameters of the model I_{pho}, I_{so}, R_s and R_{sh}. First, the parameters 'R_s' and R_{sh} are determined by solving (2-6) and (2-7) numerically using the well-known Newton-Raphson iterative method. If the iteration results in a non-divergent solution, the initial value of the variables R_s and R_{sh} should be changed. An initial value for R_s can be chosen in the range of (0-0.5) Ω and an initial value for R_{sh} is in the range of (100-10,000) Ω. Once R_s and R_{sh} are found, they are substituted directly in (2-3) and (2-5) to determine the value of the photon current I_{pho} and saturation current I_{so}.

After determining the first set of parameters, the polynomial coefficients are estimated such that the model analogously follows the behavior of the practical PV model. Namely, they are determined by equating (2-2) and its derivative with (2-1) and its derivative. Equating (2-2) with (2-1) and substituting the short circuit current point, the maximum current-voltage point and the open circuit voltage point results in the following equations:

$$\alpha_0 = I_{sc}R_s \tag{2-8}$$

$$\alpha_0 + \alpha_1 V_m + \alpha_2 V_m^2 + \alpha_3 V_m^3 = V_m + I_m R_s \tag{2-9}$$

$$\alpha_0 + \alpha_1 V_{oc} + \alpha_2 V_{oc}^2 + \alpha_3 V_{oc}^3 = V_{oc} \tag{2-10}$$

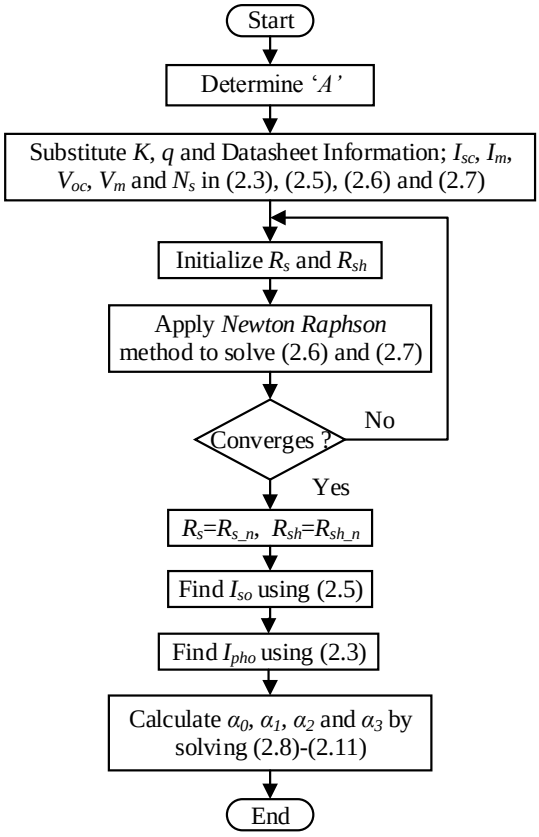

Figure 2-4: The flowchart for parameterizing the proposed PV model.

Equating the derivatives of (2-2) with that of (2-1) and substituting the maximum voltage and current point results in:

$$\alpha_1 + 2\alpha_2 V_m + 3\alpha_3 V_m^2 = 1 - R_s \times I_m/V_m \tag{2-11}$$

Equations (2-8)-(2-11) are linear and can be trivially solved analytically to determine the values of the four coefficients α_0, α_1, α_2 and α_3.

As an example, the PV module JAM5(l)-72-155 is parameterized in this paragraph utilizing the flowchart in Figure 2-4. The ideality factor of the diode A=1.8 is determined using the procedure described in [49]. Then, the model parameters R_s and R_{sh} are determined by solving (2-6) and (2-7) numerically using the well-known Newton-Raphson iterative method. The values of R_s and R_{sh} for this module equal to 0.0991 and 333.663 Ω, respectively. Finally, the model parameters are substituted in (2-3) and (2-5) to determine the photon current I_{pho} and saturation current I_{so}. The values of photon current and saturation current equal to 4.9415 A and 9. 7116×10^{-6} A, respectively. Finally, the values of

polynomial coefficients α_0, α_1, α_2 and α_3 are determined by solving the equations (2-8) - (2-11) analytically which are as follows α_0=0.4898, α_1=0.8924, α_2=0.0064 and α_3=-0.000095.

It is important to emphasize here that the proposed model represented by (2-2) can be completely simulated using direct substitution analytically without a need for numerical iterative solver. However, parameterizing the model requires solving two nonlinear equations (2-10) and (2-11) numerically. Because the model is parameterized usually a single time, this should not impose difficulties while simulating the proposed model.

The parameters at STC of other commercial PV modules are determined using the parameterization approach in Figure 2-4. These are presented in detail in Table 2.1. Furthermore, the parameters are substituted in (2-2) to plot the *I-V* and *P-V* curves for each PV module at STC. The current-voltage *I-V* and power-voltage *P-V* curves of the PV modules are shown in Figure 2-5(a) and Figure 2-5(b), respectively. It can be seen that the modeled *I-V* curves pass precisely through the three points given by the manufacturer. Moreover, *P-V* curves pass accurately through the peak power point at its corresponding voltage V_m.

2.1.3. Adjustment to Metrological Variations

The determined model parameters extracted by the flowchart in Figure 2-4 are at STC and therefore must be adjusted for temperature and irradiance variations. The photon current I_{pho} is adjusted to the temperature and irradiance using (2-12), where G denotes irradiance (KW/m^2), ΔT is the temperature difference between the module temperature and the STC temperature, and C_i is the current temperature coefficient given by the product datasheet [40]:

$$I_{ph} = G(I_{pho} + C_i \Delta T) \tag{2-12}$$

Estimating the effect of meteorological conditions on I_{so} is more challenging. Equation (2-13) is usually used to estimate the saturation current I_s for the practical model at any metrological condition, where $|B|$ is the absolute value of the voltage temperature coefficient given by product data sheets [40]:

$$I_s = \frac{I_{ph} - (V_{oc} - |B|\Delta T)/R_{sh}}{e^{\frac{q(V_{oc}-|B|\Delta T)}{N_s KTA}} - 1} \tag{2-13}$$

Analogously, (2-13) can be rewritten for the proposed circuit model shown in Figure 2-3 as follows where $\overline{V_{oc}} = V_{oc} - |B|\Delta T$:

Table 2.1: Extracted Parameters of the Proposed Model for Different PV Modules

	Mono-Crystalline		Poly-Crystalline		Thin-Film	
Parameters	JAM5(l) -72-155	JAM5(l) -72-80/SI	JAP6- 72-250	NDQ2 E3E	GE-C dTe78	NA-E 125G5
I_{pho}	4.9415	5.4411	7.8022	7.9293	1.2303	3.3706
$I_{so}\times10^{-6}$	9.7116	3.4104	4.0546	1.653	70.166	400.79
A	1.8	1.7	1.63	1.5	2.5	1.3
R_s	0.0991	0.1015	0.099	0.1166	0.9091	0.0298
R_{sh}	333.663	493.4728	352.968	98.7726	3989.9	179.80
α_0	0.4898	0.5523	0.7719	0.9234	1.1182	0.1003
α_1	0.8924	0.8620	0.8108	0.6889	0.9366	0.9924
α_2	0.0064	0.0078	0.0111	0.0283	0.0019	0.0003
$\alpha_3\times10^{-5}$	-9.5197	-11.229	-16.499	-65.238	-1.388	-41.69

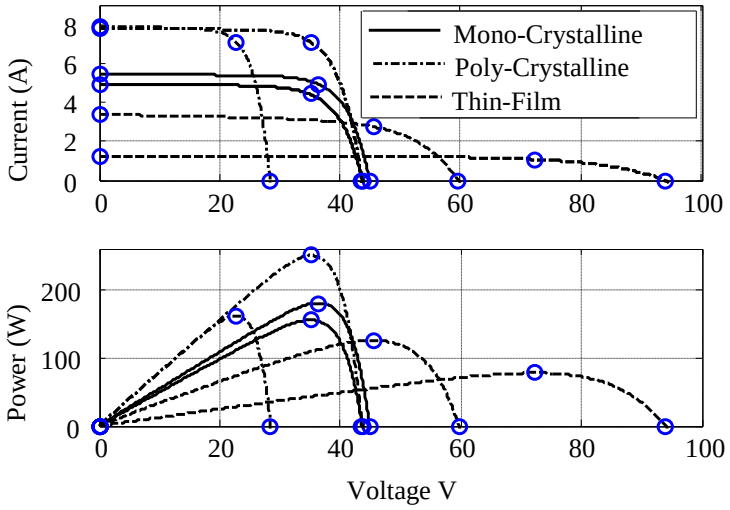

Figure 2-5: Modelled current and power curves for PV Modules in Table 2.1.

$$I_s = \frac{I_{ph} - (\alpha_0 + \alpha_1\overline{V_{oc}} + \alpha_2\overline{V_{oc}}^2 + \alpha_3\overline{V_{oc}}^3)/R_{sh}}{e^{\frac{q\left(\alpha_0+\alpha_1\overline{V_{oc}}+\alpha_2\overline{V_{oc}}^2+\alpha_3\overline{V_{oc}}^3\right)}{N_sKTA}} - 1} \tag{2-14}$$

Unfortunately, the proposed model exhibits inaccuracy at low irradiance levels. To improve the accuracy, the open circuit voltage variation due to irradiance $\Delta V_{oc}(G, T_o)$ is added to (2-14) to take the irradiance-variation effect into consideration, as shown in the following equation:

$$I_s = \frac{I_{ph} - (\alpha_0 + \alpha_1\overline{V_{oc}} + \alpha_2\overline{V_{oc}}^2 + \alpha_3\overline{V_{oc}}^3 + \Delta V_{oc}(G,T_o))/R_{sh}}{e^{\frac{q\left(\alpha_0+\alpha_1\overline{V_{oc}}+\alpha_2\overline{V_{oc}}^2+\alpha_3\overline{V_{oc}}^3+\Delta V_{oc}(G,T_o)\right)}{N_sKTA}} - 1} \quad (2\text{-}15)$$

where $\Delta V_{oc}(G,T_o)$ is the difference between open circuit voltages at an operating irradiance G and STC irradiance G_o, both at STC temperature T_o. The open circuit voltage can be approximated as follows:

$$V_{oc} \simeq \frac{N_sKTA}{q} ln(I_{ph}/I_s) \quad (2\text{-}16)$$

The difference between open circuit voltages at different irradiances $\Delta V_{oc}(G,T_o)$ is expressed in the following:

$$\Delta V_{oc}(G,T_o) = V_{oc}(G,T_o) - V_{oc}(G_o,T_o) \quad (2\text{-}17)$$

Substituting (2-16) and (2-12) in (2-17) results in:

$$\Delta V_{oc}(G,T_o) \simeq \frac{N_sKTA}{q} ln(G/G_o) \quad (2\text{-}18)$$

To compensate for the approximations while deriving (2-18), the following will replace it:

$$\Delta V_{oc}(G,T_o) \simeq Y \times ln(G/G_o) \quad (2\text{-}19)$$

Moreover, Y is determined in (2-20) where $V_{oc}(G_1)$ can be found in the curves provided by the manufacturer's datasheet:

$$Y \simeq (V_{oc}(G_1,T_o) - V_{oc}(G_o,T_o))/ln(G_1/G_o) \quad (2\text{-}20)$$

To summarize, (2-12) and (2-15) are used to adjust STC parameters I_{pho} and I_{rs} to I_{ph} and I_s at any irradiance and temperature level. Equation (2-19) finds the introduced term $\Delta V_{oc}(G,T_o)$ in (2-15), and (2-20) finds the value of the Y factor that appears in (2-19).

Finally, it is important to mention that the polynomial coefficients α_0, α_1, α_2 and α_3 are also affected by the temperature and irradiance variations. However, the effect of the meteorological conditions on the polynomial coefficients is slight and can be neglected as presented in Appendix A. Similarly, the temperature effect on the ideality factor, series and shunt resistances can also be neglected as reported in [41].

2.2. Model Evaluation

2.2.1. Model Accuracy

It was shown earlier that the proposed model can accurately pass through the four STC points provided in the manufacturer's datasheet. This section evaluates the accuracy of the model at the rest points of the curve. The evaluation is conducted by comparing the modeled *I-V* curves of the proposed model to the corresponded *I-V* curves produced by the practical model. The comparison is conducted with reference to the measurements provided in the manufacturer datasheets from different PV technologies available commercially, as shown in Figure 2-6. The deviation of the modeled *I-V* curve with reference to the measured curve for the existing models and proposed model is also presented in Figure 2-7, depicted as a percentage of the short-circuit current I_{sc}.

The comparison in Figure 2-6 demonstrates a good match between the modeled and measured data for the three PV technologies available commercially. It can also be seen that the accuracy of the proposed model highly matches that of the practical model, as shown in Figure 2-7. There are a few points where the practical model negligibly outperforms the proposed model, and similarly a few points where the proposed model negligibly outperforms the practical model. Generally, however, it can be said that both of them have the same accuracy.

To verify the effectiveness of the proposed model under various environmental conditions, three PV modules of different PV technologies are tested under a range of irradiances and temperatures. The modeled characteristic curves are compared to the measured curves provided by the manufacturer datasheet of mono crystalline, poly crystalline and amorphous thin film PV modules, as shown in Figure 2-8, Figure 2-9 and Figure 2-10, respectively. The resulting curves show a good match between the measured curves and the modeled curves. The slight deviations between the measured and modeled curves are due to measurement errors and to imperfections in the model.

The accuracy of the proposed model is also investigated and compared numerically with the existing models at different irradiance and temperature levels as shown in Table 2.2. The root mean square RMS, maximum and minimum modeling deviation represented as percentage of the short circuit current I_{sc} is summarized for each model type and under different meteorological conditions. It is shown that the accuracy improves going from the ideal, through simplified to practical model. Moreover, the accuracy of the proposed model is highly close to the accuracy of the practical model.

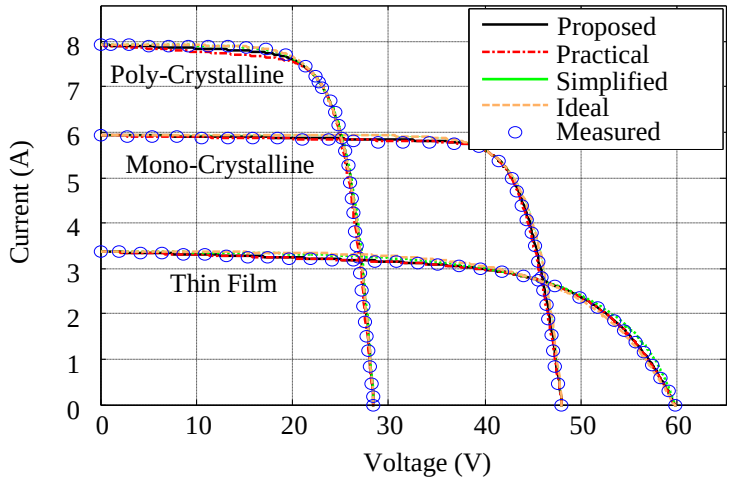

Figure 2-6: Modelled and measured current curves for mono-crystalline, poly-crystalline and thin-film PV modules.

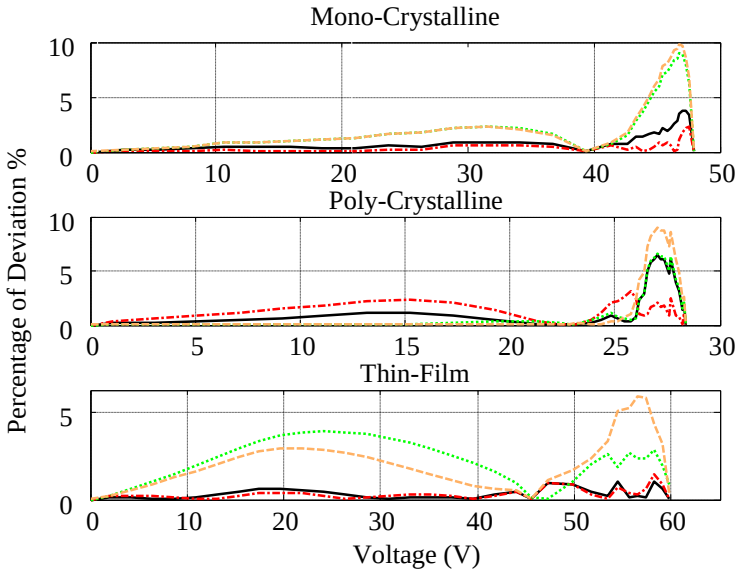

Figure 2-7: Deviation in the practical and proposed models with respect to measured data.

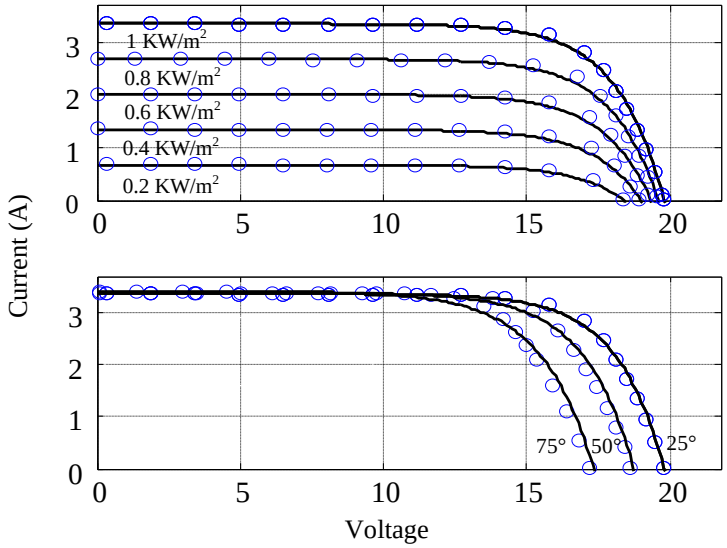

Figure 2-8: Modelled and measured current curves for a mono-crystalline PV module under different irradiances and temperatures.

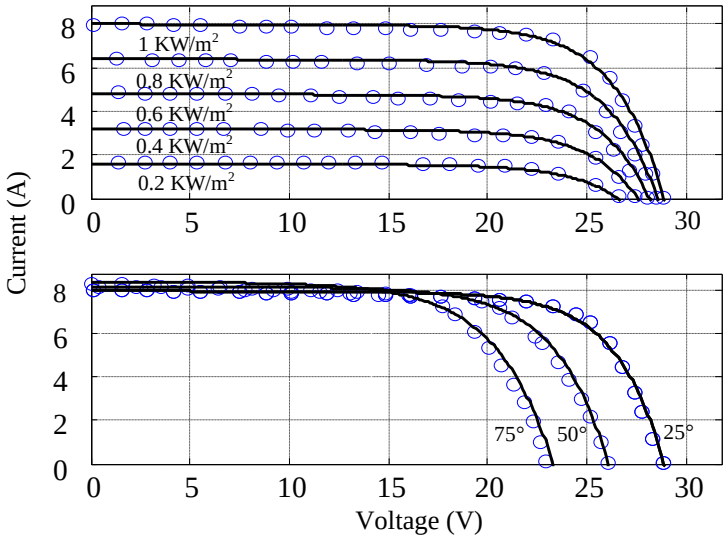

Figure 2-9: Modelled and measured current curves for a poly-crystalline PV module under different irradiances and temperatures.

Table 2.2: The Percentage of Modeling Deviation of the Proposed Model and Existing Models at Various Temperature and Irradiance Levels

Irradiance G and Temperature T	Ideal Model			Simplified Model			Practical Model			Proposed Model		
	Min	Max	RMS	Min	Max	RMS	Min	Max	RMS	Min	Max	RMS
G = 1 kW/m^2 & T=25°C	0.04	9.8	4.61	0.04	2.70	1.21	0.04	2.44	0.59	0.02	2.55	0.55
G =0.8 kW/m^2 & T=25°C	0.01	4.0	1.54	0.01	1.56	0.97	0.01	1.78	0.59	0.01	1.73	0.79
G =0.6 kW/m^2 & T=25°C	0.04	10.4	2.31	0.01	2.90	1.76	0.02	3.08	0.93	0.02	2.93	1.15
G =0.4 kW/m^2 & T=25°C	0.01	13.9	4.27	0.01	2.88	1.90	0.01	4.48	1.55	0.01	3.47	1.30
G =0.2 kW/m^2 & T=25°C	0.03	15.9	4.09	0.02	2.75	1.87	0.01	6.24	1.50	0.01	1.82	0.72
G = 1 kW/m^2 & T=50°C	0.02	13.2	6.90	0.37	15.69	6.80	0.03	3.05	1.31	0.04	3.22	1.92
G = 1 kW/m^2 & T=75°C	0.14	14.2	7.13	0.17	20.51	7.54	0.02	3.60	1.50	0.30	3.87	1.43

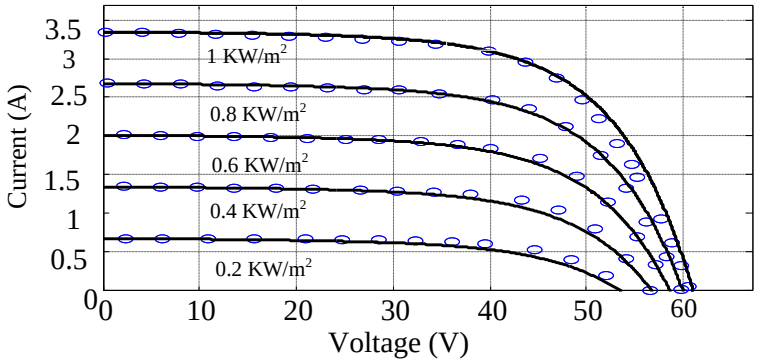

Figure 2-10: Modelled and measured current curves for a thin-film PV module under different irradiances.

2.2.2. Computational Time

The main motivation for this chapter, as highlighted in the introduction, is building a PV model that can reduce the high computational time of the practical PV model. This section evaluates the computational time needed to run a simulation of a PV module from zero to open circuit voltage V_{oc}, using the proposed model in MATLAB. This is then compared to the available models in the literature, i.e., practical, simplified and ideal PV models. The model is also compared to the Lambert based PV model [51, 52]. A poly-crystalline module is chosen to be simulated from 0 to V_{oc}, using the proposed model and other models for computational time comparisons. The extracted parameters shown in Table 2.1 and Equations (2-12) and (2-15) are utilized to build the model in SIMULINK environment shown in Figure 2-11 below. The simulation is used to plot the *P-V* curve for the module, operating under 0.8 KW/m^2 of irradiance and 60°C of temperature. The proposed model and other available models in the literature are used in the same computer and for the same discrete time step. The resulting computational time, normalized over the computational time of the ideal model, for the proposed model and other models is

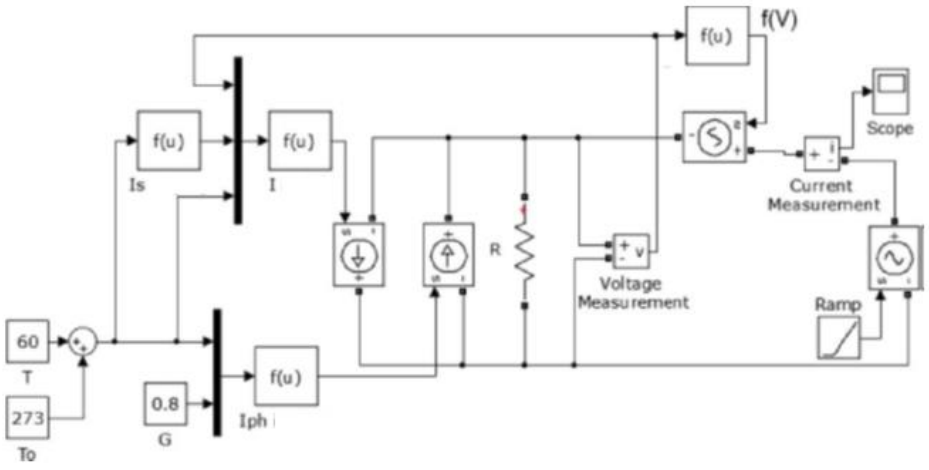

Figure 2-11: MATLAB-SIMULINK simulation of the proposed PV model.

summarized in Table 2.3. The computational time was determined by the clock function several times, and the average value of the measurements is recorded. Table 2.3 shows that the proposed model has lower computational time compared to that of the practical, simplified and Lambert models. The computational time of the proposed model almost equals that of the simple ideal model. This is because the proposed model relies on the non-transcendental equation, which does not require a numerical solver, as demonstrated earlier. Although the reduction of the computational time with respect to the practical model does not appear significant when simulating one PV module, there are substantial advantages when simulating a larger system, as demonstrated in the next section.

2.3. Case Study: Partially Shaded PV System

In this section, the accuracy and the computational time of the proposed model under partial shading conditions are investigated. Studying partial-shaded impact on a system is an active area of research and is of significant importance to designing PV systems [53]. It is also essential for testing maximum power point tracking algorithms proposed for these systems [16, 54]. Furthermore, studies of energy prediction needs to consider shade levels affecting the system in order to obtain real values of available power throughout the day.

As illustrated earlier, the challenge in such studies is the need for simulating an enormous number of series and parallel connected PV modules simultaneously, because each PV unit might be subjected to a different irradiance level. This results in a high computational time and therefore oftentimes becomes challenging to simulate and study these systems.

Table 2.3: Computational Time Comparison for the Proposed and Existing Models

Used Model	Normalized Time (s)
Ideal Model	1.000
Simplified Model	1.190
Practical Model	1.210
Lambert Model	3.254
Proposed Model	1.036

2.3.1. Model Accuracy

This section verifies the accuracy of the proposed model under partial shading conditions. The PV system under study consists of 12 series connected PV modules as shown in Figure 2-12. Each PV module is of type Yingli YL-165 and contains 48 series connected PV cells with 3 bypassed diodes where each diode is connected to 16 PV cells. The shading scenario and irradiance distribution of the PV modules in the system are shown in Figure 2-12. Four PV modules are fully illuminated receiving 0.97 KW/m^2 while the rest of PV modules are partially shaded. One third of a partial shaded PV module receives fully illuminated irradiance of 0.97 KW/m^2 whereas the rest receives 56% of the fully illuminated irradiance.

The proposed model is used to simulate the system shown in Figure 2-12 in SIMULINK. One PV module is modeled using 48 series connected PV cells with three bypassed diodes. The entire system is then modeled by series connecting 12 PV modules together. The same system is also re-simulated using the practical PV model. It is important to mention that parameterizing a PV cell is similar to that of a PV module except that the value of the open circuit voltage V_{oc} and maximum voltage V_m provided by manufactures datasheet must be divided by the number of PV cells N_s in the PV module. The resulted *I-V* curves in both cases are compared to experimental data, provided in [43], as shown in Figure 2-13. As it can be shown, the proposed model can simulate partial shaded PV systems accurately.

2.3.2. Computational Time

As mentioned earlier in the introduction, a quick approach to model PV systems is conducted by using one aggregated PV model for an arbitrary number of PV modules [44]. Unfortunately, this approach can only be applied on homogeneous PV systems in which all units receive same irradiance, and thus cannot be applied on partial shaded systems. Each PV unit in partial shaded PV system must be modeled using a separate PV model because each unit might have a different irradiance level. This results in a high computational time. This section shows the advantage of the proposed PV model in reducing the computational time when simulating partially shaded PV systems. The partially shaded PV system under study is shown in Figure 2-14. The system consists of 10 parallel connected columns of PV

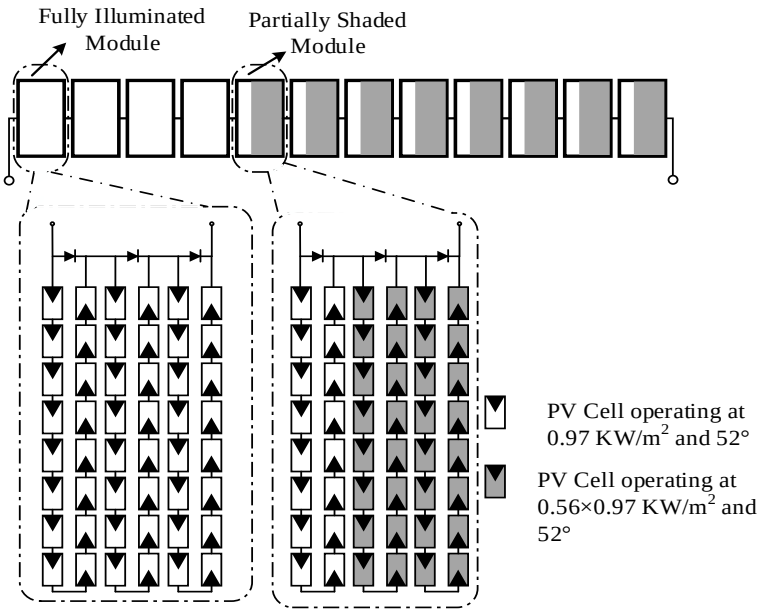

Figure 2-12: A partially shaded PV system composed of twelve series PV modules.

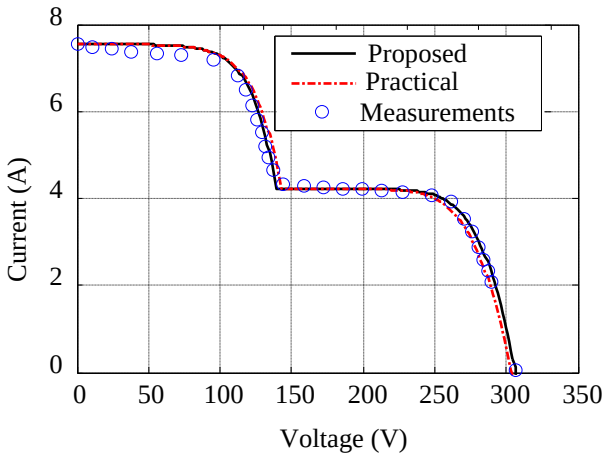

Figure 2-13: The modeled current curves using both the proposed and practical models compared to the experimental data.

strings; each PV column consists of 10 series-connected PV modules, and each module has a bypassing diode. The system is subjected to four different irradiance levels: 1 KW/m^2, 0.5 KW/m^2, 0.3 KW/m^2 and 0.1 KW/m^2, all under 60°C of temperature, as illustrated in the figure. The simulation is conducted to simulate the voltage-power curve of the system from 0 to V_{oc} with 0.1 V of discrete voltage step. The simulation is conducted in MATLAB Simulink where each PV module is represented by the proposed PV model connected in parallel to a bypass diode.

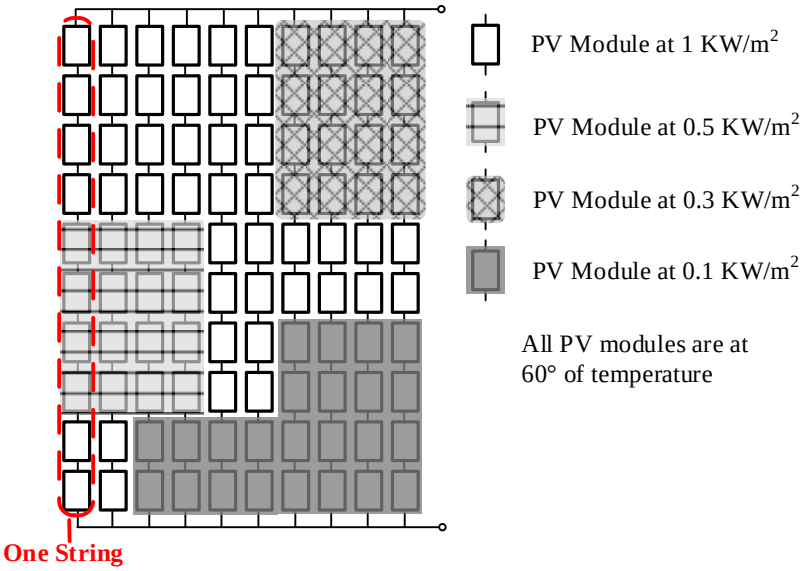

Figure 2-14: The Partially shaded photovoltaic system under study.

In Figure 2-14, the only string simulated in the system is the left-most PV column. The simulation is repeated for the two left-most columns, then three, then four, and so on, until the whole 10 PV columns in the system are reached. The resulting computational time in each scenario is recorded in Table 2.4 for both the proposed and practical PV models. The simulation is repeated for the case of non-shaded PV system where all the PV modules of Figure 2-14 receive full irradiance of 1 KW/m^2. The results are also recorded in Table 2.4. It is noteworthy that all of the simulations are conducted in the same computer and at the same discrete time step.

Table 2.4 shows two important results. The first is that the proposed model has a lower computational time than the practical PV model. The second is that the percentage reduction in computational time for the proposed model, with respect to the practical model, increases with the size of the simulated system for both shaded and unshaded PV system.

When one string in the PV system in Figure 2-14 is simulated in the shaded system, the percentage of reduction in computational time is 32.36%. However, when the complete PV system of Figure 2-14 is simulated, a computational time reduction of 51.28% is recorded. This is shown in Figure 2-15, which plots the computational time for both the proposed and practical models. The computational time, when simulating a partial-shaded or non-shaded PV system, increases exponentially with the size of the PV system. Furthermore, the rate of time increase in the practical time is higher than that of the proposed model. This indicates that the reduction in computational time featured in the proposed model is proportional to the number of PV modules in the simulated system. This can be generalized for systems

Table 2.4: Computational Time of the Practical and Proposed Models at Different System Sizes

No. of PV Strings	Practical Model (s)		Proposed Model (s)		Reduction in time %	
	Unshaded system	Shaded System	Unshaded system	Shaded System	Unshaded system	Shaded System
1	2.57	5.5	1.51	3.72	41.14	32.36
2	7.52	12.15	4.38	7.87	41.67	35.23
3	16.51	24.78	8.61	14.07	47.85	43.22
4	32.60	43.63	15.22	23.82	53.29	45.4
5	54.08	73.12	24.79	37.95	54.16	48.1
6	84.97	106.78	38.72	54.58	54.43	48.89
7	120.29	152.7	54.59	77.94	54.62	48.96
8	166.68	215.51	74.83	107	55.10	50.35
9	224.52	291.04	99.38	144.34	55.73	50.7
10	294.48	383.5	129.08	186.84	56.16	51.28

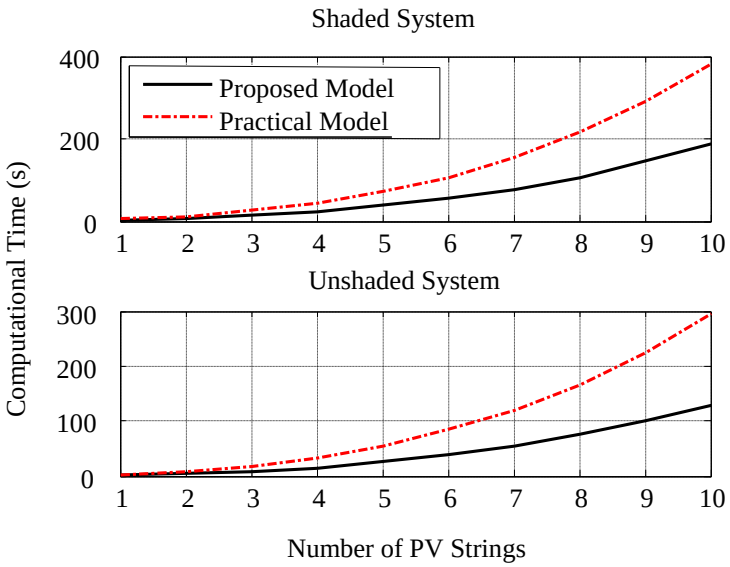

Figure 2-15: The computational time of the proposed and practical models at different system sizes under shaded and unshaded conditions.

working both under shaded and unshaded conditions as demonstrated. Therefore, the proposed model not only decreases the computational time, the reduction increases exponentially with the size of a PV system. This feature of the proposed model provides a clear advantage when simulating a large PV power system.

2.3.3. Comparison to the Lambert based PV Model

Simplified Lambert function based PV models are employed in the literature to model partially shaded PV systems with improved computational speed. In this section, the Lambert modeling approach presented in [55] is applied on the proposed model and the overall performance is compared to the modeling performance resulted when instead Lambert model is adopted. The relation between the output current *I* and terminal voltage *V* of a PV module in the Lambert model is represented in the following equations [43]:

$$V = (I_{ph} + I_s).R_{sh} - (R_s + R_{sh}).I - a \times \text{Lambert}(W) \quad 2\text{-}21)$$

$$W = \frac{R_{sh} \times I_s}{a} e^{\left(\frac{R_{sh}.(I_{ph}+I_s-I)}{a}\right)} \quad 2\text{-}22)$$

The partial shaded PV system under study is a PV string composed of 15 series connected PV modules operating at different irradiance and temperature levels. The value of irradiance and temperature at each of the PV module is shown in Table 2.5.

The simulation is conducted to simulate the voltage-power curve of the system from 0 to V_{oc} with 0.1 *V* of discrete voltage step. First of all, only one PV module is simulated which is the PV module number 1. The simulation is repeated for the two PV modules 1 and 2, then three, then four, and so on, until the whole 15 PV modules in the string is reached. The resulting computational time in each scenario is recorded in Table 2.6 for both the proposed and Lambert PV model proposed in [55]. Furthermore, the computational times are plotted in Figure 2-16 for both the proposed model and the Lambert model. Table 2.6 and Figure 2-16 show clearly that the proposed model provide reduced computational time compared to the Lambert model. As an example, when simulating the whole PV string, 93% reduction in computational time is resulted. Moreover, they show that the reduction in computational time increases with increasing the size of PV string.

2.4. Discussion

This chapter highlighted the shortcomings found in the available PV models, which suffer either from excessive computational time or from inaccuracy. It then clarified the need for an accurate and low computational time PV model for modeling partially-shaded PV systems.

To meet this need, the chapter proposed an accurate photovoltaic model that featured a lower computational time. The proposed model relies on the practical model and reduces the computational time by replacing the model series resistance with a third-degree polynomial voltage-dependent source. It mimics the accurate characteristics of the practical model without depending on the implicit

Table 2.5: Irradiance and Temperature Profile

Module #	Irradiance KW/m^2	Temperature C°	Module #	Irradiance KW/m^2	Temperature C°
1	1.000	72°	9	0.400	39°
2	0.700	47°	10	0.260	32°
3	0.100	25°	11	0.575	29°
4	0.250	27°	12	0.500	39°
5	0.850	27°	13	0.950	34°
6	0.530	42°	14	0.755	49°
7	0.620	33°	15	0.280	43°
8	0.715	37°	-	-	-

Table 2.6: Computational Time of Lambert and Proposed Models at Different String Sizes

Number of PV Modules	Lambert Model [55] (s)	Proposed Model (s)	Reduction in time %
1	0.0282	0.0196	30.31
2	0.1194	0.0501	58.05
3	0.2530	0.0844	66.62
4	0.4536	0.1243	72.58
5	0.7722	0.1726	77.65
6	1.1892	0.2217	81.36
7	1.7383	0.2789	83.95
8	2.4069	0.3391	85.91
9	3.2240	0.3831	88.11
10	4.1966	0.4472	89.34
11	5.3429	0.5218	90.23
12	6.6170	0.5928	91.04
13	7.9478	0.6518	91.79
14	9.5378	0.7193	92.45
15	11.1761	0.7783	93.03

transcendental equation, thus providing a lower computational time. The proposed model consists of current source, diode, shunt resistant and polynomial voltage dependent voltage source.

The effectiveness of the proposed model over the practical model was verified by comparing their computational times. Moreover, the accuracy of the model was verified by measuring data at different temperatures and irradiances in commercially available mono-crystalline, poly-crystalline and thin-film PV technologies. A case study of a partially shaded PV system was then conducted to show the effectiveness of the proposed model under partial shading conditions. The advantage of using the proposed model in these conditions is amplified, because the percentage of the reduction in computational time increases nonlinearly with the number of connected PV units.

In spite of the reduction in the computational time achieved by the proposed circuit model in this chapter, it is still considered too large for some model-based online applications. These applications

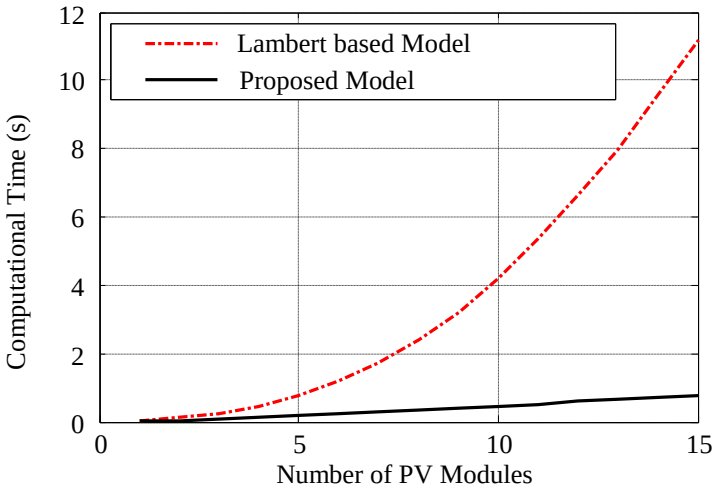

Figure 2-16: Computational time of the proposed and Lambert models at different sizes.

require estimating the power peaks of the power-voltage curves of partially shaded PV systems in few seconds. Using the circuit model to simulate the entire power curve and then finding the power peaks is time consuming and might reach to hundreds of seconds as demonstrated in this chapter. Therefore, the literature lacks many model-based tools that would improve PV systems. For this reason, next chapter will develop a fast modeling tool for finding the power peaks of partially shaded PV systems in few seconds suitable for developing online applications.

Chapter 3 FAST POWER-PEAK ESTIMATOR FOR PARTIALLY SHADED PV SYSTEMS

Unlike homogeneous PV systems whose output power curves exhibit only a single power peak, partially shaded PV systems are characterized by multiple power peaks. These peaks and their corresponding MPP voltages can be determined by simulating the power curve of a partially shaded PV system using numerous connected PV circuit models. Although utilizing the circuit model proposed in the previous chapter can reduce the length of the computational time required for conducting such simulations, computational time is still too long for some useful online applications.

An example is the fact that, although model-based MPPTs have been successfully implemented for improving dynamic MPPT performance in homogeneous PV systems, none yet exists for use with partially shaded PV systems. Model-based MPPTs require a determination of the PV system power peaks in a few seconds, which is infeasible with existing PV models that can require hours for large systems.

This chapter proposes a novel power-peak estimator capable of determining the power peaks of large PV systems with a reduced computational time in the range of only a few seconds. Rather than simulating the entire power curve, the proposed estimator finds the power peaks directly by utilizing three developed rules that govern the formation of power peaks in partially shaded PV systems. The proposed estimator was then used, for the first time, for the development of a model-based MPPT. The developed MPPT can successfully improve the dynamic power-extraction performance of nonhomogeneous PV systems.

3.1. Rules Governing the Formation of Power-Peaks in Partially Shaded PV Systems

As mentioned, the proposed modeling approach relies on three developed rules governing the formation of power peaks in partially shaded PV systems. The first rule finds the power peaks of partially shaded series PV units connected without bypass diodes, such as those depicted in Figure 3-1(a). The second rule determines the power peaks of partially shaded series PV units connected with bypass diodes, such as those shown in Figure 3-1(b). The third rule finds the power peaks of partially shaded PV units connected in parallel, such as those shown in Figure 3-1(c). The combined three rules can find the power peaks of partially shaded PV systems composed of series PV units (connected with and without bypass diodes) and parallel PV strings, such as those shown in Figure 3-1(d).

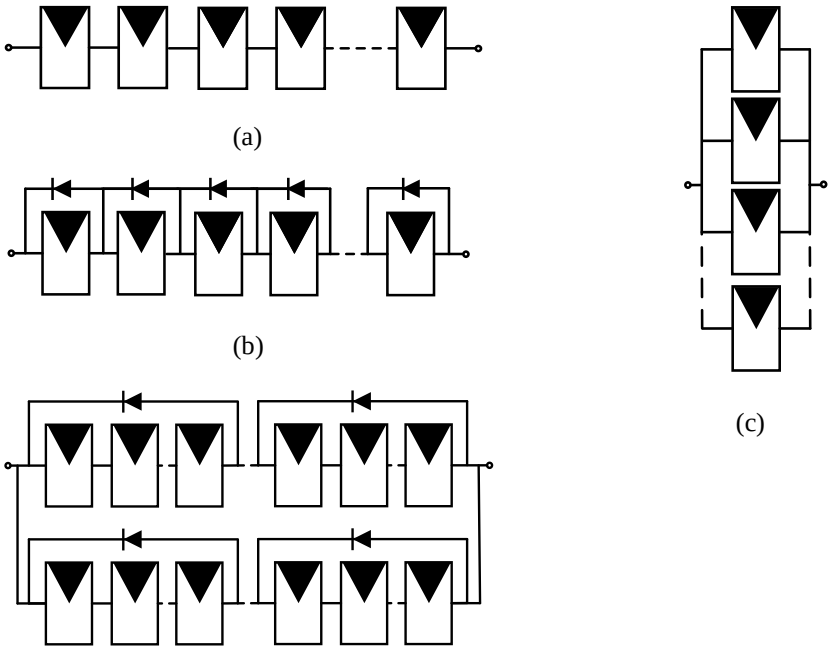

Figure 3-1: PV systems: a) series PV units connected without bypass diodes; b) series PV units connected with bypass diodes; c) parallel PV units; and d) series PV units connected in parallel.

The three rules presented in this section are based on the Lambert PV circuit model [55]. The relation between the output current *I* and terminal voltage *V* of a PV module in the Lambert model is represented in the following equations [43]:

$$V = \left(I_{ph} + I_s\right) \times R_{sh} - (R_s + R_{sh}).I - a \times Lambert(W) \tag{3-1}$$

$$W = \frac{R_{sh} \times I_s}{a} e^{\left(\frac{R_{sh}.\left(I_{ph}+I_s-I\right)}{a}\right)} \tag{3-2}$$

where the parameter a is equal to N_sKTA/q. The photon and saturation currents are calculated using the following equations [40]:

$$I_{ph} = G \times (I_{sc} + C_i.\Delta T) \tag{3-3}$$

$$I_s = [(I_{sc} + \alpha \times \Delta T) - \frac{V_{oc} - |B|\Delta T}{R_{sh}}]/[e^{\frac{q(V_{oc}-|B|\Delta T)}{N_sKTA}} - 1] \tag{3-4}$$

3.1.1. First Rule

It is known that the output power curve of series PV units connected without bypass diodes always has a single power peak [56]. The value of the current at this single maximum power point (MPP) can be calculated by equating the summation of the derivatives of the power-current curves corresponding to the series PV units to zero, as expressed in the following:

$$\sum_{i=1}^{n_s} \frac{dP_i}{dI} = 0 \tag{3-5}$$

where n_s refers to the number of series connected PV units. The derivative of the power-current curve of a PV unit dP/dI is expressed as follows:

$$\frac{dP}{dI} = V + I \times \frac{dV}{dI} \tag{3-6}$$

where dV/dI is the voltage derivative with respect to current and is expressed in the following:

$$\frac{dV}{dI} = -(R_s + R_{sh}) - \frac{R_{sh}\left(I_{ph} + I_s - I\right)Lambert(W)}{1 + Lambert(W)} \tag{3-7}$$

Substituting (3-1) and (3-7) in (3-6) results in:

$$\frac{dP}{dI} = R_{sh} \times \left(I_{ph} + I_s\right) - \frac{R_{sh} \times I\left(I_{ph} + I_s - I\right) \times Lambert(W)}{1 + Lambert(W)} - 2I \times (R_s + R_{sh}) - a \times Lambert(W) \tag{3-8}$$

Substituting (3-8) in (3-5) produces:

$$\sum_{i=1}^{n_s} R_{sh} \times \left(I_{ph_i} + I_{s_i}\right) - 2I \times (R_s + R_{sh}) - a_i \times Lambert(W_i) - \frac{R_{sh} \times I \times \left(I_{ph_i} + I_{s_i} - I\right)Lambert(W_i)}{1 + Lambert(W_i)} = 0 \tag{3-9}$$

Solving (3-9) for n_s number of series PV units determines the MPP current of the series PV units. Equation (3-9) can be easily solved using any numerical method, such as the well-known Newton-Raphson technique. The value of the power peak at the determined MPP current, resulting from solving (3-9), can be calculated by summing the powers of all series-connected PV units generated at the MPP current using the following equation:

$$\sum_{i=1}^{n_s} P_i = I \times \sum_{i=1}^{n_s} V_i = I \times \sum_{i=1}^{n_s} \left(\left(I_{ph_i} + I_{s_i}\right)R_{sh} - (R_s + R_{sh})I - a_i \times Lambert(W_i)\right) \tag{3-10}$$

To summarize, the first rule states that, for any series PV units connected without bypass diodes, there is a single power peak, which can be calculated using (3-10), while the corresponding MPP current can be determined by solving (3-9).

3.1.2. Second Rule

The output power curve of series PV units, connected with bypass diodes, could have multiple peaks rather than only one peak [45, 57]. The value of the MPP currents at the power peaks can be calculated by equating the summation of the derivatives of the power-current curves for all series PV units to zero, as expressed in the following equation:

$$\sum_{j=1}^{n_d}\left(Z_j \times \frac{dP_j}{dI}\right) = 0 \tag{3-11}$$

where n_d refers to the number of diode-bypassed PV units and Z_j is an integer modeling the effect of a bypass diode. The integer Z_j is equal to one when the photon current I_{ph} of the j_{th} PV unit is higher than the current passing through the series units; otherwise, it is equal to zero.

If a bypassed PV unit is composed of series-connected PV units, such as in the system shown in Figure 3-2, then equation (3-11) should be adjusted as follows:

$$\sum_{j=1}^{n_d} Z_j \frac{dP_j}{dI} = \sum_{j=1}^{n_d} Z_j \times \left(\sum_{i=1}^{n_s} \frac{dP_i}{dI}\right)_j = 0 \tag{3-12}$$

Substituting (3-8) in (3-12) results in:

$$\sum_{j=1}^{n_d} Z_j \left(\sum_{i=1}^{n_s}\left(R_{sh}\left(I_{ph_i} + I_{s_i}\right) - \frac{R_{sh} \times \left(I_{ph_i} + I_{s_i} - I\right) Lambert(W_i) I}{\left[\left(1 + Lambert(W_i)\right)\right]} - 2I \times (R_s + R_{sh}) - a_i \times Lambert(W_i)\right)\right)_j = 0 \tag{3-13}$$

Solving (3-13) for any set of series PV units connected with bypass diodes produces the value of the MPP current corresponding to one of the power peaks of the system. Because multiple power peaks could exist, equation (3-13) should be solved several times at various initial guesses to determine the MPP currents corresponding to all power peaks. Similar to (3-9), equation (3-13) can be easily solved by any numerical method.

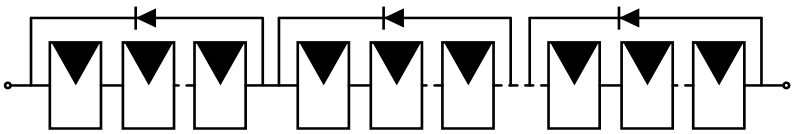

Figure 3-2: Series connected PV units with and without bypass didoes.

The power peak at a determined MPP current, resulting from solving (3-13), can be calculated by summing the powers generated from all the series-connected PV units operating at the MPP current, considering the voltage drop in the bypassed diodes V_d, using the following equation:

$$\sum_{j=1}^{n_d} P_j = \sum_{j=1}^{n_d} \left(Z_j \times \left(\sum_{i=1}^{n_s} P_i \right) - (1 - Z_j) \times n_s I V_d \right)_j = \sum_{j=1}^{n_d} \left(Z_j \left(I \times \sum_{i=1}^{n_s} V_i \right)_j - (1 - Z_j) n_s I V_d \right)_j \quad (3\text{-}14)$$

Substituting (3-1) in (3-14), equation (3-14) becomes:

$$\sum_{j=1}^{n_d} P_j = \sum_{j=1}^{n_d} \left(Z_j \times \sum_{i=1}^{n_s} \left(\left(I_{ph_i} + I_{s_i} \right) \times R_{sh} I - (R_s + R_{sh}) \times I^2 - a_i \times I \times Lambert(W_i) \right) - (1 - Z_j) \times n_s I . V_d \right)_j \quad (3\text{-}15)$$

In summary, the second rule states that, for any series PV units connected with bypass diodes, the MPP currents can be calculated by solving (3-13) at different initial guesses, and the power peaks are determined using (3-15).

3.1.3. Third Rule

The output power curve of parallel PV units could have multiple power peaks [56]. The value of the corresponding MPP voltages can be calculated by equating the summation of the derivatives of the power-voltage curves for all parallel PV units to zero, as expressed in (3-16), and by equating the voltages of the parallel PV units, as in (3-17):

$$\sum_{k=1}^{n_p} \frac{dP_k}{dV} = 0 \quad (3\text{-}16)$$

$$V_1 = V_x, \text{for all } x = [2, 3, \ldots k] \tag{3-17}$$

where n_p refers to the number of parallel PV units. If a paralleled PV unit is composed of series-connected PV units, equation (3-16) should be adjusted as follows:

$$\sum_{k=1}^{n_p} \frac{dP_k}{dV} = \sum_{k=1}^{n_p} \left(\sum_{j=1}^{n_d} \left(Z_j \times \frac{dP_j}{dI} \right) \times \sum_{j=1}^{n_d} \left(Z_j \times \frac{dI_j}{dV} \right) \right) = 0 \tag{3-18}$$

Substituting (3-7) and (3-12) in (3-18) results in:

$$\sum_{k=1}^{n_p} \left(\left(\sum_{j=1}^{n_d} Z_j \times \left(\sum_{1}^{n_s} \frac{dP_i}{dI} \right)_j \right) \times \left(\sum_{i=1}^{n_s} Z_j \times \left(\sum_{i=1}^{n_s} \frac{dI_i}{dV} \right)_j \right) \right) = 0 \tag{3-19}$$

Solving (3-19) with the equations represented in (3-17), for any number *k* of parallel PV units, produces the set of currents [I_1, I_2,..,I_k] passing through the paralleled PV strings at one power peak of the system. Because multiple power peaks could exist, the equations should be solved several times at various initial guesses to determine the sets of currents corresponding to all power peaks.

The value of the power peak corresponding to a determined set of currents can be calculated by summing the powers of all parallel connected PV units generated at the determined set of currents, using the following equation:

$$\begin{aligned} \sum_{k=1}^{n_p} P_k &= \sum_{k=1}^{n_p} \left(\sum_{j=1}^{n_d} \left(Z_j \sum_{i=1}^{n_s} P_{i\ j} - (1 - Z_j) \times n_s V_d \right)_j \right)_k \\ &= \sum_{k=1}^{n_p} \left(\sum_{j=1}^{n_d} \left(Z_j \left(I \times \sum_{i=1}^{n_s} V_i \right) - (1 - Z_j) \times n_s I V_d \right)_j \right)_k \end{aligned} \tag{3-20}$$

Substituting (3-1) in (3-20) results in:

$$\begin{aligned} \sum_{k=1}^{n_p} P_k = \sum_{k=1}^{n_p} \Bigg(\sum_{j=1}^{n_d} \Bigg(Z_j \sum_{i=1}^{n_s} \Big((I_{ph_i} + I_{s_i}) R_{sh} I - (R_s + R_{sh}) I^2 - a_i I Lambert(W_i) \Big) \\ - (1 - Z_j).n_s.I.V_d \Bigg)_j \Bigg)_k \end{aligned} \tag{3-21}$$

In summary, the third rule states that, for any parallel PV units, the set of currents corresponding to a power peak can be determined by solving (3-19) with the equations represented in (3-17), and the value of the power peak can be calculated using (3-21).

3.2. The Proposed Modeling Tool

This section presents the proposed modeling algorithm that determines the power peaks of partially shaded PV systems. The algorithm utilizes the three rules presented in the previous section to quickly determine the peaks of a PV system without simulating the entire power curve.

The algorithm starts by applying the first rule, represented in equation (3-9), to the groups of PV units connected without a bypass diode to determine the MPP currents of the groups. The initial guess for solving (3-9) for a group is best chosen to be 90% of the group's photon current, which approximately equals the photon current of the PV unit receiving the lowest irradiance level in the group.

Once the MPP currents of all the groups of PV units connected without diodes are calculated, the second rule, represented in equation (3-13), will be applied to the groups of PV units connected with bypass diodes (PV strings). The initial guesses needed to solve (3-13) for a PV string are the MPP currents resulting from applying the first rule to the groups of PV units inside the PV string. The integer Z_j for a group is equal to one if the photon current of the group is higher than the used initial guess.

Finally, the third rule, represented by (3-17) and (3-19), will be applied to find the power peaks and their corresponding currents of the entire system. Applying the third rule produces the set of currents passing through the parallel PV strings at one of the power peaks. To find the sets of currents corresponding to all power peaks, the third rule will be applied at various sets of initial guesses. The number of required sets of initial guesses equals the number of MPP currents resulting from applying the second rule. This means that a set of initial guesses is produced from each MPP current resulting from the second rule. To obtain a set of initial guesses from an MPP current, the MPP current is first substituted in the corresponded PV string to find the string voltage. The resulting voltage is used to calculate the currents in all of the parallel strings. These currents are a set of initial guesses. This process is repeated for all MPP currents resulting from the second rule to find all sets of initial guesses. It is important to mention that when the resulting voltage is used to calculate the current in a parallel string, all the diodes inside the string are firstly assumed not activated. Then, the voltage of each group is calculated using the resulted current. If a negative voltage appears in any of the group, the calculation is repeated assuming that the diode of the group with minimum photon current is activated. If again any of

the resulted voltages is negative, the diode of the group with minimum photon current, excluding the already deactivated group, is deactivated.

A summary of the proposed algorithm is shown in the flowchart in Figure 3-3. The proposed algorithm is illustrated further using the example of a partially shaded PV array, as shown in Figure 3-4. The PV array is composed of two PV strings, each with two series PV modules. The used PV modules consist of 36 PV cells and 3 bypassing diodes. The profile of the irradiances is illustrated in the same figure. The inputs to the algorithm are the irradiances and temperatures received by all PV cells of the array. First, the photon and saturation currents (I_{ph}, I_s) of all the PV cells are calculated using (3-3) and (3-4). Next, the photon current of each group of series PV units connected without diodes is estimated by finding the photon current of the PV unit receiving the lowest irradiance in each group. Then, (3-9) is solved for all groups of PV cells connected without bypass diodes (circled by a black dotted line). Since there are seven groups of PV cells connected without bypass diodes which have dissimilar shading patterns in Figure 3-4, equation (3-9) is solved seven times. The resulting currents from solving (3-9) for the series groups in a PV string are used as initial guesses to solve (3-13) for the PV strings (circled by a blue dashed line). Equation (3-13) will be solved three times (corresponding to the three different initial guesses) for the first string, and five times for the second PV string. After (3-13) is solved for all PV strings, the third rule is applied to the parallel PV units (circled by a red dashed line). First, the resulting MPP currents from solving (3-13) are used to find the set of initial guesses for the third rule. Each MPP current is substituted in the corresponding PV string to find the string voltage, which is then used to find the currents in all of the strings. Solving (3-17) and (3-19) (rule 3) for the entire system using all of the sets of initial guesses produces the sets of currents corresponding to the power peaks of the system. Because there are eight sets of initial guesses (corresponding to the eight times that equation (3-13) is solved), equations (3-17) and (3-19) will be solved eight times. Finally, substituting each set of currents in (3-21) determines the corresponding power peak. Equation (3-21) will be solved eight times, similar to (3-17) and (3-19).

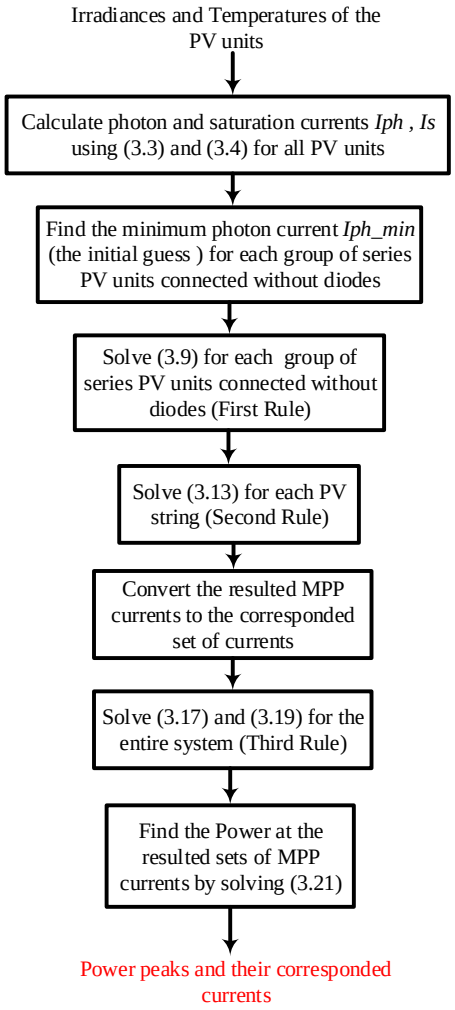

Figure 3-3: Flowchart summarizing the proposed modelling tool.

3.3. Evaluation of the Proposed Modeling Tool

3.3.1. Accuracy

This section evaluates the accuracy of the proposed modeling approach in finding the power peaks of partially shaded PV systems. The evaluation is conducted by comparing the modeled power peaks (using the proposed approach) to those resulting from simulating the entire *P-V* curve (existing approach). The Lambert function implementation in MATLAB is conducted via the Halley's method, presented in [58].

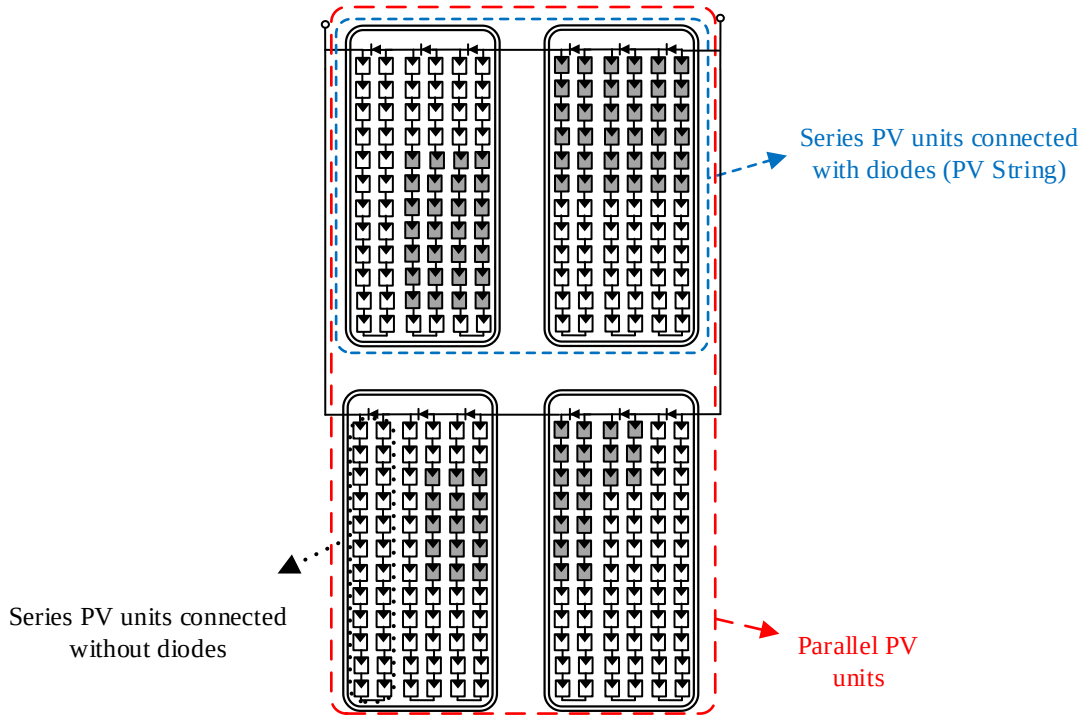

Figure 3-4: A 2×2 PV array composed of series PV units connected without bypassed diodes; series PV units connected with bypass diodes and parallel PV units.

The system under study is composed of twelve series-connected PV modules, as shown in Figure 3-5. Each PV module is of the type "Yingli YL-165" and contains 48 series-connected PV cells with 3 bypassed diodes, where each diode is connected to 16 PV cells. The system is first modeled using the proposed modeling approach, after which the results are compared to those resulting from the simulation, as shown in Figure 3-6. It can be seen that the modeled power peaks using the proposed approach are highly close to the power peaks resulting from using circuit simulation. The numerical values for the extracted peaks are also compared in Table 3.2. The table reveals that the accuracy of the proposed approach is high where the percentage error does not exceed 0.4%.

3.3.2. Computational Time

The effectiveness of the proposed approach to quickly find the power peaks of a partially shaded PV system is verified in this section. The computational times required to find the power peaks of a partially shaded PV system using the proposed approach are recorded and then compared to the computational times that result when the circuit simulation is used. The discrete voltage step used is 0.1 V in all cases.

Table 3.2 reveals that the proposed modeling approach significantly reduces the computational time compared to the circuit simulation. Furthermore, it shows that the computational time of the proposed

Table 3.1: Comparison between the Modeled and Measured Power Peaks

Proposed Modeling Approach		Existing Modeling Approach		Percentage Deviation %	
Current (A)	Power (W)	Current (A)	Power (W)	Current %	Power %
6.9843	935.7	7	938.3	0.224	0.267
4.0292	1037.7	4.04	1040.9	0.277	0.307

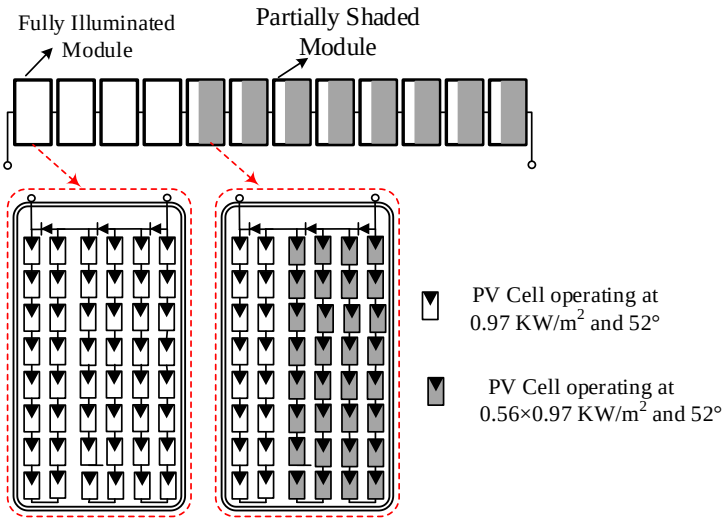

Figure 3-5: Partially shaded PV system composed of twelve series-connected PV modules.

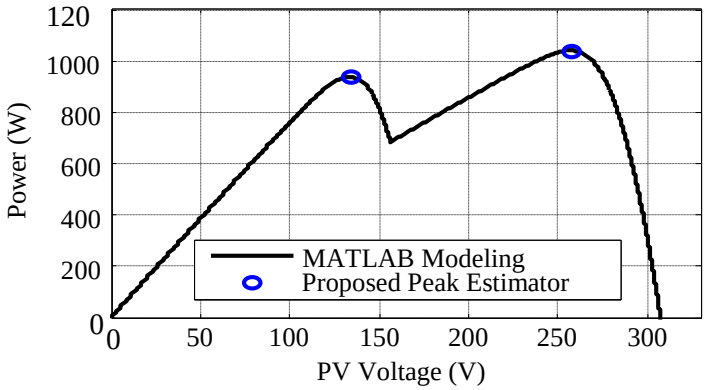

Figure 3-6: The power curve of the system under study and the estimated power peaks using the proposed tool.

Table 3.2: Computational Time Comparison at Different System Sizes

No. of PV Strings	Global Power Peak		Computational Time	
	Current (A)	Power (W)	Circuit Simulation	Proposed Approach
1	1.86	578.23	66 s	0.1970 s
2	3.73	1156.5	09 m: 18 s	0.2120 s
3	5.59	1734.7	28m: 11 s	0.2260 s
4	7.97	2486.4	50 m: 52 s	0.4820 s
5	10.35	3240.8	1 h: 34 m: 11 s	0.5630 s
6	14.13	4128.8	2 h: 27 m: 10 s	0.9230 s
7	17.90	5094.	3 h: 29 m: 40 s	1.5220 s
8	21.66	6086	4 h: 55 m: 05 s	1.8410 s
9	25.41	7087	6 h: 42 m: 33 s	2.0850 s
10	29.24	8138.9	8 h :44 m:14 s	2.2570 s

approach does not increase significantly with the increase of system size, unlike circuit simulation. This shows a clear advantage for the proposed modelling approach over the existing approach, particularly when modelling large PV systems.

The system under study is composed of a 10×10 PV array with an irradiance and temperature profile shown in Figure 3-7. Each PV module is of the type Mono Crystalline JAM5(l)-72-155 and consists of 72 PV cells and 3 bypass diodes. First, the left-most PV string is only considered for modeling. The modeling is then repeated for two and three PV strings until reaching all ten PV strings. The resulting global power peaks, using the proposed modeling approach and the needed computational times, are recorded in Table 3.2. The peaks are also compared to those that result from circuit simulation. It is worth mentioning that each group of PV cells receiving the same irradiance is simulated using a separate circuit PV model, and that all models are then connected in series and parallel to form the system under study.

3.4. Comparison with the Empirical Approaches

A method to model the power peaks of partially shaded PV systems using empirical equations is available in the literature [59, 60]. It estimates the current, voltage and power of the possible peaks in partially shaded PV systems with simplified empirical expressions. This section compares this method with the proposed approach in this chapter. The system under study is composed of 10×10 PV modules operating under the shading scenario depicted in Figure 3-7. The entire power curve of the system is

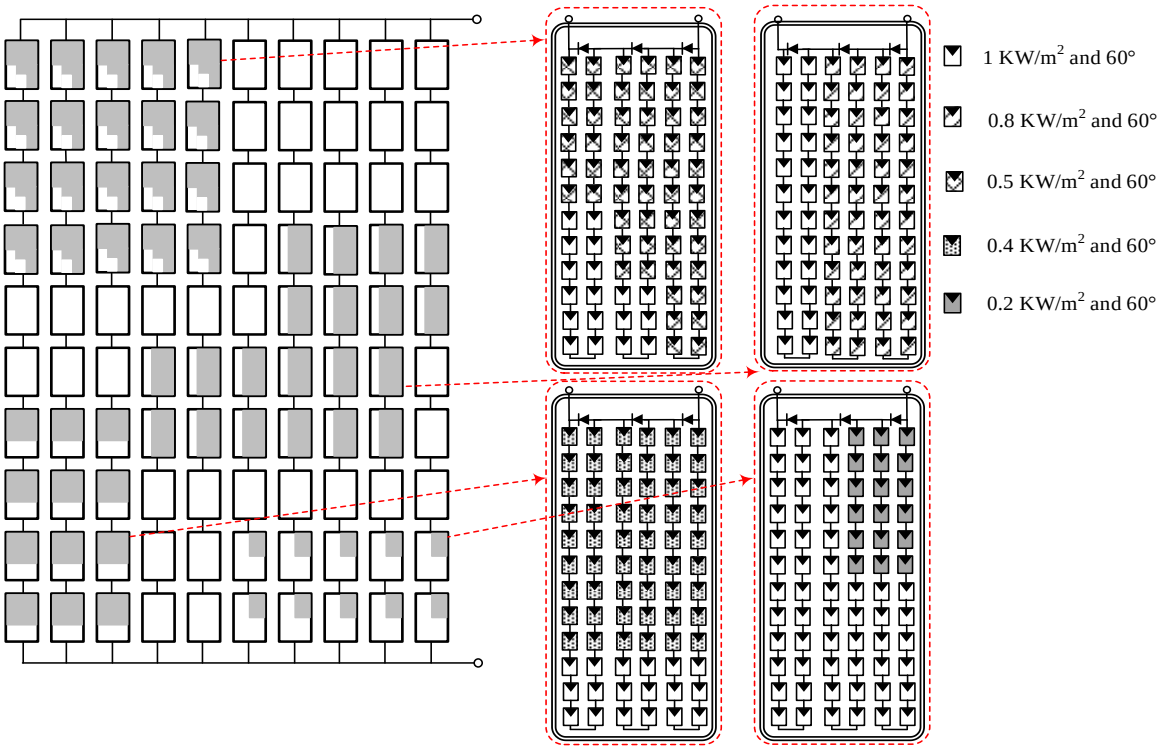

Figure 3-7: A 10×10 partially shaded PV system.

simulated first using circuit simulation. The resulting peaks are used as a benchmark to evaluate the accuracy of the proposed and empirical peak estimators. The discrete voltage step used in the simulation is 0.1 *V*, and the time needed to simulate the system is 880 s.

Although there are several empirical approaches available in the literature [59, 60], the method proposed in [60] is selected for comparison because it is the latest method and has the best reported accuracy among the available methods. Table 3.3 compares the accuracy and the computational time of the proposed and the empirical power peak estimators. As can be seen, the computational time in the simplified empirical method is smaller than that of the proposed method. However, the accuracy of the empirical approach is poor and might not be accepted, as the error can exceed 15%. In contrast, the proposed approach can produce highly accurate results.

Another disadvantage of the empirical method is that it assumes that the PV cells connected with bypass diodes receive the same atmospheric conditions. It cannot be used when the PV cells connected with bypass diodes work at dissimilar conditions. Other disadvantage is that the method finds a large number of possible power peaks, not only the true power peaks. More specifically, the method produced

Table 3.3: Comparison between the Proposed and Simplified Empirical Peak Estimators

	Proposed Peak Estimator			Empirical Peak Estimator in [60]		
Power Peaks	1st	2nd	3rd	1st	2nd	3rd
Voltage Error %	0.15	0.22	0.11	16.87	9.93	10.7
Power Error %	0.04	0.05	0.03	10.5	11.38	15.6
Comp. Time		0.991 s			9 ms	

more than twelve possible power peaks, whereas there are only three power peaks in the system shown in Figure 3-8. It then becomes the user's responsibility to choose the true power peaks among the possible peaks, which can be an impossible task if the user has not previously obtained the power curve.

3.5. Case Study: Developing a Model-based Maximum Power Point Tracker

This section utilizes the proposed modeling approach, successfully evaluated in the previous section, to develop a model-based maximum power point tracker (MPPT) for partially shaded PV systems. Similar to model-based MPPT methods available in the literature for homogeneous PV systems, the proposed method starts with obtaining the irradiance and temperature received by a PV system. The irradiance and temperature can be either measured using irradiance and temperature sensors or indirectly using current and voltage sensors. The irradiance and temperature data are then fed to the proposed modeling approach proposed in this chapter to determine the current (or voltage) that delivers the global maximum power of the PV system. Once this is determined, it is used as a reference for the power converter connected to the PV system to extract its maximum power.

To test the effectiveness of the developed model-based MPPT in tracking the maximum power of partially shaded PV systems, a partially shaded PV system composed of 2×2 PV array, shown in Figure 3-9, is simulated in Simulink. The proposed model-based MPPT method is implemented in the PV system for maximum power point tracking. The PV module used in the system is of the type mono-crystalline JAM5(l)-72-155.

First, the system operates on the shading scenario appearing in Figure 3-9(a) for 10 sec. Then, the system operates on the shading scenario of Figure 3-9(b) for 10 sec. Finally, it operates back again on the first shading scenario for another 10 sec. The power-voltage curves of the systems under the two different shading scenarios are shown in Figure 3-10.

The extracted power of the system is depicted in Figure 3-10 and compared to the extracted power when the Perturb and Observe (P&O) method is implemented instead of the proposed approach. As can be seen in the figure, the proposed algorithm guarantees tracking the global maximum power point,

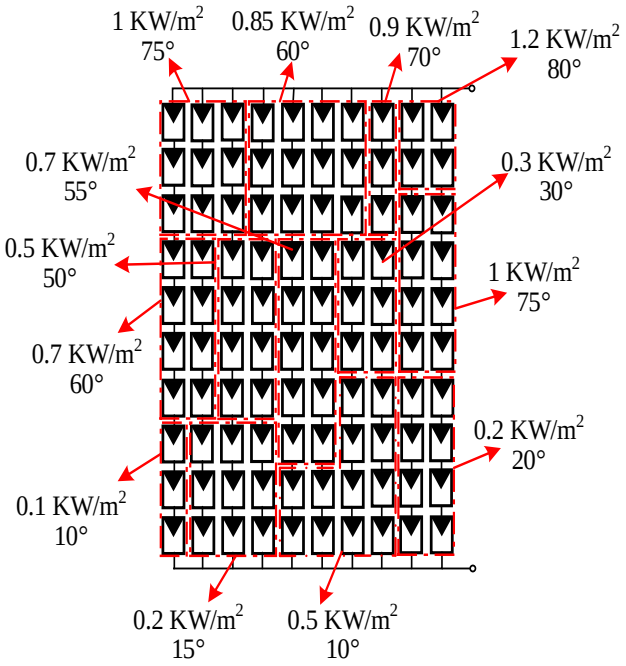

Figure 3-8: A partially shaded photovoltaic system.

thereby avoiding being trapped in a local peak, as occurs in the P&O method. This means no misleading-power losses results when using the proposed model-based MPPT method.

In addition to the verification conducted using the circuit simulation, the effectiveness of the proposed method is validated in real-time using OPAL-RT real-time simulator (RTS). The system shown in Figure 3-9 is used again for verification in real-time simulation. The first scenario is applied for 10 s. The second scenario is then applied for another 10 s before operating the system again for 10 s on the first scenario. The scaled voltage and power waveforms are shown in Figure 3-12(a) and Figure 3-12(b), respectively. As can be seen, the voltage at maximum power in the first and second scenarios is around 27 V and 62 V, respectively. This complies with the information revealed in Figure 3-10. Moreover, the power generated in the first and second scenarios complies with the information revealed in Figure 3-10 and Figure 3-11.

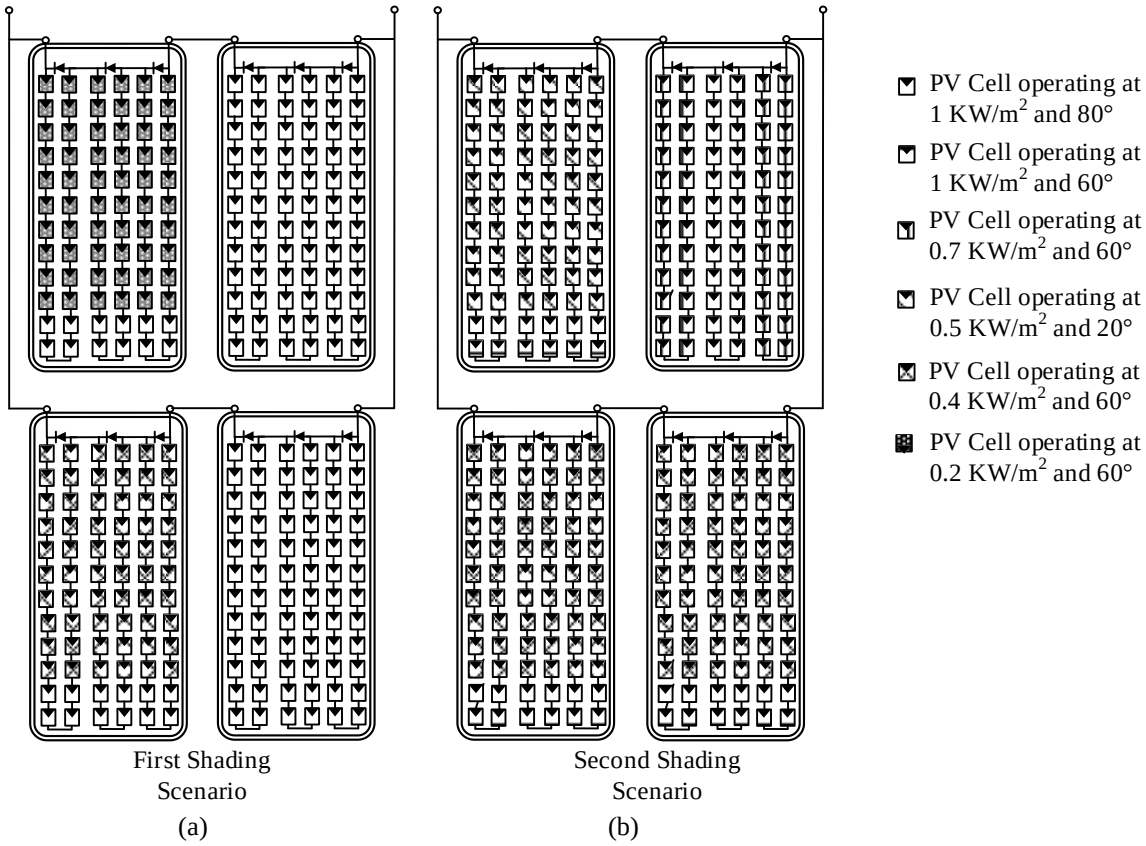

Figure 3-9: Partially shaded PV system under different shading scenarios.

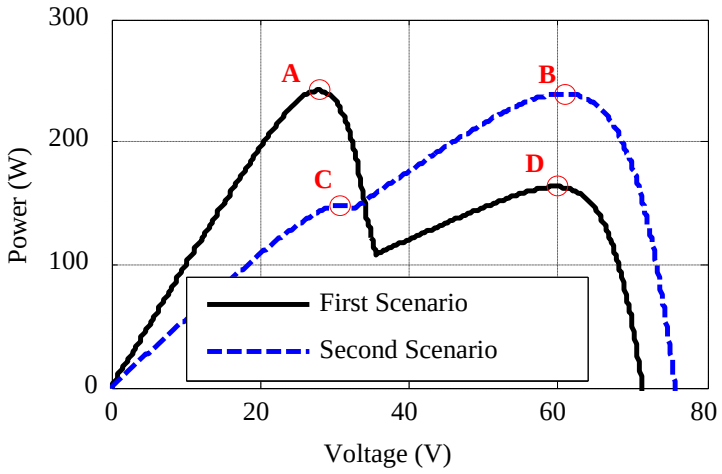

Figure 3-10: The power curves of the PV systems shown in Figure 3-9.

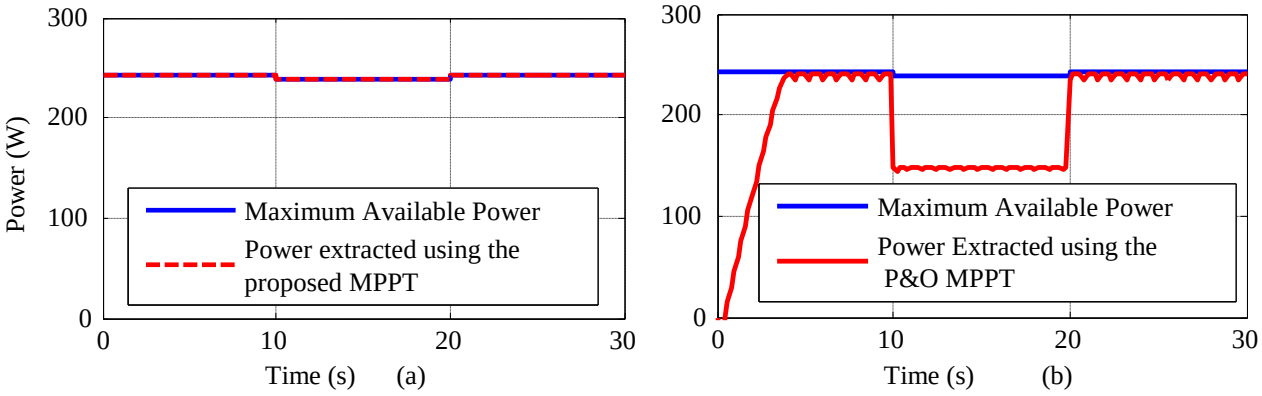

Figure 3-11: The extracted power using (a) the proposed MPPT and (b) P&O MPPT.

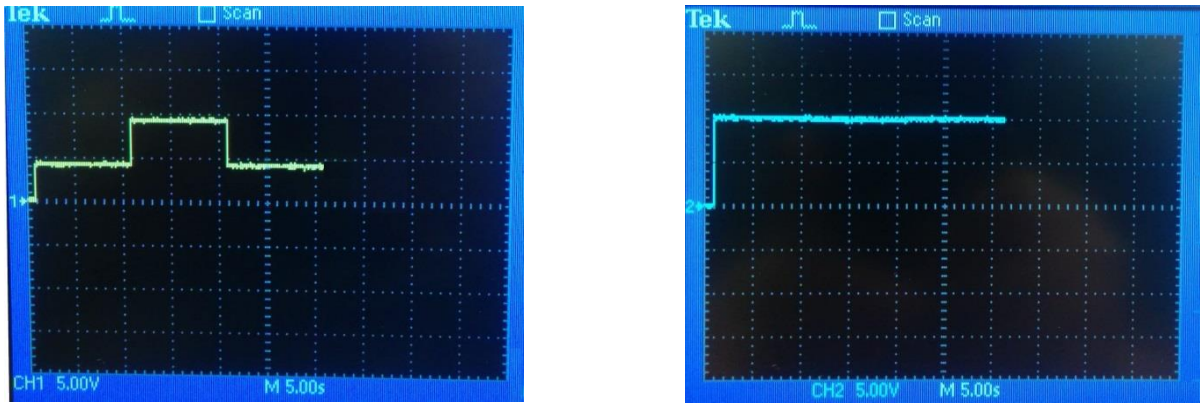

(a) (b)

Figure 3-12: The resulted waveforms of the real time simulation (a) voltage (with scaling factor= 7) waveform and (b) power (with scaling factor=25) waveform.

3.6. Discussion

This chapter proposed a fast modeling tool for partially shaded PV systems. The proposed approach utilizes three developed rules governing the formation of power peaks in partially shaded PV systems to determine their power peaks without simulating the entire power curve and thus saves significant computational time. The effectiveness of the proposed modeling approach to find the power peaks quickly and accurately was verified using MATLAB simulation.

The proposed modeling approach was also utilized in this chapter to build, for the first time, model-based MPPT for partially shaded PV systems. The developed MPPT enhances the dynamic performance compared to the existing heuristic MPPT techniques. Moreover, the developed approach guarantees the tracking of the global maximum power without getting trapped in a local power point and thus decreases

the misleading power losses. The effectiveness of the developed MPPT was verified using MATLAB and real time simulation.

One disadvantage of the proposed model-based MPPT in this chapter is the needed irradiance measurement for each PV cell in the PV system. This means that hundreds of current and voltage sensors are required for each PV module which impedes the practicality of the method. Moreover, as the modeling accuracy is deteriorated with aging of PV modules, the accuracy of the tracking of the proposed model-based MPPT would be affected. These two challenges will be addressed in the next chapter using an introduced interdisciplinary solution to support the practicality of the proposed model-based MPPT.

Chapter 4 A NOVEL MPPT TECHNIQUE BASED ON AN IMAGE OF PV MODULES

Tracking the GMPP in partially shaded PV systems is usually challenging as mentioned earlier in Chapter 1 because the conventional MPPT algorithms (such as P&O, hill climbing, incremental conductance and fuzzy logic…etc.) can get trapped in a local power peak and thus miss the true GMPP [61]. Therefore, numerous MPPT techniques have been developed in the literature for tracking GMPP of partially shaded PV modules. In [62], a short circuit pulse based MPPT is proposed but requires measuring the short circuit current of the PV system periodically. A similar method, but based on open circuit voltage measurement, is available in [63]. Both methods cause momentary power losses due to the periodic disconnection of the PV system for short circuit current and open circuit voltage measurements [61].

The line search algorithm with Fibonacci sequence, presented in [64], uses the Fibonacci sequence to track the GMPP under partially shaded conditions. It is similar to the conventional well-known Hill climbing method except that the perturbation in this method is adaptive and determined by the Fibonacci sequence. The major drawback of this method is the possibility of missing the GMPP under some shading conditions [19, 65].

The load-line MPPT approach proposed in [66] uses the computed load line to find the vicinity of the GMPP. However, the GMPP cannot be obtained if the GMPP lies on the left side of the load line [19]. In [67], an instantaneous operating power optimization approach is proposed. It relies on the linear relationships between the max current and max power as well as the max current and short circuit current to estimate the GMPP. However, all the voltage factors of all the maxim power peaks (MPPs) have to be previously known which means that the method is system dependent and can only be used for specific shading patterns [19].

A new observation about the shape of power-voltage curves of partially shaded PV systems is utilized to build an effective and fast MPPT method in [68]. The observation states that the power peaks in the left and right sides of the GMPP decreases in a descending manner. However, the comprehensive study in [69] demonstrated that this observation is not correct for all shading scenarios and therefore the method cannot guarantee finding the GMPP.

The Dividing Rectangles Technique proposed in [70] employs a Lipschitz condition and advanced mathematical tools to track the GMPP. However, if the initial point in the algorithm is not chosen properly, the controller may get trapped in a local power point [61]. Another method is proposed in [16]

which relies on a constant power operation to track the GMPP. Unlike the majority of the methods which track the power peak by incrementing or decrementing the current or voltage, this method directly increments power using a constant power electronic converter. The deficiency of this method is the slow tracking due to the small power perturbation that is required to detect small power differences between power peaks [71].

Biological optimization algorithms such as Artificial Bee Colony [18] and particle swarm [19, 72, 73] have been extensively utilized for maximum point tracking. They are probably the most effective methods available so far in the literature for tracking the GMPP. However, these methods suffer from slow settling time due to the need to scan the power curve [18, 65]. Moreover, they rely heavily on the preciseness of a few parameters [74] and cause oscillations in output power before reaching GMPP [18, 54].

In addition to the highlighted drawbacks in the aforementioned techniques, the majority require a periodic scanning of the power curve. Unfortunately, this has several drawbacks [71]. It causes a reduction in the extracted power because it forces the PV system to operate on non-maximum power points. Also, it disturbs the tracking during normal operation (homogeneous conditions) of the system causing further power losses. Moreover, it does not guarantee the GMPP operation when the shading pattern is changing rapidly.

A relatively different solution is developed in [75] in which a thermal camera is employed to find the GMPP. The thermal camera provides the temperatures of the PV cells, and then empirical approximations are used to locate the GMPP. However, the method could suffer from poor accuracy due to the approximations used. Moreover, the expensive cost of thermal cameras hinders the practical implementation of the method.

The previous chapter proposed a promising model-based MPPT that has the ability to find the GMPP without the need for scanning the power curve. However, it was indicated that the method is unsuitable for practical implementation due to the excessive number of the required irradiance sensors, and the impreciseness in the used PV model. This chapter introduces an interdisciplinary solution to solve these challenges. The first challenge is addressed innovatively by relying on an image of PV module, obtained by an optical camera, to estimate the irradiances instead of using irradiance sensors. The second challenge is resolved by merging the well-known iterative P&O MPPT with the proposed model-based MPPT to correct any inaccuracy in the determined GMPP resulted from the model`s impreciseness.

The chapter starts by presenting the proposed method which estimates the irradiances from a captured image. Then, it adjusts the estimated irradiances to the elevation and azimuth angles of the

lighting source. Finally, a developed prototype is used to experimentally validate the proposed MPPT under various shading scenarios.

4.1. Proposed Irradiance Estimation Method

In the proposed irradiance estimation approach, a camera periodically takes images of the PV module's surface as shown in Figure 4-1. The captured images are processed to extract the incident irradiances on the cells of the PV module. This requires a knowledge of two relations as shown in Figure 4-2: first, the camera's response function which is the relation between the reflected radiance in the direction of the camera and the intensity of the corresponding image, and second, the reflectance of the PV cell which is the relation between the incident radiance on a PV cell and the reflected radiance in the direction of the camera. A pre-knowledge of these two relations is required to estimate the incident irradiance on a PV cell from its captured image. The following describes the pre-characterization of both relations.

4.1.1. Camera's Response Function

Detectors found in optical cameras consist of an array of rectangular grid of photo-sensors sensitive to light. Each photo-sensor is a small rectangular box that converts light into voltage. Any digital image is represented by a matrix of numbers, called pixels, representing the intensity of light received by the corresponded photosensitive sensors. A digital image $M(x, y)$ denotes the image intensity at pixel (x, y) and encodes the intensity recorded by the photo-sensors of the array contributing to that pixel. $M(x, y)$ is a bit in the range [0-255] (typically, 0 is black and 255 is white) [76].

The relation between the received intensity of light at a photo-sensor (x, y) and the corresponding intensity of a pixel $M(x, y)$ is not a linear relationship. There is usually nonlinear mapping called camera response function that determines how radiance in the scene becomes pixel values in the image.

In the literature, there are many methods to determine the response function of a camera. An effective method is presented in [77] to recover a response function using a set of images taken for the same scene at different exposure durations. The exposure duration is the time during which the aperture of the camera opens while capturing an image.

The algorithm in [77] is based on utilizing a property of imaging systems known as reciprocity. It states that only the term $G\times\Delta t$, where G is the irradiance and Δt is the exposure duration, is important where halving G and doubling Δt will not change the intensity of a pixel Z. The input to the algorithm is a number of photographs taken of the same scene at different exposure durations. A set of equations can be written by applying the reciprocity property for all pixels as the following: $Z=f(\Delta t\times G)$ where f is the

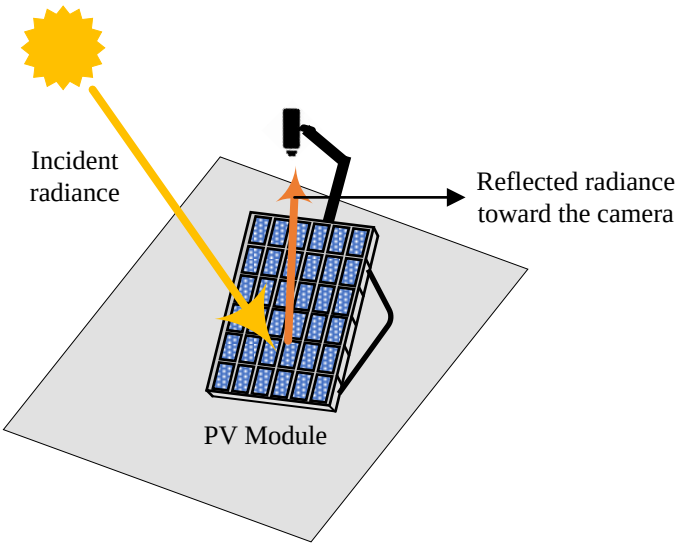

Figure 4-1: The proposed system for estimating the incident irradiance.

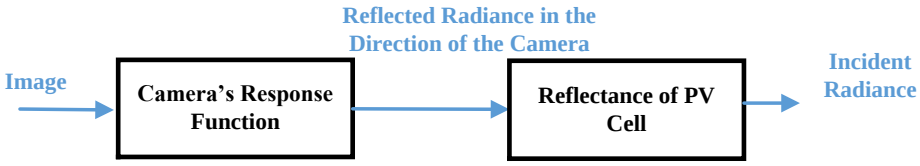

Figure 4-2: Flowchart for the proposed irradiance estimation method.

response function. The unknowns (f and G) can be found by solving the written equations in a least squares error minimization.

Using the described algorithm, the response function of a Canon Power Shot A620, which is the camera used in this research, is estimated. Four images for an arbitrary scene are captured at different exposure durations as shown in Figure 4-3. They are inputted to the coded algorithm to estimate the response function. The resulting response function is depicted in Figure 4-4. As seen, the response function contains a mapping for all pixel values from 0 to 255 to a corresponded irradiance. It is important to note that the corresponding irradiance, y-axis in Figure 4-4, is determined up to an unknown scale factor F. However, this will not pose a problem as will be shown later.

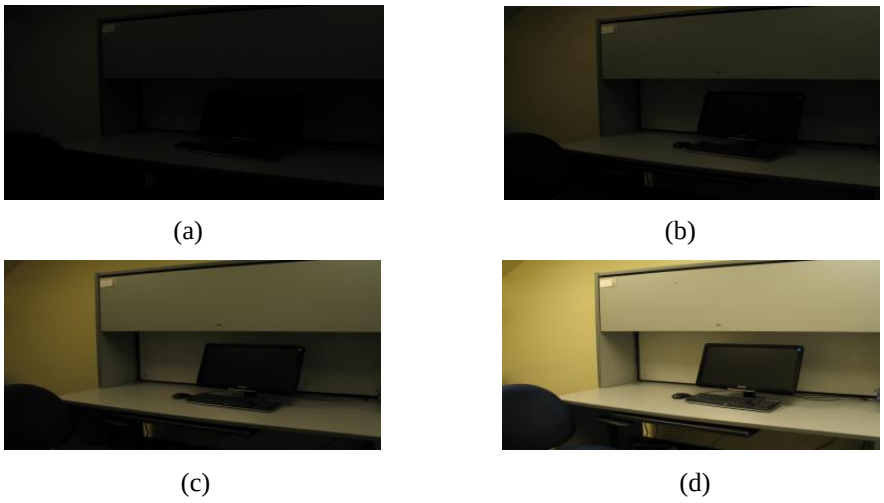

Figure 4-3: Four images taken by Canon Power Shot A620 at different exposure durations.

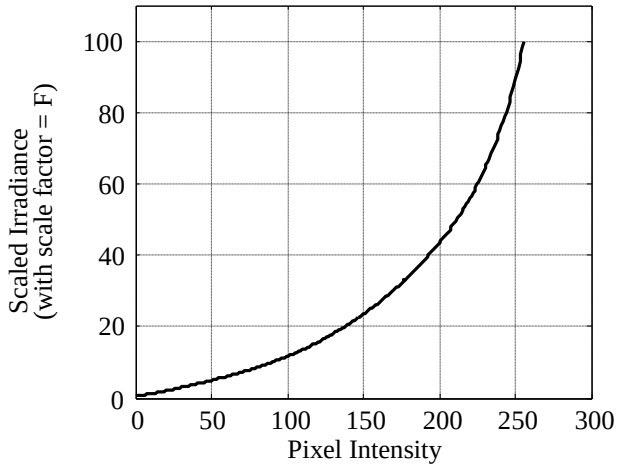

Figure 4-4: The response function for Canon Power Shot A620

4.1.2. Reflectance of PV Cell

The reflectance of a PV cell refers to how much of the incident radiance is reflected in the direction of the camera. It is the ratio between the reflected radiance in the direction of the camera and the incident radiance on the PV cell. It is entirely a surface property and is not dependent on the incident light.

Measuring the reflectance of a PV cell requires capturing an image of the cell at a known level of incident irradiance. The ratio between the reflected irradiance in the direction of the camera, which is the outcome of processing the captured image through the camera's response function (refer to Figure 4-2) and the known incident irradiance is the reflectance of the PV cell.

First, a monocrystalline PV cell is captured by a Canon Power Shot A620 camera under a known level of irradiance (462 W/m^2). The captured image is mapped through the response function shown in Figure 4-4. The ratio between the resulting array of numbers to the known irradiance is depicted in Figure 4-5 which is the reflectance of the PV cell. Because the used response function is scaled to a factor *F*, the resulting reflectance is also scaled to the same factor. The two high reflectivity lines in the reflectance map represent the two metallic current collecting grids in PV cells.

4.1.3. Experimental Verification

Once both the camera response function and the reflectance of the PV cell are extracted, they are used to estimate the incident irradiances on the PV cell from its captured images. In this section, the captured images of the PV cell are at six different levels of irradiances as depicted in Figure 4-6. Each captured image is used with the two extracted relations, in the previous section, to find the incident irradiance.

The images are first mapped through the camera response function shown in Figure 4-4 and then the mean of the resulting array, which represents the radiance reflected to the camera, is divided by the mean of the reflectance array shown in Figure 4-5 to find the incident irradiance of the PV cell. Because both the irradiance reflected to the camera and the reflectance is scaled to the same factor *F*, the division will cancel the unknown *F* factor. Table 4.1 summarizes the estimated irradiance levels using the proposed approach and compares them to the measured irradiances. The absolute deviation between the estimated and measured irradiances is shown also in the Table. It can be seen that the error is acceptable, revealing an effective and accurate estimation. It is also important to mention that the parameters of the used camera such as the aperture and exposure duration require fine tuning one time at the installation of the system. The tuning can be roughly conducted such that the captured images at fully illuminated and shaded conditions are not too bright or too dark. This is to ensure that the data in the captured images are not distorted.

4.2. Adjustment to Lighting Source Angles

In this section, it is shown that the reflectance of PV cells changes with variation in lighting source angles both elevation and azimuth angles. Because sun location in the sky changes during the day, it is important to investigate the effect of the sun angles on the proposed irradiance estimation method. A geniophotometer, shown in Figure 4-7, is used for this purpose which is a device used to allow

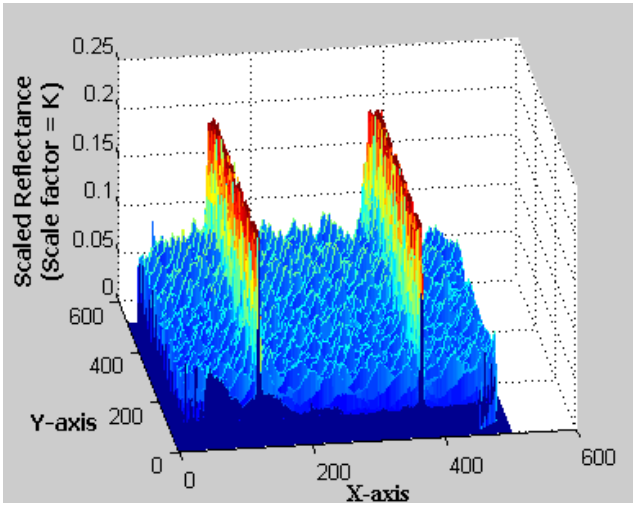

Figure 4-5: The reflectance map of a mono-crystalline PV cell.

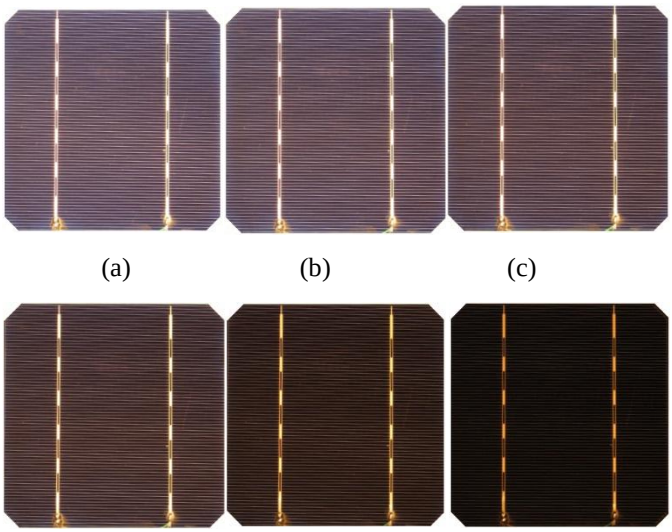

(a) (b) (c)

(d) (e) (f)

Figure 4-6: Images of the PV cell under various irradiance levels.

positioning the lighting source at various angles in the semi-sphere surrounding the PV cell. The azimuth angle of the lighting source is varied from 0° to 180° with a step of 10°, and at each step the elevation angle is also varied between 0° and180° covering all the possible angles in the semi-sphere above the solar cell. At each angle, an image is captured, the irradiance is measured and the mean reflectance is calculated. Figure 4-8 plots the resulting reflectance values versus the elevation angles at different azimuth angles. Furthermore, the reflectance for the complete range of angles is plotted in 3d as shown in Figure 4-9. The data in the figure can be saved in a look-up table to be used for irradiance estimation

Table 4.1: Comparison between the Measured and Estimated Irradiances of the PV Cells shown in Figure 4-6

Image #	Measured (W/m^2)	Estimated (W/m^2)	Absolute Error
(a)	410	423.8	13.8
(b)	368	387.2	19.2
(c)	310	339.4	29.4
(d)	230	256.2	26.2
(e)	134	165.6	31.6
(f)	63	83.2	20.2

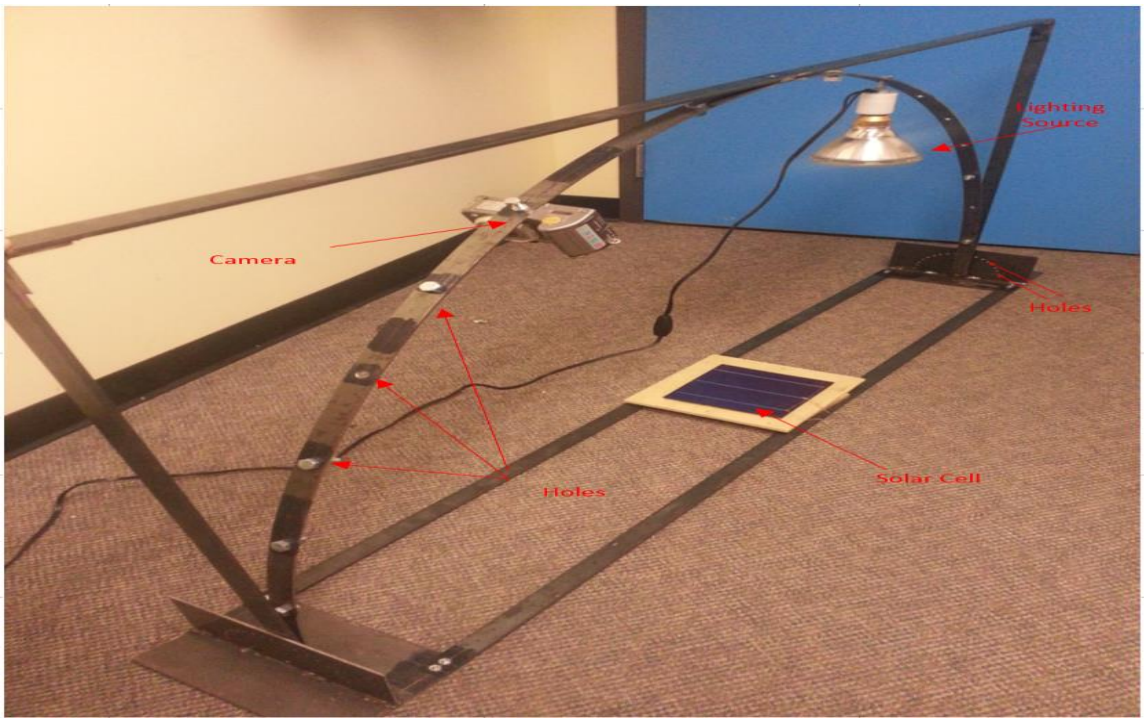

Figure 4-7: The geniophotometer constructed by the author.

at different lighting source angles. The sun elevation and azimuth angles at any time of the day and at any day of the year can be calculated via the equations provided in [78, 79]. Once the angles are obtained, they are used to find the mean reflectance of the PV cell using Figure 4-9 and then the irradiance is estimated as described in the previous section.

To experimentally test the effectiveness of the proposed irradiance estimation method at different angles, the experiment conducted in the previous section is repeated outdoor at different times of the day.

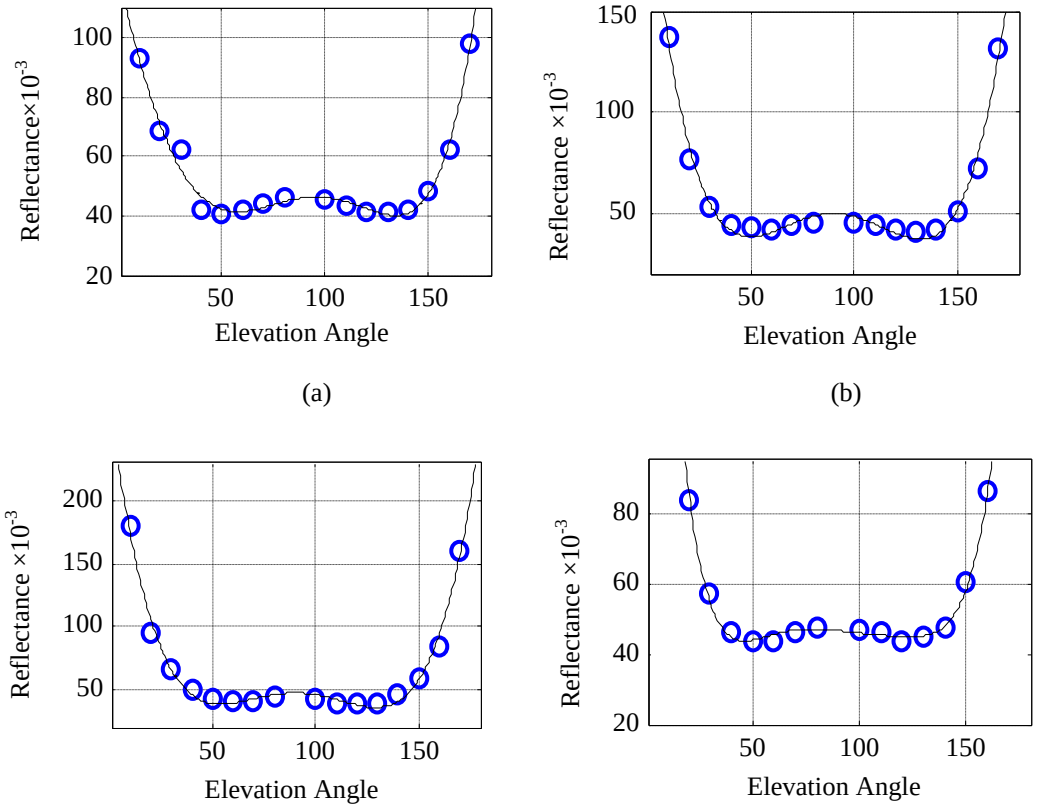

Figure 4-8: The variation of reflectance versus the elevations angles at different azimuth angles: (a) 0°, (b) 40°, (c) 90° and (d) 140°.

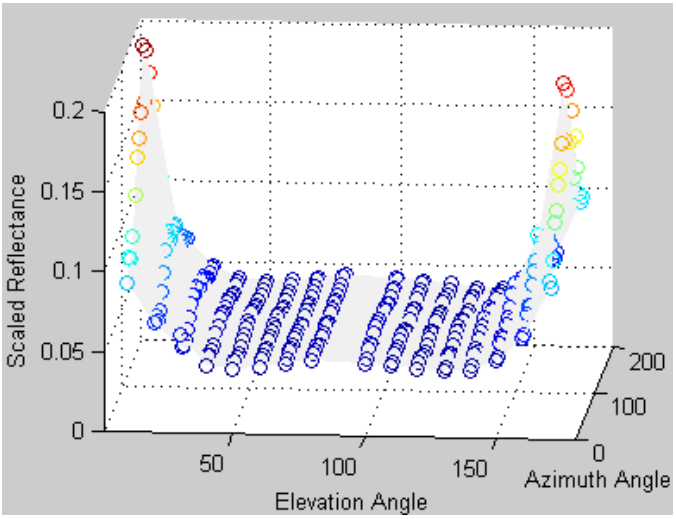

Figure 4-9: The reflectance at various elevation and azimuth angles.

Ten images were captured at different irradiance levels at different times. Then, the irradiances were estimated from the captured images considering the different angles of the sun at time the image was captured. The resulting estimated irradiances were compared to the measured irradiances in
Table **4.2**. The sun angles for the image are also provided in the table. As seen, the table reveals a good accuracy for the proposed method.

4.3. Temperature Estimation

The presented model-based MPPT requires the irradiances and temperatures of the PV cells. The estimation of the irradiances is already discussed in the previous section. The temperatures can be determined from the estimated irradiances through the thermal model of PV modules presented in [80]. The difference between the atmospheric and PV cell temperatures is directly related to the irradiance G received by the PV cell as in the following where K_e is a constant determined empirically:

$$\Delta T = K_e \times G \tag{4-1}$$

Based on this relation, knowing the temperature of a reference cell will be sufficient to estimate the temperatures of the remaining cells. This means that measuring the temperature of one PV cell in the PV module can determine the temperatures of the rest. This is represented in the following equation where T_{co} and G_{co} are the temperature and irradiance of the reference PV cell.

$$T = T_{co} + K_e \times (G - G_{co}) \tag{4-2}$$

4.4. Experimental Prototype

A method for estimating the irradiances from a captured image of the PV module as well as its temperatures was already presented. Although its accuracy was already experimentally verified, the overall model-based MPPT method combining the irradiance estimation method and the power-peaks estimator is not yet validated. This section aims to validate the proposed method including irradiance estimation, temperature estimation and power-peaks estimator. A prototype composed of eight PV cells, connected with two bypass diodes, and a camera is developed to test the effectiveness of the proposed technique experimentally under two different shading patterns as shown in Figure 4-10. The electrical characteristics of the entire PV module are as follows: the short circuit current I_{sc}= 2.95 A, the operating current I_m= 2.73 A, the open circuit voltage V_{oc}=4.96 and the operating voltage V_m = 4 V.

Table 4.2: Comparison between the Measured and Estimated irradiances under Various Sun's Angles

Measured (W/m^2)	Elevation Angle	Azimuth Angle	Estimated (W/m^2)	Absolute Error
675.3	40.20	10.9	683.7	8.4
701.4	39.60	9.5	705	3.6
536	25.20	15.0	516.9	19.0
217.2	23.60	17.0	255.9	39.0
448	22.70	18.0	410.7	37.0
369.5	21.90	19.0	350.9	19.0
232	21.00	20.0	258.2	26.0
289.2	21.00	20.0	280	9.2
213.3	13.20	28.4	160.0	53.3
84.7	13.20	28.4	100.4	15.7

First, the captured images were mapped through the camera response function, shown in Figure 4-4, to find the irradiance reflected in the direction of the camera. Then, the reflectance of the PV cells, presented in Figure 4-9, was used to estimate the incident irradiances on the different solar cells of the prototype. After estimating the irradiances, the temperature of the solar cells were determined using (4-2). Then, the power-peaks estimator was used to find the GMPP. The resulting GMPPs were plotted in Figure 4-11 along with the measured power curves. The measured GMPPs are 3.27 V and 1.01 V in the first and second scenarios respectively, while the estimated GMPPs are 3.6V and 0.83V. As noticed, the estimated GMPPs lie in the measured GMPP vicinity and very close to the exact GMPP. The small error can be attributed to the impreciseness of the PV model and irradiance estimation. However, it can be safely compensated by the P&O MPPT merged with the proposed model-based MPPT. The time needed for the proposed MPPT to find the GMPP, including the time of the image processing as well as the time of the peak estimator equals to 0.1 s. This means that the proposed method can effectively operate under fast-changing environmental conditions.

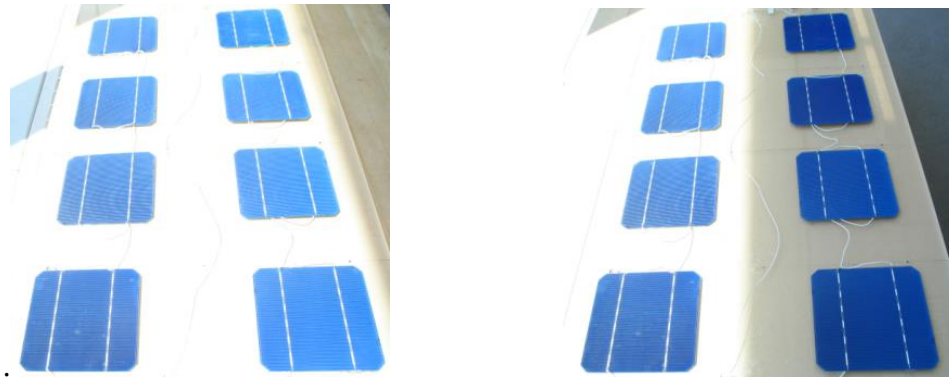

(a) (b)

Figure 4-10: Solar PV array test platform under: (a) unshaded and (b) partially shaded conditions.

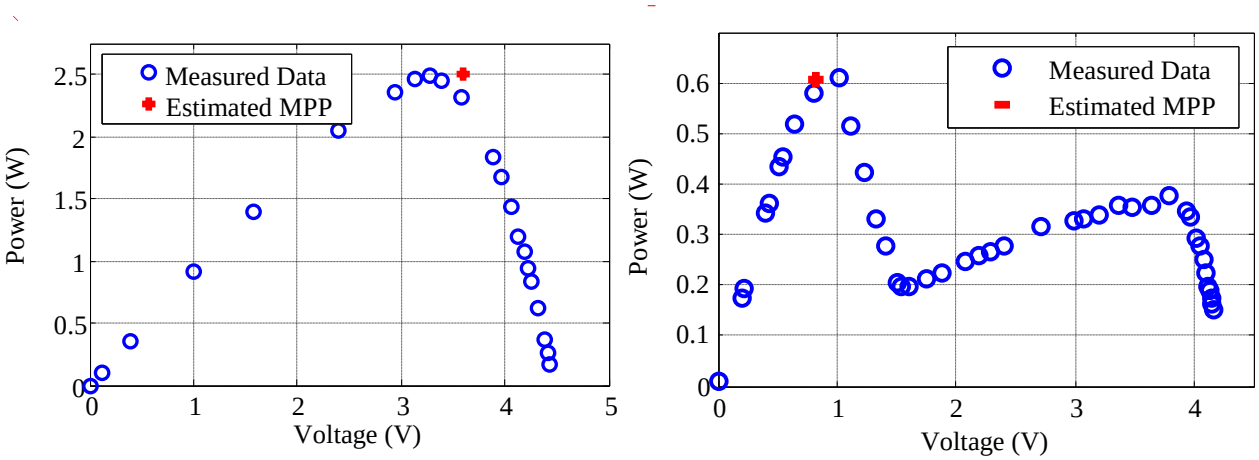

(a) (b)

Figure 4-11: Measured PV curves and estimated GMPP in both shading scenarios.

4.5. Economic Feasibility of the Proposed Method

Although it was mentioned that a camera would be needed for each micro inverter in the proposed method, it has not yet been discussed whether this arrangement is economically feasible. In this section, the cost of energy savings gained by using the proposed method is quantified and compared to the cost of the camera and other hardware requirements.

It might be useful here to review the two sources of power losses in optimization-based MPPT methods, as these are eliminated in the proposed method. The first is the power loss during the periodic scanning time in which the PV module is forced to work on non-maximum power points. The second

occurs when shading scenario changes between two successive scans. In this case, the PV module will be working on the previous GMPP, not the true GMPP, until the next scan. This means the PV module will not generate its maximum power after the change in shading scenario until the subsequent scan. These two sources of power losses are eliminated in the proposed method, as it does not require a heuristic scanning and can find the GMPP analytically after changes in the shading scenario.

The energy losses due to these two sources in the optimization based methods will now be quantified and their cost will be compared to that of the camera. The P-V curve of the PV module used in the comparison under a random shading scenario is plotted in Figure 4-2. In the comparison, it is supposed that the periodic scanning in the optimization-based methods occurs every 15 minutes for 2-second durations (typically used assumptions in the available methods). It is assumed that there would be an abrupt irradiance change every one hour throughout a day having 10 hours of illumination. An abrupt change in the irradiance is also expected to occur approximately in the midst of two successive curve scans (after 5 minutes of the scanning). Therefore, the system would work on the local point for the rest ten minutes until the next scanning every time the system experience abrupt change in the irradiance.

The losses during the scanning time can be calculated by multiplying the scanning duration (2 sec) by the number of scans in a day (40 scans) and fifty percent of the GMPP (165 W), assuming that the scanning causes a 50% power loss. This results in 1.83 W.h. of energy per day. Similarly, the power losses occurring between the successive scans due to the changes in shading scenarios can be calculated by multiplying the difference between the GMPP power (105 W) and the local peak power (19 W) by the number of times a change in shading scenario occurs in a day (10 times) and its duration (10 min), which is equal to 143.3 W.h. per day. The price of this energy is $34 per year, calculating the Canadian feed in tariff at 0.642 $/KWh.

In addition to the needed camera in the proposed approach, it requires a camera interfacing hardware, mounting arrangement and a temperature sensor. The average cost of the DSP camera module, which consists of a camera and an interfacing hardware to the DSP, is 25$. Mounting hardware for a camera could be less than 10$. Temperature sensors are available with less than 5$. This means that the added hardware costs approximately 40$. Adding 10% additional cost for any extra hardware results in a total cost of 44$. Considering this cost and the cost of energy savings, the payback period for the required hardware of the proposed method is less than a year and a half.

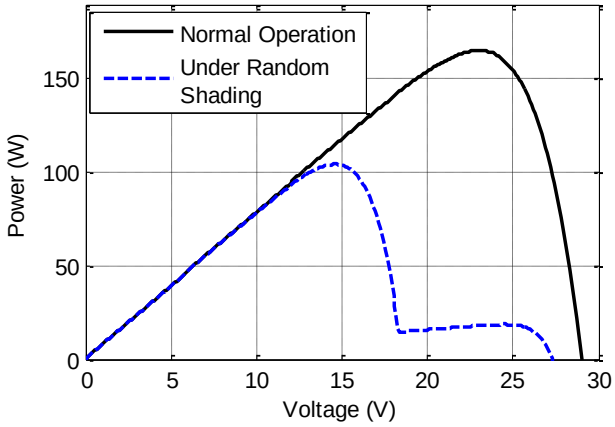

Figure 4-12: Power-voltage curves of a PV module under normal operating and random shading conditions.

4.6. Discussion

This chapter proposes a practical model-based MPPT method that is able to track the GMPP of partially shaded PV systems without the need for periodic curve scanning. The proposed method utilizes the images captured by an optical camera to estimate the incident irradiances, and then uses the estimated irradiances to find the GMPP analytically via the power-peak estimator, which is developed using the mathematical model of PV modules in the previous chapter. The proposed MPPT is also combined with the P&O MPPT to correct any inaccuracy in the determined GMPP which can exist due to any imprecision in the irradiance estimation or the model.

The proposed irradiance estimation method utilizes two relations, which must be pre-characterized, to determine the incident irradiances: the camera response function and the solar cell reflectance. These two relations are first determined in this chapter for the camera and solar cell, and then utilized to find the incident irradiances. A Geniophotometer was built by the author to find the reflectance variations at various sun angles. The effectiveness of the overall proposed irradiance estimation method is experimentally verified. Further experimental validation was also carried out to verify the effectiveness of the whole model-based MPPT method under various shading scenarios.

The proposed MPPT is the first model-based MPPT method developed for partially shaded PV systems. The existing methods are heuristic and require scanning the power curve to find the GMPP which causes power losses. The proposed method analytically determines the GMPP and thus removes the required curve scanning. Therefore, it can uniquely eliminate the first form of power losses in

partially shaded PV systems: misleading-power losses. The second form of power losses in partially shaded PV systems, termed as mismatch power losses, will be covered in the next chapter.

Chapter 5 ENHANCED RECONFIGURATION METHOD FOR MINIMIZING MISMATCH POWER LOSSES

In addition to power losses caused by mistracking the GMPP, partially shaded PV systems experience another form of power losses due to power mismatch occurring between their series-connected PV modules as illustrated in the first chapter. PV array reconfiguration has been reported as an effective solution for minimizing these losses. As shown in Figure 5-1, the PV system is divided into two groups: fixed and reconfigurable. Each PV module in the reconfigurable group is connected to all rows of the fixed group through switches and is continuously relocated during the operation of the system [21]. First, the irradiance of each PV module is estimated, and then the modules are relocated to satisfy the irradiance equalization principle which states that mismatch power losses are minimized when the summations of irradiances in all the PV rows are approximately equal [81]. This ensures that the MPP currents for all rows are almost equal and thus minimizes the mismatch power losses.

While all available reconfiguration methods follow this general irradiance equalization principle, the methods differ in how the principle is applied. The simplest PV reconfiguration technique for minimizing partial shading losses is presented in [82]. The reconfigurable PV module that receives the highest illumination is connected to the fixed PV row that receives the lowest illumination, and this is repeated until all the reconfigurable PV modules are connected to the fixed PV rows. Although simple, this is a slow method, as it requires measurements and processing after connecting each PV module. In other words, the reconfigurable PV modules are not connected simultaneously to the fixed rows.

In [81], the sums of irradiances in the PV rows are calculated in all the possible configurations, and then the configuration producing the best equalization is selected. Because of the massive number of possible configurations that exist in a PV system, this method becomes impractical for large PV systems due to the excessive computational time required.

An optimization-based PV reconfiguration method is also proposed in [21]. Choosing the best configuration is treated as a quadratic programming problem that is solved by using the branch and bound algorithm. In this approach, the goal is to find the configuration that minimizes the difference between the irradiance summations of the PV rows. This method, however, is impractical for large PV systems due to the long time delay needed to solve the optimization problem, as will be shown in this chapter.

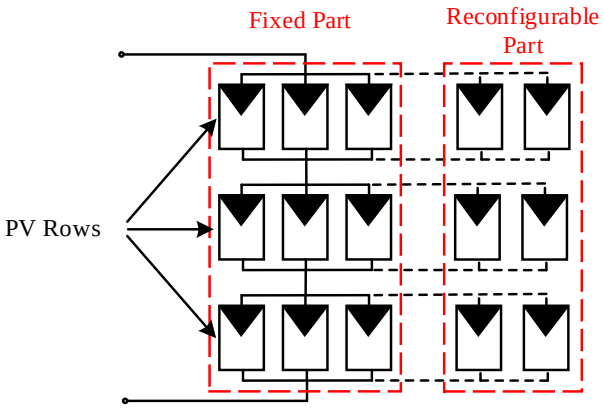

Figure 5-1: A PV system composed of fixed and reconfigurable parts.

In the reconfiguration method proposed in [83], a simple and fast algorithm that is able to find the best configuration in reduced time was developed. However, this method does not always guarantee finding the best configuration and might result in a PV configuration that is not optimal, thus impeding the exploitation of the maximum available power.

To summarize, the existing available PV reconfiguration methods either have impractically large time delay requirements or are unable to guarantee minimizing the mismatch losses. To resolve these challenges, this chapter proposes a new reconfiguration method which features a simple algorithm that can quickly find the best configuration, minimizing the power losses, in a fast computational time.

An overview of the reconfiguration method adopted in this work is first presented, followed by a description of the proposed reconfiguration algorithm. Then, a comprehensive comparison is carried out using MATLAB to validate the effectiveness of the method over existing methods under various shading scenarios. A case study of a large PV system is conducted to show the improvement in energy due to the reduced time delay of the proposed method.

5.1. PV Reconfiguration Review

As mentioned, a PV system is divided into two parts: fixed and reconfigurable. Each PV module in the reconfigurable part is connected to all the PV rows of the fixed part through switches, where only one switch among the switches connected to a PV module is turned on at the same time. The number of switches needed for a PV system is composed of n_f number of fixed modules, n_r number of reconfigurable modules, and r number of rows equal to n_r of double-poles r-throws switches. It is worth mentioning that decreasing the number of reconfigurable PV modules has the advantage of reducing the

number of required switches. However, it also causes a reduction in the available power in some shading scenarios.

The reconfigurable PV modules are connected to the fixed rows to fulfil the irradiance equalization principle, which is to reconfigure the PV panels such that the sums of irradiances in all the PV rows are equal. This is illustrated in Figure 5-2, which shows a PV system consisting of nine reconfigurable PV modules and zero fixed PV modules, before and after reconfiguration. As can be seen, the summations of irradiances in all the rows after reconfiguring the system are equal. While it is not always possible to find a configuration which results in exactly equal summations of irradiances, the goal remains to minimize the difference between the summations in irradiances.

To illustrate how reconfiguring PV modules could increase the extracted energy of a PV system, the PV curves for both scenarios shown in Figure 5-2 are plotted in Figure 5-3. As can be seen, the GMPP for the same system changes with reconfiguration. An increase from 480 W to 600 W is achieved in this example, as illustrated in the figure. It is important to note that while reconfiguration mitigates the majority of mismatch power losses, it does not completely eliminate them. The mismatch still exists in the parallel-connected PV modules, although it disappears in series-connected PV modules. This is the reason for the appearance of a small power peak in the power curve of the system after configuration, as shown in Figure 5-3.

5.2. Proposed Reconfiguration Algorithm

This section presents the proposed algorithm that finds the PV configuration that minimizes mismatch power losses. The proposed algorithm is based on the irradiance equalization principle, which is similar to the available algorithms in the literature, but is distinguished by its simplicity and reduced time delay.

The flowchart of the proposed algorithm is depicted in Figure 5-4. To find the new PV configuration, the following steps are required:

1- Calculate the row irradiances, which are the summations of the irradiances received by the PV modules of each row.
2- Identify the two rows that have the highest and lowest row irradiances.
3- Replace, one by one, all the PV modules in the row receiving the lowest irradiance with the PV modules in the row receiving the highest irradiance.

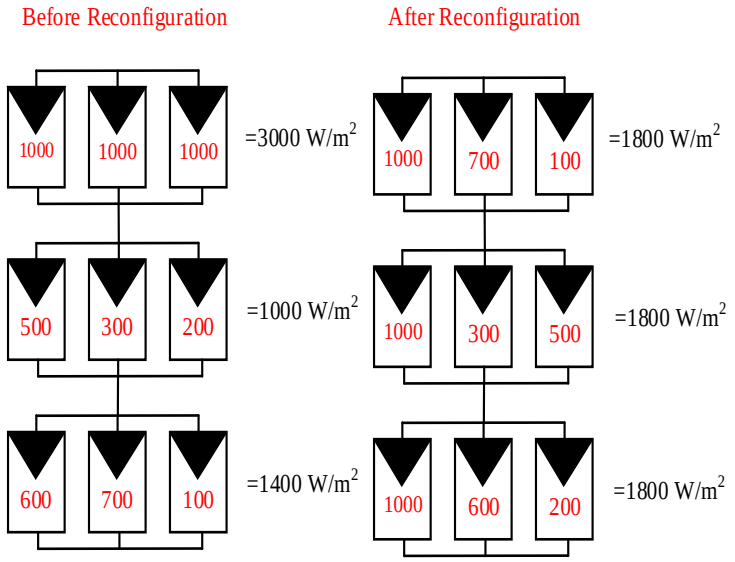

Figure 5-2: An example of a PV system before and after reconfiguration.

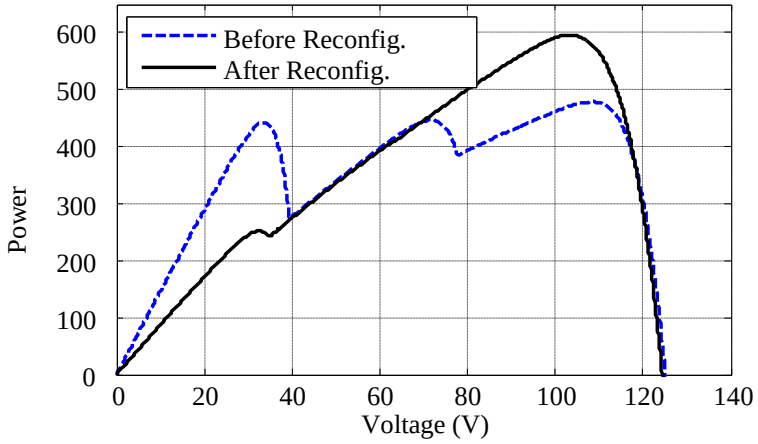

Figure 5-3: The power curves of the PV system before and after reconfiguration.

4- At each replacement, the new row irradiances for both rows will be calculated and the replacement will be approved if the lowest row irradiance of both rows after the replacement exceeds the lowest row irradiance before the replacement.

5- If a replacement is approved, steps 3 and 4 will be repeated by identifying the new rows receiving the lowest and highest row irradiances.

6- Otherwise, none of the replacements will be approved, and step 4 will be repeated between the PV row receiving the lowest row irradiance and the PV row receiving the second-highest (then third-highest, fourth-highest, etc.) row irradiance.

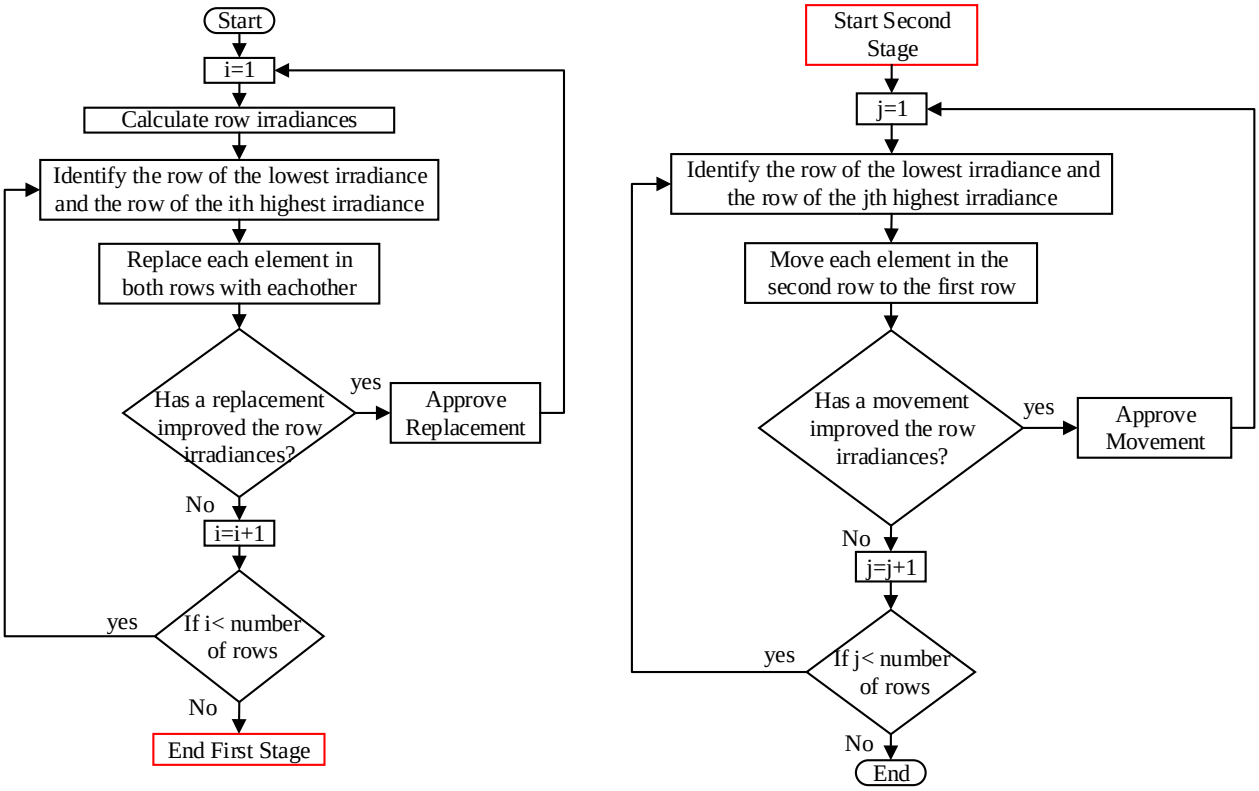

Figure 5-4: Flowchart illustrating the proposed algorithm.

7- If any replacement is approved, the process will be repeated from the beginning between the rows of highest and lowest row irradiances.

After this procedure is conducted for all the PV rows, a new configuration that fulfills the irradiance equalization principle will result. However, the new configuration will have the same reconfigurable PV modules in all the PV rows. This means that there could be more replacements that result in better configurations if the number of reconfigurable PV modules in the rows was allowed to be different. To further reconfigure the PV system to result in a better configuration that is not constrained by the number of PV modules in the rows, the algorithm will proceed as follows:

8- Move all the PV modules in the PV row that has the highest row irradiance to the PV row that has the lowest row irradiance, one by one.

9- If moving a PV module results in an improvement in the row irradiances, then the movement is approved, and this process will be repeated for the new PV rows that have the highest and lowest irradiances.

10- However, if no movements were approved, then this process will be repeated between the PV rows receiving the lowest row irradiance and second-highest (third-highest, fourth-highest, etc.) row irradiance.

The algorithm will be better understood by applying it to the partially shaded PV system shown in Figure 5-5. The system is composed of 9 fixed PV modules and 9 reconfigurable PV modules. The incident irradiance on each PV module is indicated inside each module. As can be seen, the row irradiances (4700 W/m^2, 3200 W/m^2, and 2600 W/m^2) are not equal and there is a significant difference between them. The goal of applying the proposed algorithm is to reconfigure the reconfigurable PV modules in Figure 5-5 to result in equal row irradiances.

The proposed algorithm starts by identifying the two rows that give in the highest and lowest row irradiances, which are the first and third rows (4700 W/m^2 and 2600 W/m^2), respectively. Then each PV module in the row receiving the lowest irradiance (2600 W/m^2) will be replaced with each PV module in the row receiving the highest irradiance (4700 W/m^2). This will replace the PV module receiving 100 W/m^2 with the PV module receiving 1000 W/m^2, as shown in the first table of Figure 5-6. This replacement will be approved because the lowest row irradiance (3500 W/m^2) after the replacement, shown in the second table in Figure 5-6, is higher than the lowest row irradiance (2600 W/m^2) before the replacement, as shown in the first table. Because the replacement is approved, this process will be repeated and the new PV rows receiving the lowest and highest row irradiances will be identified, which are 3800 W/m^2 and 3200 W/m^2, respectively, as seen in the second table in the figure. Then, the PV module (200 W/m^2) in the second row will be replaced by the PV module (100 W/m^2) in the first row.

This replacement will not be approved, however, as it will not result in better row irradiances. The same result also occurs when replacing the PV module (100 W/m^2) with the PV module (800 W/m^2). In contrast, replacing the PV module (200 W/m^2) with the PV module (700 W/m^2) will be approved because the lowest row irradiance (3300 W/m^2) after the replacement, shown in the third table, is higher than the lowest row irradiance (2300 W/m^2) before the replacement, shown in the second table.

The process will be repeated and the PV rows receiving the lowest and highest row irradiances, which are (3300 W/m^2 and 3700 W/m^2), respectively, as shown in the third table, will be identified. The PV module (200 W/m^2) will then be replaced with the PV module (100 W/m^2), as shown in the third table. Since the replacement results in row irradiances (3400 W/m^2 and 3600 W/m^2) shown in the fourth table are higher than the lowest row irradiance prior to the replacement (3300 W/m^2), the replacement will be approved. The process will be repeated for all the PV modules in the first row in the fourth table

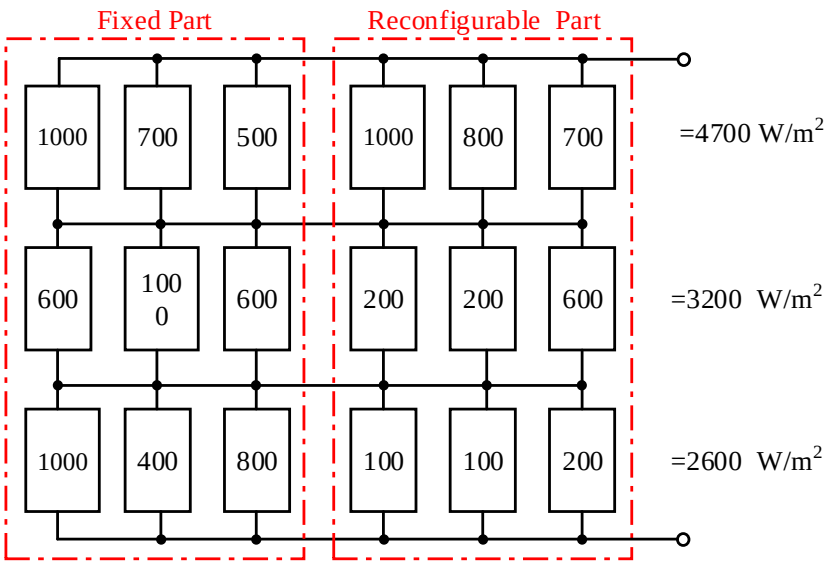

Figure 5-5: The partially shaded PV system under study.

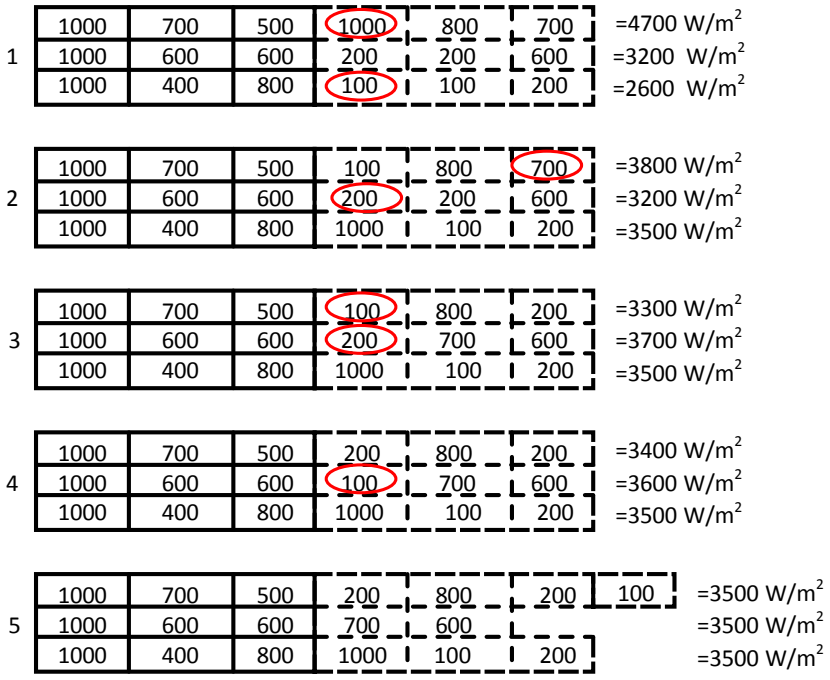

Figure 5-6: A step-by-step illustration on how the PV system shown in Figure 5-6 is reconfigured using the proposed algorithm.

with all the modules of the second and third PV rows. However, no replacement will be approved. This means that no further improvement is possible.

At this point, the second part of the algorithm will start. All the PV modules of the second row in the fourth table (which receives the highest row irradiance) will be added to the first row (which receives the lowest row irradiance). As illustrated, moving the PV modules (700 W/m^2 and 600 W/m^2) results in no improvement, but the PV module (100 W/m^2) will be moved, as it improves the situation. As seen in the fifth table, all the row irradiances are equal, which means the irradiance equalization principle is satisfied. This second part of the algorithm removes the constraint that the number of PV modules in all rows must be equal. This allows for a better configuration to appear and it does not have a negative impact on the system.

5.3. Test and Validation

5.3.1. Accuracy Verification

This section verifies the effectiveness of the proposed reconfiguration algorithm using MATLAB simulation. The PV system under study is a 6×6 PV array consisting of two fixed and four reconfigurable PV columns, as shown in Figure 5-7(a). The first two columns of the PV modules, which are indicated by the solid line, are fixed and the rest of PV modules, which are indicated by the dashed lines, are reconfigurable. The test is conducted under two different shading scenarios.

The first shading scenario is shown in Figure 5-7 (a). As can be seen, the minimum row irradiance is 800 W/m^2 while the maximum is 4000 W/m^2, which indicates a sizeable variation between them. This means that mismatch power losses exist in this system. To reduce these losses, the proposed algorithm, described in Figure 5-4, is applied to reconfigure the system. The resulting configuration is depicted in Figure 5-7 (b). As shown, the row irradiances in the new configuration are equal, which means that the mismatch power losses are minimized. The power curves for this PV system before and after reconfiguration are plotted in Figure 5-8. It can be seen that the available maximum power for the system after reconfiguration (1950 W) is higher than the power prior to reconfiguration (1750 W). This is due to reducing the mismatch power losses.

The simulation is also repeated for a second shading scenario shown in Figure 5-9(a). As can be seen, there is a large variation in the row irradiances from 1700 W/m^2 to 6000 W/m^2, which indicates the existence of high mismatch power losses in the system. After applying the proposed algorithm, the system is reconfigured, as shown in Figure 5-9(b). Although it is not possible in this shading scenario to equate all the row irradiances, the proposed algorithm found a better configuration that reduced

1000	1000	1000	100	100	400	=3600 W/m^2
500	400	100	500	500	800	=2800 W/m^2
100	1000	1000	100	600	300	=3100 W/m^2
100	100	200	100	100	200	=800 W/m^2
200	300	700	500	600	800	=3100 W/m^2
1000	1000	300	200	600	900	=4000 W/m^2

(a)

1000	1000	300	100	100	400		=2900 W/m^2
500	400	700	500	800			=2900 W/m^2
100	1000	1000	100	600	100		=2900 W/m^2
100	100	1000	900	600	200		=2900 W/m^2
200	300	500	500	600	800		=2900 W/m^2
1000	1000	100	200	200	300	100	=2900 W/m^2

(b)

Figure 5-7: The PV system under first shading scenario a) before reconfiguration and b) after reconfiguration.

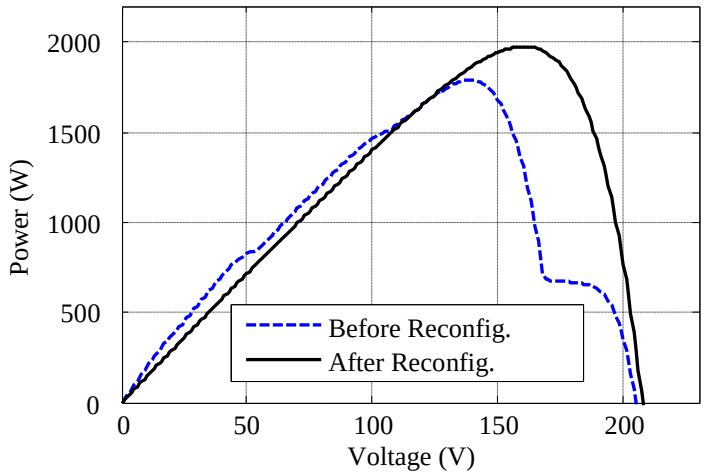

Figure 5-8: The power curves for the PV system under first shading scenario before and after reconfiguration.

the differences between the row irradiances. This means that the mismatch power losses are minimized after reconfiguration. The power curves for the system before and after reconfiguration are plotted in Figure 5-10. The available power increases from 1700 W to 2550 W after reconfiguration due to reducing the mismatch power losses.

1000	1000	1000	1000	1000	1000	=6000 W/m^2
500	500	600	650	800	1000	=4050 W/m^2
500	500	900	100	100	900	=3000 W/m^2
1000	1000	650	750	850	100	=4350 W/m^2
200	200	500	450	500	800	=2650 W/m^2
200	150	100	150	100	1000	=1700 W/m^2

(a)

1000	1000	100	600	900			=3600 W/m^2
500	500	450	650	650	800	100	=3650 W/m^2
500	500	1000	750	900			=3650 W/m^2
1000	1000	100	500	850	100		=3550 W/m^2
200	200	1000	1000	500	800		=3700 W/m^2
200	150	1000	1000	150	1000	100	=3600 W/m^2

(b)

Figure 5-9: The PV system under second shading scenario a) before reconfiguration and b) after reconfiguration.

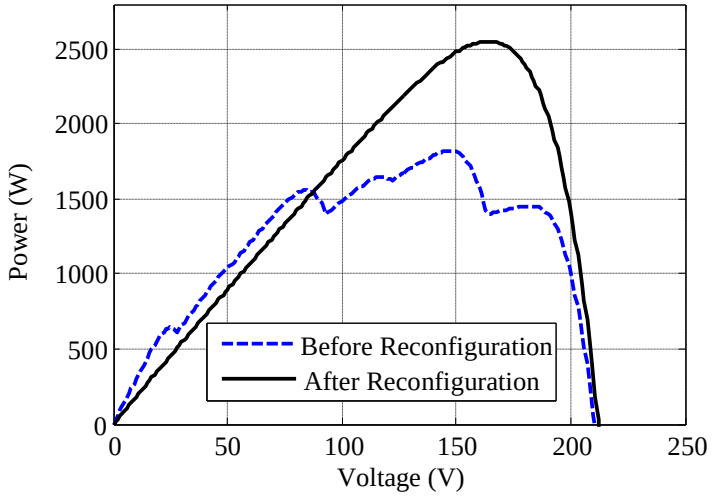

Figure 5-10 The power curves for the PV system under second shading scenario before and after reconfiguration.

5.3.2. Comparison with Existing Methods

As mentioned in the introduction, the available PV reconfiguration methods in the literature either have high accuracy but long time delay (such as the method presented in [21]), or they have negligible time delay but do not lead to large reduction in mismatch power losses (such as the method proposed in [83]). In this section, it is shown that the proposed method combines both advantages – high accuracy and negligible time delay– in the available techniques.

First, the accuracy of the reconfiguration methods in [21] and [83] will be compared with that of the proposed method. These two methods are used as a benchmark for the comparison because they are the newest and most effective methods presented in the literature. Next, the computational time needed to find the optimal configuration in the existing and proposed methods will be evaluated. The method proposed in [82] is not included in the comparison because it is an older approach that requires the PV modules to be physically connected and disconnected during the search for the best configuration.

The PV system used in this comparison is shown in Figure 5-11(a). The PV configurations that resulted after applying the reconfiguration methods in [21] and [83] are shown in Figure 5-11(b) and Figure 5-11(c), respectively. The PV configuration that resulted after applying the proposed reconfiguration method is shown in Figure 5-11(d).

As can be seen, while there is still a variation in the row irradiances after applying the method in [83], the row irradiances are equal after applying the proposed method and the one in [21]. This indicates that the power mismatch losses of the method in [21] and in the proposed method are lower than that of the method in [83]. The power curves for the system before and after reconfiguration of both the existing methods and the proposed method are depicted in Figure 5-12. It is clear that the proposed method is able to generate maximum power similar to the method in [21]. However, the method in [83] is unable to generate this maximum power due to inaccurate reconfiguration, as was discussed in the introduction.

The computational time required to find the best configuration in the proposed and existing methods is also compared and summarized in Table 5.1. As shown, the time delay in the proposed method is very short and may even be negligible, similar to the method in [83]. However, the time delay in [21] is longer, as was discussed in the introduction.

5.4. Case Study: Large PV System

The main feature of the proposed reconfiguration method presented in this chapter is the reduced time delay compared to other methods in the literature. Although this feature was already tested and verified in the previous section, its advantages and impact on the efficiency of PV systems have not been yet presented. In this section, a large PV system is tested under both the proposed method (fast reconfiguration) and the method in [21] (slow reconfiguration), and the energy generated in both cases is compared. This will show how the reduction in time delay affects the generated energy of partially shaded PV systems.

The chosen PV system is composed of 600 PV modules comprised of 30 rows and 20 columns; of these, ten columns are fixed and ten columns are reconfigurable. A shadow of a moving cloud above the

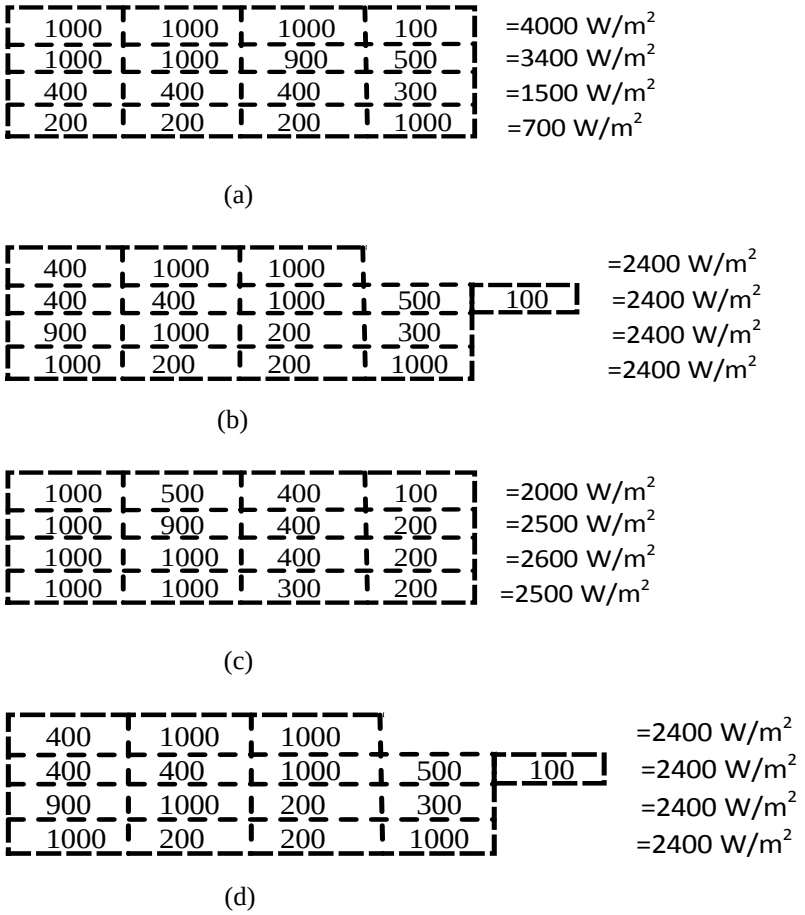

Figure 5-11: A PV system under a random shading a) before reconfiguration, b) after the reconfiguration presented in [21], b) after the reconfiguration presented in [83] and d) after the proposed reconfiguration.

PV system is simulated, as shown in Figure 5-13. First, the shadow will shade the first PV row, and then it will continue moving to shade the adjacent rows, where it can shade six adjacent PV rows at once.

Ideally, the reconfiguration would occur instantaneously, and there would be no time delay between the moment when a shadow covers a PV row and the moment the PV system operates on the new configuration. Under such conditions, a PV system always works on the best configuration because the reconfiguration occurs faster than the change in the shading scenario. However, in reality, there is a time delay, which is the computational time of the reconfiguration method. As was shown in the previous section, the time delay for the proposed and existing methods are 0.01 s and 76 s, respectively. Assuming that the cloud shadowing will move from one module to another in 3 seconds, the shadow will move

Table 5.1: Comparison between the Proposed and Existing Methods

Methods	Improvement in Power %	Computational time (s)
The method in [21]	41.8	76
The method in [83]	32.4	0.001
The Proposed method	41.8	0.01

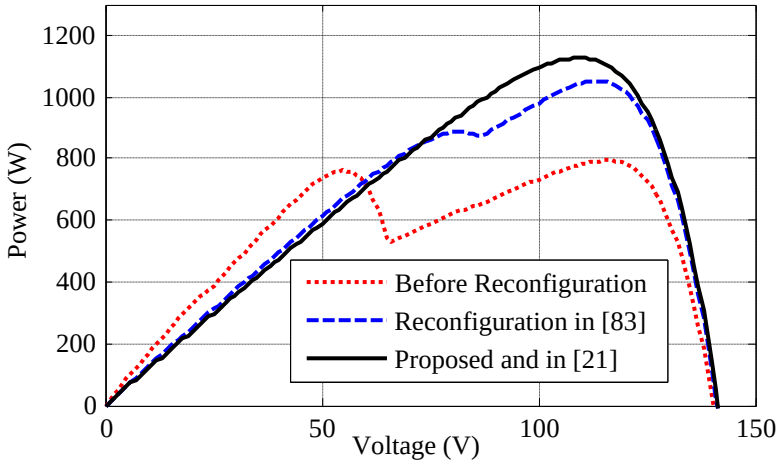

Figure 5-12: The power curves for the PV system after reconfiguration using both the proposed and existing reconfiguration.

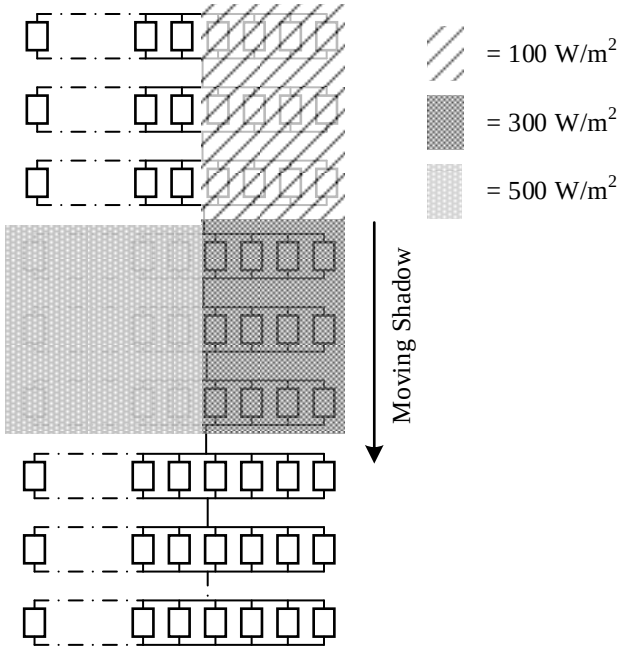

Figure 5-13: The large PV system under study under a moving shadow.

from the first row to the last row in less than the time needed for the reconfiguration method in [21]. This means that the system will not be able to operate at the established configuration during the shade movement, which would affect the harvested energy.

On the other hand, in the proposed method, the PV system will be able to operate on its optimal configurations during the shade movement from one row to another. However, the small time delay of this method also causes energy losses. The energy losses in both methods are quantified and summarized in Table 5.2. As can be seen, while the energy losses in the existing reconfiguration reach 8.55%, they do not exceed 0.3% in the proposed method, which reveals the superiority of this method.

The aforementioned analysis was also repeated for the two cases when the ratio between fixed and reconfigurable PV modules is 5-15 and 15-5, respectively, instead of 10-10 for the same system. The results are summarized in Table 5.3 and Table 5.4, respectively. As noted, the improvement in efficiency achieved by using the proposed reconfiguration is nearly the same in all cases. Furthermore, it is clear that the harvested energy is improved with increases in the number of reconfigurable PV modules, although the increase is negligible for this type of shading scenario.

5.5. Discussion

The existing PV reconfiguration methods either have high accuracy but suffer from long time delay, or they have negligible time delay but do not result in large reduction in the mismatch power losses. This chapter proposed a new PV reconfiguration that combines both advantages of the available methods: finding a better configuration in a negligible time delay.

The effectiveness of the proposed method was validated using MATLAB. The method was tested under different shading scenarios and showed its effectiveness in finding a better configuration. The proposed method was also compared with existing configuration methods in terms of time delay and accuracy. It was shown that the proposed method has high accuracy and low computational time. Finally, a case study conducted on a large PV system revealed that the proposed method's negligible time delay reduces mismatch-power losses and thus increases the efficiency of partially shaded PV systems.

It is also important to mention that although the proposed method was able to find the same configurations resulted from the optimized based reconfiguration techniques in all the cases covered in this thesis, the proposed method, similar to any heuristic based techniques, may not guarantee finding the optimal configurations under all cases.

After mitigating the two forms of power losses, prevailing in partially shaded PV systems, in this chapter and the previous chapter, the tracking-power losses existing in homogeneous PV systems will be

Table 5.2: Comparison between the Existing and Proposed Methods (10 Fixed and 10 reconfigurable PV modules)

Methods	Harvested Energy (KJ)	Efficiency %
Instantaneous Reconfiguration	5851.87	100
Reconfiguration in [21]	5351.67	91.45
Proposed Reconfiguration	5836.86	99.74

Table 5.3: Comparison between the Existing and Proposed Methods (5 fixed and 15 reconfigurable PV module)

Methods	Harvested Energy (KJ)	Efficiency %
Instantaneous Reconfiguration	5856.884	100
Reconfiguration in [21]	5351.678	91.374
Proposed Reconfiguration	5841.72782	99.74

Table 5.4: Comparison between the Existing and Proposed Methods (15 fixed and 5 reconfigurable PV modules)

Methods	Harvested Energy (KJ)	Efficiency %
Instantaneous Reconfiguration	5850.456	100
Reconfiguration in [21]	5351.678	91.474
Proposed Reconfiguration	5835.49266	99.74

covered in the next chapter. Although the available MPPT methods combining model based and heuristic techniques effectively mitigates tracking power losses, they have not been desirable and utilized due to the required temperature measurement which increases the implementation complexity and cost compared to heuristic techniques. In the next chapter, a new temperature estimator is proposed that is able to estimate the temperature of PV system without the need for temperature measurements, increasing the desirability and practicality of these MPPT methods in comparison to the existing heuristic techniques.

Chapter 6 AN ENHANCED MPPT METHOD COMBINING MODEL-BASED AND HEURISTIC TECHNIQUES

Many MPPT algorithms exist in the literature for homogeneous PV systems. The most commonly used one is the hill climbing technique which keeps altering the duty cycle of the power electronic converters in the direction which results in an increase in the generated power [84, 85]. A similar method is the P&O which works exactly as the hill climbing technique except that the perturbation here is in the voltage instead of the duty cycle [86, 87]. A small step size in both methods reduces the oscillations around the maximum power point but results in slow tracking speed, while a big step size results in fast tracking but with high oscillations [88].

To eliminate the output power oscillations, the incremental conductance MPPT method was proposed [89]. It is based on the fact that the slope of the *P-V* curve is equal to zero at MPP, positive to the left and negative to the right of the MPP point. The max power is then tracked by comparing the incremental conductance $\Delta I/\Delta V$ to the instantaneous conductance I/V. Once the system reaches the MPP, the operation is preserved at the same point without oscillations. Modified incremental conductance MPPT methods have also appeared to improve the tracking accuracy under rapid irradiance variations [74, 90].

Fuzzy logic controller-based MPPT techniques are also available [91]. Compared to the conventional methods, they improve the tracking performance under varying atmospheric conditions. However, many parameters need to be selected based on trial and error and thus it is greatly affected by the knowledge of the user. Neural networks have been also utilized in the MPPT to find the optimum voltage point [92, 93], but they require extensive training and the use of enormous amounts of data at various temperature and irradiance conditions.

Ripple correlation control MPPT exploits the current and voltage ripples inherent in PV systems to extract information about the power gradient in order to evaluate if the PV system operates close to the maximum power point [94, 95]. Extremum seeking control [96, 97] and adaptive extremum seeking control approaches [98] track the MPP by establishing a feedback system that is able to produce an oscillatory behavior around the equilibrium point. Optimization algorithms are also adopted to find the MPP, such as particle swarm optimization [99] and biological swarm chasing algorithm [100].

The aforementioned methods are known as heuristic techniques and their operation can be summarized as: disturbing the PV system, observing the effect and then taking the appropriate action

[101]. The main disadvantage of such techniques is their slow tracking speed and poor performance in the rapidly changing irradiance [102].

Model-based MPPTs have recently appeared in the literature to improve the tracking speed and dynamic performance of the MPPTs [103]. Relying on the mathematical model of the PV system in addition to the temperature and irradiance measurements, the MPP point is analytically determined. The weakness in the model based MPPTs is the need for irradiance and temperature sensors, which increases their implementation cost. The authors in [102] proposed an improved model–based MPPT that does not require an irradiance meter. Their method relies on the PV model inverse as well as the voltage and current measurements to estimate the irradiance received by the PV system mathematically. However, its efficiency is highly affected by the PV model accuracy which is not perfect and decreases with the aging of PV systems. Similar methods are presented in [103-107] in which the PV model is utilized to find the MPP voltage. Unfortunately, they do not perform accurately in case of any mismatch between the real and modeled characteristics of the PV system. To improve the accuracy of the model-based MPPTs while maintaining its high tracking speed, an MPPT method combining both the model-based and heuristic techniques is proposed in [101]. The method merges a heuristic method and the PV mathematical model to obtain accurate and high speed tracking. The disadvantage of this method in comparison to the heuristic techniques is the need for temperature measurement.

This chapter proposes an enhanced combined heuristic and model-based MPPT method which eliminates the need for temperature measurement. The proposed method relies on a new set of derived equations that estimate the temperature utilizing the current and voltage measurements. It combines the well-known P&O and the model-based methods to obtain an accurate and high speed tracking. Furthermore, the proposed MPPT uniquely relies on a recently developed simple non-transcendental PV circuit model, presented in chapter 2, featuring lower computational effort to reduce the computational complexity of the tracking.

In this chapter, the proposed temperature estimator is first derived. Then, it is utilized to build the enhanced MPPT method combining model-based and heuristic techniques. Next, a comprehensive comparison with the available methods is conducted to show the effectiveness of the proposed method. Finally, an experimental setup is built to validate the proposed method.

6.1. Proposed Temperature Estimator

As indicated, the main contribution of this chapter is to eliminate the temperature measurement required in the combined heuristic and model based MPPT methods. This section derives a mathematical

temperature estimator which will be used to replace the temperature measurement. The mathematical estimator is derived relying on the polynomial based PV circuit model presented in chapter 2.

Taking the derivative of both sides of (2.2) with respect to the voltage *V* results in:

$$\frac{dI}{dV} = \frac{-qI_s(\alpha_1 + 2\alpha_2 V + 3\alpha_3 V^2)}{N_s KTA} e^{\frac{q(\alpha_0+\alpha_1 V+\alpha_2 V^2+\alpha_3 V^3)}{N_s KTA}} - \frac{\alpha_1 + 2\alpha_2 V + 3\alpha_3 V^2}{R_{sh}} \tag{6-1}$$

Substituting the saturation current equation (2-15) in (6-1) and manipulating yield:

$$\begin{aligned} &\frac{I_{sc} + C_i\Delta T - (\alpha_o + \alpha_1\overline{V_{oc}} + \alpha_2\overline{V_{oc}}^2 + \alpha_3\overline{V_{oc}}^3)/R_{sh}}{e^{\frac{q(\alpha_o+\alpha_1\overline{V_{oc}}+\alpha_2\overline{V_{oc}}^2+\alpha_3\overline{V_{oc}}^3)}{N_s KTA}}} \times \frac{-q(\alpha_1 + 2\alpha_2 V + 3\alpha_3 V^2)}{N_s KTA} \\ &\times e^{\frac{q(\alpha_0+\alpha_1 V+\alpha_2 V^2+\alpha_3 V^3)}{N_s KTA}} - \frac{\alpha_1 + 2\alpha_2 V + 3\alpha_3 V^2}{R_{sh}} - \frac{dI}{dV} = 0 \end{aligned} \tag{6-2}$$

Equation (4-2) has three unknowns: the temperature *T*, current *I* and voltage *V*. Knowing the current and voltage, which are continuously measured, the temperature of the PV module can be estimated. The term dI/dV appearing in (4-2) can be discretized and represented as $\Delta I/\Delta V$ where ΔV and ΔI are the difference between the present and previous successive voltages and currents. An iterative technique, such as the Newton Raphson method, is needed to solve (4-2). Therefore, the first derivative of (4-2) with respect to the temperature will be required which is represented as follows:

$$\frac{X_3 T - X1}{T^2} \times e^{\frac{X2}{T}} + \left(\frac{X_1}{T}\right) e^{\frac{X_2}{T}} \times \left(\frac{X_4 T - X_2}{T^2}\right) = 0 \tag{6-3}$$

where the variables X_1, X_2, X_3 and X_4 are expressed as follows:

$$\begin{aligned} X_1 = (I_{sc} + C_i\Delta T - (\alpha_o + \alpha_1(V_{oc} - |B|\Delta T) + \alpha_2(V_{oc} - |B|\Delta T)^2 + \alpha_3(V_{oc} - |B|\Delta T)^3)/R_{sh}) \\ \times \frac{-q(\alpha_1 + 2\alpha_2 V + 3\alpha_3 V^2)}{N_s KA} \end{aligned} \tag{6-4}$$

$$\begin{aligned} X_2 = [q(\alpha_1 V + \alpha_2 V^2 + \alpha_3 V^3 - \alpha_1(V_{oc} - |B|\Delta T) - \alpha_2(V_{oc} - |B|\Delta T)^2 \\ - \alpha_3(V_{oc} - |B|\Delta T)^3)]/(N_s KA \end{aligned} \tag{6-5}$$

$$\begin{aligned} X_3 = [C_i - \frac{\alpha_1|B| + 2\alpha_2|B|(V_{oc} - |B|\Delta T) + 3\alpha_3|B|(V_{oc} - |B|\Delta T)^2}{R_{sh}}] \\ \times \frac{q(\alpha_1 + 2\alpha_2 V + 3\alpha_3 V^2)}{N_s KA} \end{aligned} \tag{6-6}$$

$$X_4 = [q(\alpha_1|B| + 2\alpha_2|B|(V_{oc} - |B|\Delta T) + 3\alpha_3|B|(V_{oc} - |B|\Delta T)^2)]/(N_s KA) \tag{6-7}$$

The temperature estimation procedure is summarized in the flowchart of Figure 6-1. It starts by measuring the current and voltage of the PV system, and then substituting the datasheet information (I_{sc},

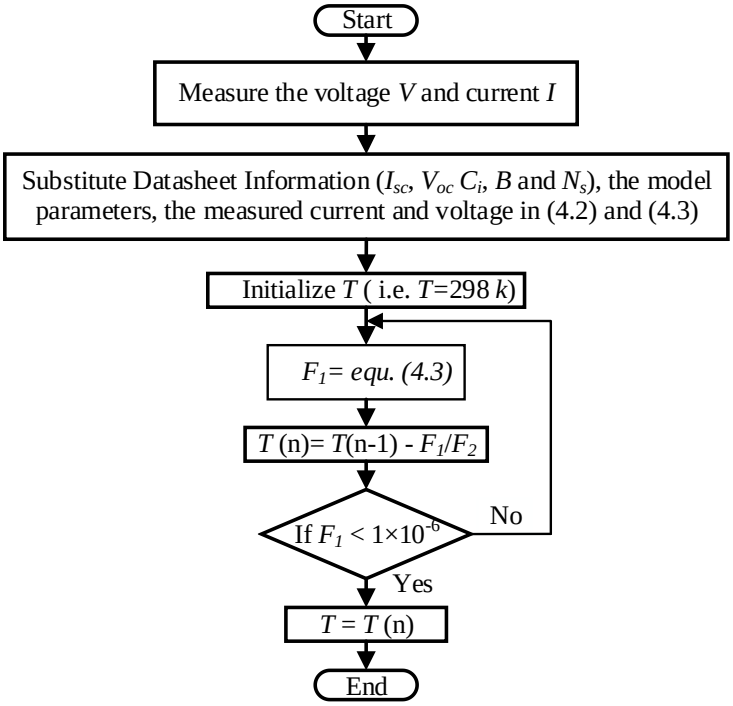

Figure 6-1: Flowchart illustrating the temperature estimation procedure.

V_{oc}, C_i, B and N_s), model parameters (α_0, α_1, α_2, α_3, A, and R_{sh}), measured voltage V and current I in equations (6-2) and (6-3). Next, the Newton Raphson method is used to solve (6-2) to find the temperature T. The STC temperature (T= 298 k) can be efficiently used as the initial guess. The iterations will run until the error becomes as low as 1×10^{-6} and the resulting temperature will be the final estimated temperature.

To test the accuracy of the proposed temperature estimator, a PV system composed of a PV module equipped with an MPPT method, as shown in Figure 6-2, is built in MATLAB. As illustrated, the estimator uses the measured current and voltage for estimating the operating temperature.

As shown, the output of the temperature estimator is the estimated temperature, while the inputs are the current and voltage of the PV module. The temperature and irradiance profiles inputted to the simulated PV system are plotted in Figure 6-3. The irradiance is initially at 1000 W/m^2, then changed to 400 W/m^2 and lastly elevated to 800 KW/m^2. The temperature started at 70°, then fell to 50° and finally to 25°.

The resulting averaged estimated temperatures using the proposed temperature estimator are depicted in Figure 6-4. As seen, they highly match the real temperatures at the various values of the irradiances

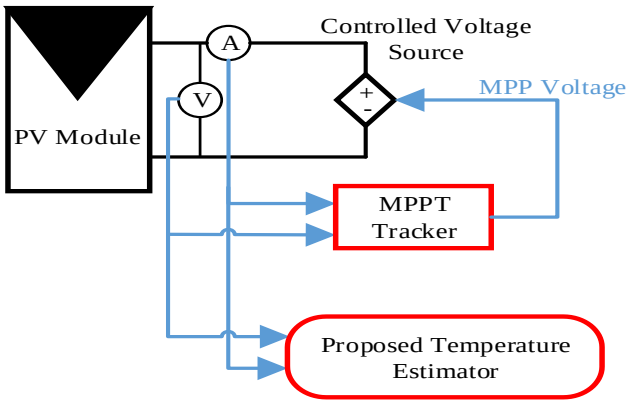

Figure 6-2: Simulated PV system connected to the temperature estimator.

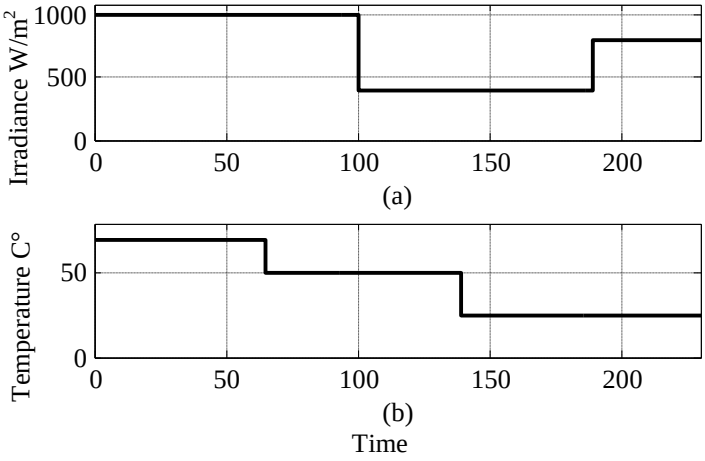

Figure 6-3: The irradiance and temperature profiles used in the system under study.

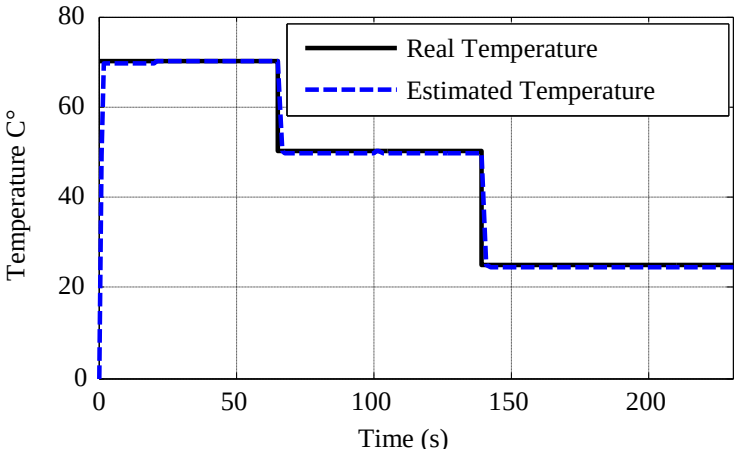

Figure 6-4: The real and estimated temperatures.

Table 6.1:Comparison between the Estimated and Actual Temperatures at Different Irradiances

Irradiance W/m^2	Temperature C°	Estimated Temperature C°	Absolute Error C°
1000	70	70.0094	0.0094
1000	50	50.0087	0.0087
400	50	50.0083	0.0083
400	25	24.8082	0.1918
800	25	24.8086	0.1914

and temperatures. Moreover, the absolute error between the real and estimated temperatures is shown in Table 6.1. The table reveals the high accuracy of the estimator.

6.2. The Developed MPPT Method

This section presents the proposed combined heuristic and model-based MPPT method. The proposed MPPT utilizes the well-known heuristic P&O MPPT method, for accurate maximum power point tracking, and the polynomial-based PV model, for accelerating the tracking speed. It is also equipped with the proposed temperature estimator to eliminate the temperature measurement.

6.2.1. P&O MPPT

The P&O MPPT method is based on perturbing (incrementing or decrementing) the voltage of the PV system and then observing the corresponding change in the output power. If it results in an increase in the output power, the perturbing is maintained in the same direction to increase the extracted power. Otherwise, the perturbing direction is reversed. This process continues throughout the operation of the PV system.

A flowchart summarizing the operation of the P&O MPPT method is depicted in Figure 6-5. It starts by measuring the PV voltage and current, and then calculates the power. If the power increases compared to its previous value, then the PV voltage is perturbed by a voltage step ΔV in the same direction as the previous perturbation. However, if the current power decreases in comparison with its previous value, then the PV voltage is perturbed by a voltage step ΔV in the opposite direction of the previous perturbation.

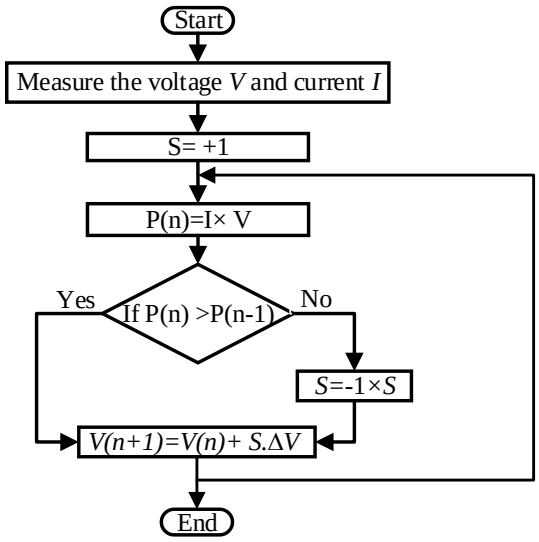

Figure 6-5: The flowchart summarizing the P&O MPPT operation.

The P&O method is distinguished by its simplicity and accuracy but suffers from slow tracking speed. The tracking speed is directly related to the size of the selected voltage step where small step size, which is mandatory for accurate tracking, results in slow tracking speed as highlighted in the introduction. The voltage step can have an adaptive size to increases the speed of the accurate tracking [108].

To demonstrate the slow tracking speed of the P&O method, the created circuit model simulation in the previous section is simulated again, using the P&O MPPT. The P&O method utilized is adaptive where the voltage step size changes depending on how the operating point is close to the maximum power. The resulting simulated power, under same irradiance and temperatures shown in Figure 6-3, is plotted in Figure 6-6. The plot reveals the slow dynamics of the P&O method which causes power losses particularly under quick variations in irradiance. As seen, the P&O method does not guarantee extracting the maximum available power immediately after the atmospheric variations as it requires time delay until it generates its maximum available power.

6.2.2. Model-Based MPPT

This subsection builds a model based MPPT relying on the polynomial based PV model. The objective is to derive a relation between the MPP current and voltage and then utilize it for the MPPT tracking. Using the information that the derivative of the power at the MPP is equal to zero, the following equation can be written:

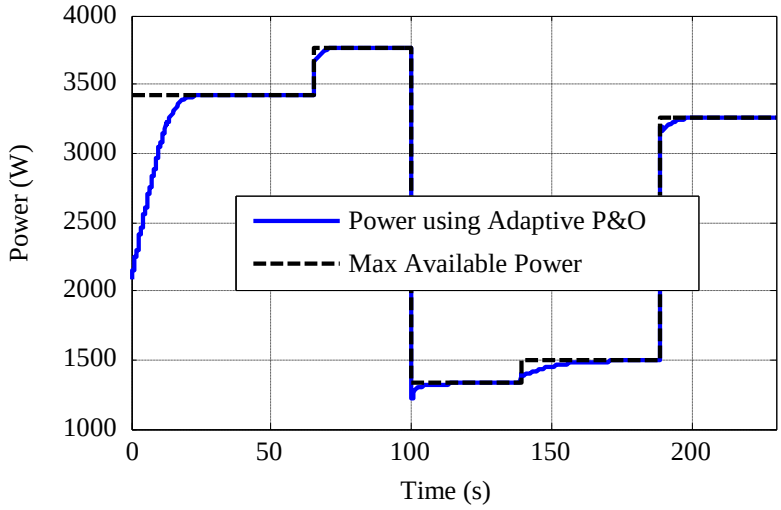

Figure 6-6: The simulated power resulted when using the adaptive P&O MPPT.

$$\frac{dP}{dV} = \frac{dI}{dV} \times V + I = 0 \tag{6-8}$$

Substituting the derivative dI/dV from (6-1) in (6-8) and manipulating yield:

$$\frac{-qI_s(\alpha_1 V_m + 2\alpha_2 V_m^2 + 3\alpha_3 V_m^3)}{N_s KTA} e^{\frac{q(\alpha_0+\alpha_1 V_m+\alpha_2 V_m^2+\alpha_3 V_m^3)}{N_s KTA}} + I_m - \frac{\alpha_1 V_m + 2\alpha_2 V_m^2 + 3\alpha_3 V_m^3}{R_{sh}} = 0 \tag{6-9}$$

The resulting equation (6-9) relates the MPP current I_m and voltage V_m at any value of temperature T. A distinguishing feature of (6-9) is that it does not depend on the irradiance, and thus it eliminates the need for measuring or estimating it. Therefore, the MPP voltage can be determined by substituting the measured current and the temperature in (6-9). Another distinguishing characteristic of (6-9) is that it provides a non-transcendental relation between V_m and I_m as it is of the form $I_m=f(V_m)$.

Relying on (6-9), the proposed model-based MPPT can be constructed in Simulink as shown in Figure 6-7. The proposed MPPT needs current measurement and knowledge of the temperature in order to solve (6-9). The resulting MPP voltage is then supplied to the controlled voltage source.

To test the effectiveness of the developed model based MPPT, the system, shown in Figure 6-7, is simulated under the irradiance and temperature profile shown in Figure 6-3. The resulting simulated power is depicted in Figure 6-8. As seen, the model based MPPT shows fast tracking dynamics under the variations in irradiance and temperature. As can be noted, the maximum available power is extracted

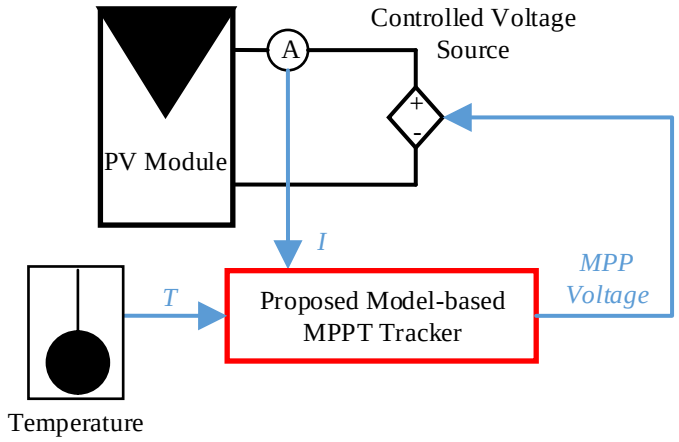

Figure 6-7: The simulated PV system using the proposed model based MPPT tracker.

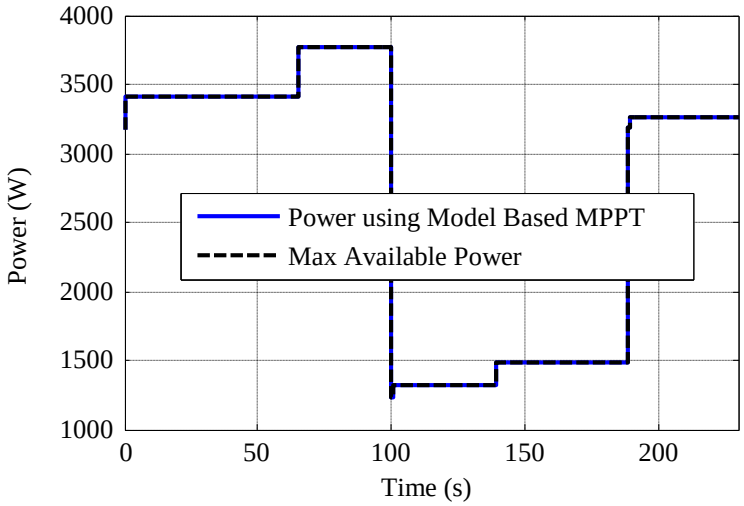

Figure 6-8: The simulated power resulted when using the model based MPPT method.

almost immediately after any change in the atmospheric conditions.

Although the model based MPPT exhibits high accuracy in tracking the maximum available power as shown in Figure 6-8, any deviation between the PV model and real characteristics of the PV module, which is predicted particularly with the aging of the system, is expected to affect the accuracy of the tracking. To illustrate this effect, a 10% error is intentionally inserted in the PV model, and then the operation of the model based MPPT is repeated. The resulting extracted power in this case is plotted in Figure 6-9. As shown, significant power losses result, which is the main drawback of the model based MPPTs.

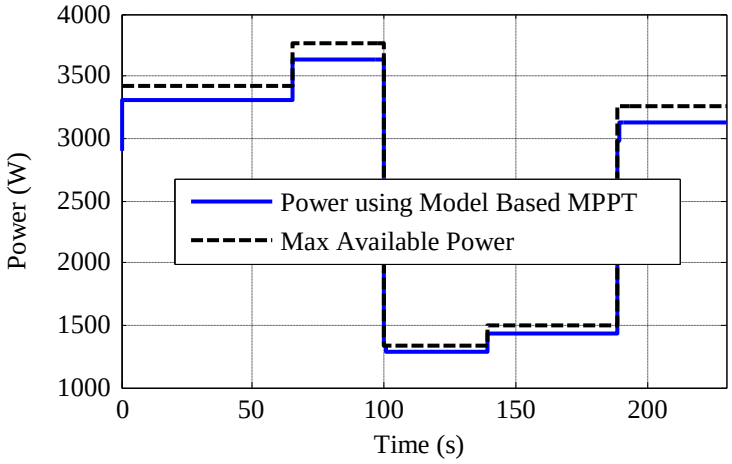

Figure 6-9: The simulated power resulted when using the model based MPPT method subjected to PV model inaccuracy.

6.2.3. Proposed Combined P&O and Model-based MPPT

It was shown in the preceding sections that the heuristic adaptive P&O method can achieve high accuracy in tracking the maximum available power but suffers from slow tracking dynamics. On the other hand, the model based MPPT exhibits high tracking speed but its accuracy is highly affected by the PV model imprecision.

This section combines the P&O MPPT method with the proposed model based MPPT technique for obtaining efficient and high speed tracking. The operation of the proposed combined MPPT is summarized in the flowchart of Figure 6-10. As noted, it sums the determined MPP voltages using both P&O and model-based methods. First, the measured current and voltage are used to estimate the temperature using the proposed temperature estimator. Then, the temperature, along with the current, are utilized to determine the MPP voltage. Once the MPP voltage V_m is determined, it is summed with the voltage V_p determined using the P&O MPPT.

To test the effectiveness of the proposed MPPT, a Simulink model for the PV system under study is used again for simulating the system under the irradiance and temperature profile shown in Figure 6-3. The simulated system embedded with the proposed combined P&O and model-based MPPT is depicted in Figure 6-11. The resultant maximum power extracted is shown in Figure 6-12. As seen, the proposed MPPT can achieve high dynamic response and accurate tracking. The simulation is also repeated to test the performance under an inaccuracy in the PV model. A 10% deviation in the PV model is intentionally added and the resulting power is plotted in Figure 6-13. As it is clear, it is not affected by the PV model impreciseness, providing a clear advantage over the model-based MPPT.

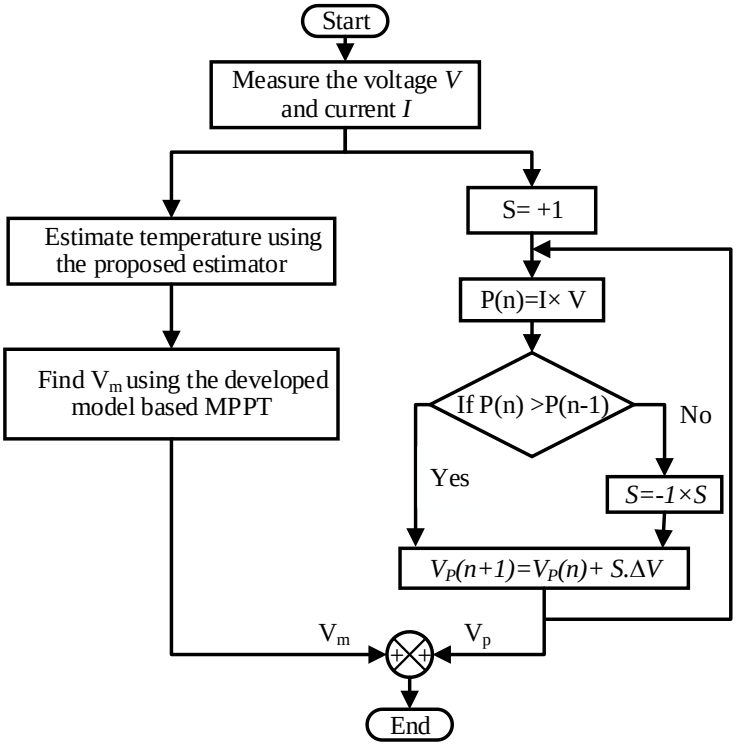

Figure 6-10: The flowchart summarizing the operation of the proposed combined P&O and Model-based MPPTs.

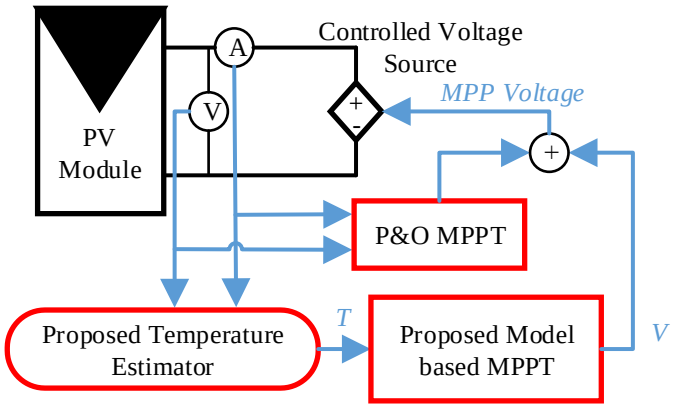

Figure 6-11**:** The simulated PV system with the proposed combined P&O and model based MPPT tracker.

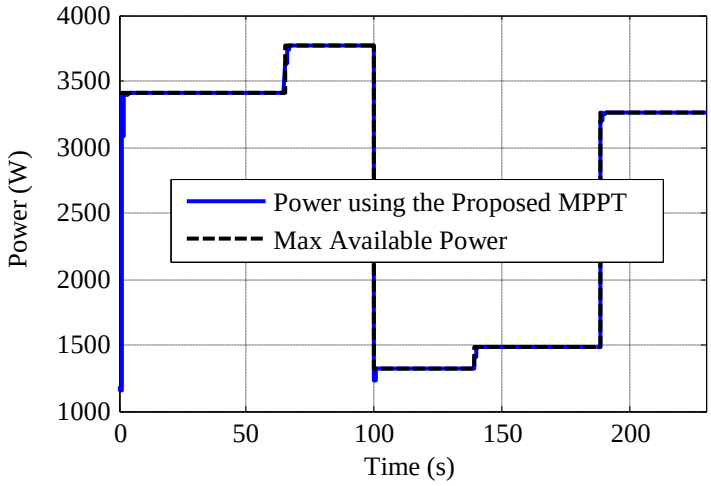

Figure 6-12: The simulated power waveform resulted when using the proposed combined model based and P&O MPPT method.

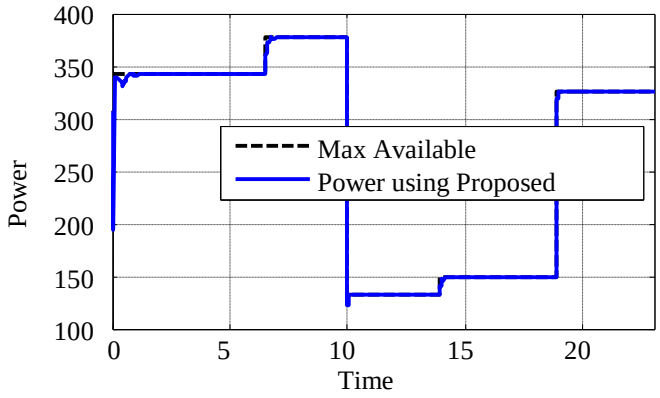

Figure 6-13: The simulated power resulted when using the proposed combined model based and P&O MPPT method subjected to PV model inaccuracy.

Comparing the power waveforms resulting from using the adaptive P&O shown in Figure 6-6 and the proposed combined model based and heuristic method shown in Figure 6-13 reveals the high speed of the proposed approach in comparison with the heuristic approach. The adaptive P&O is chosen because it has higher speed compared to the basic P&O method. Table II presents a quantitative comparison in terms of transient efficiency, tracking speed and steady state accuracy. The transient efficiency is the ratio between the extracted power to the available power during the transient period, while the steady state accuracy is at the steady state period. As shown, while the steady state accuracy is almost the same in both methods, the proposed method exhibits higher transient efficiency (around 3%

Table 6.2: Comparison between the Proposed and the Adaptive P&O Methods

	Transient Efficiency		Tracking Speed		Steady State Accuracy	
Time Period	Adaptive P&O	Proposed Technique	Adaptive P&O	Proposed Technique	Adaptive P&O	Proposed Technique
0 - 65 s	89.94 %	97.53 %	25 s	4 s	99.98 %	99.99 %
65 - 100 s	99.30 %	99.68 %	14 s	2 s	99.99 %	99.98 %
100 - 140 s	99.04 %	99.78 %	20 s	4 s	99.99 %	99.98 %
140 - 190 s	98.13 %	99.82 %	36 s	2 s	99.97 %	99.98 %
190 - 230 s	99.68 %	99.97 %	18 s	3 s	99.99 %	99.99 %
Average	96.74 %	99.24 %	22.6 s	3 s	99.99 %	99.99 %

more), as well as higher tracking speed. This will result in power savings particularly in fast changing atmospheric conditions.

To measure the improvement in the overall energy under real environmental conditions, a comparison between the energy generated by one PV module using both methods over long period of time is conducted. Real irradiance and temperature measurements provided in [13] were used for the comparison. The power gained by replacing the adaptive P&O method with the proposed method is plotted in Figure 6-14. At initial operation of the system, the power gained is high (about 70W), but reduces at steady state. The rest gain occurs at the irradiance variations. This shows the advantage of the proposed method in enhancing the dynamic performance of tracking. The gain is also quantified and summarized in Table 6.3. As shown, the proposed method increases the energy gained by 2%.

6.3. Real Time Simulation

In addition to the verification conducted using Simulink, the effectiveness of the proposed method is validated in real-time using OPAL-RT (RTS). The PV system and the proposed MPPT algorithm are implemented in the RTS. The current and voltage of the virtual PV system are connected to the implemented MPPT, and the reference voltage determined by the MPPT algorithm is connected to the virtual PV system.

The system used for the real time simulation consists of a PV array, DC boost converter and a DC bus. The real time simulation is conducted under the irradiance and temperature profile shown in Figure 6-3. The resulting real time power waveform is shown in Figure 6-15. As seen, the resulting power waveform complies with the simulated waveform.

Table 6.3 Accumulated Energy

MPPT Method	Energy
Adaptive P&O MPPT	461.8 KJ
Proposed MPPT	471.3 KJ
Improvement	2.06 %

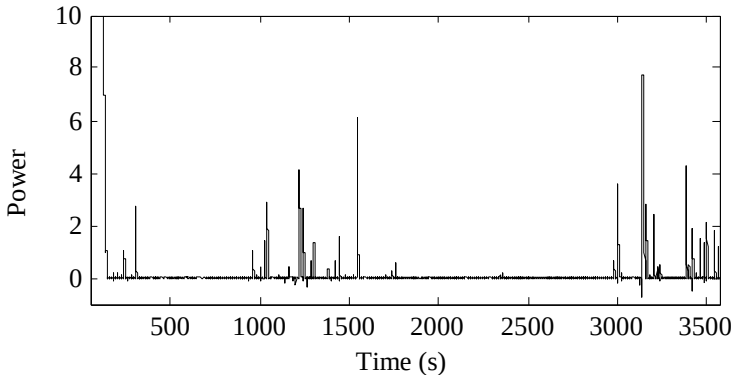

Figure 6-14: Power gained by using the proposed method over the adaptive P&O.

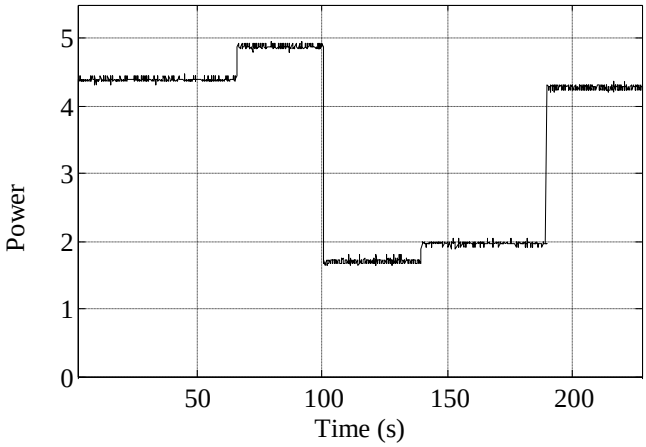

Figure 6-15: The power waveform of the real time simulation (scaling factor=790).

6.4. Experimental Set-up

This section verifies the effectiveness of the proposed method experimentally. The experimental setup, which is shown in Figure 6-16, consists of a PV module of the type Sharp ND-123UJF, data acquisition

Figure 6-16: The used experimental setup.

device (PCI-1716), DC power supply (BK- 1687B), resistive load and computer, where the PV module, the resistive load and the power supply are connected in parallel. A schematic diagram for the experimental setup is depicted in Figure 6-17. As seen, the current and voltage of the PV module are first measured and inputted to the data acquisition device which is connected to the computer. The measured current and voltage are filtered and then used by the proposed method, which is implemented in the computer through MATLAB, to find the temperature. The estimated temperature is filtered and updated periodically to the model based MPPT which finds the MPP voltage. Then, the determined MPP voltage is sent through the data acquisition device to the DC voltage supply to operate the PV module on this MPP voltage. The function of the resistor connected in parallel with the voltage supply is to dissipate the current generated by the PV module.

The described experimental system was used to verify the effectiveness of the proposed method and to compare it to the model based MPPT. First, the algorithm started to extract the maximum available power, and then the irradiance of the PV module was decreased. The algorithm was successfully able to find the new maximum power point. To verify that the extracted power is the truly available maximum power, the *I-V* curves of the PV module was measured twice under both irradiance values. The extracted power was equal to the measured power in both scenarios. Moreover, this test was exactly repeated for the model based MPPT. As expected, the resulted power of the model based MPPT is lower than that of the proposed method. As was illustrated before in this chapter, this is due to the mismatch between the PV model used in the model based MPPT and the actual characteristic of the PV module.

Table 6.4:Accumulated Energy

MPPT Method	Energy
Model based MPPT	25.12 KJ
Proposed MPPT	26.96 KJ
Improvement	7.3 %

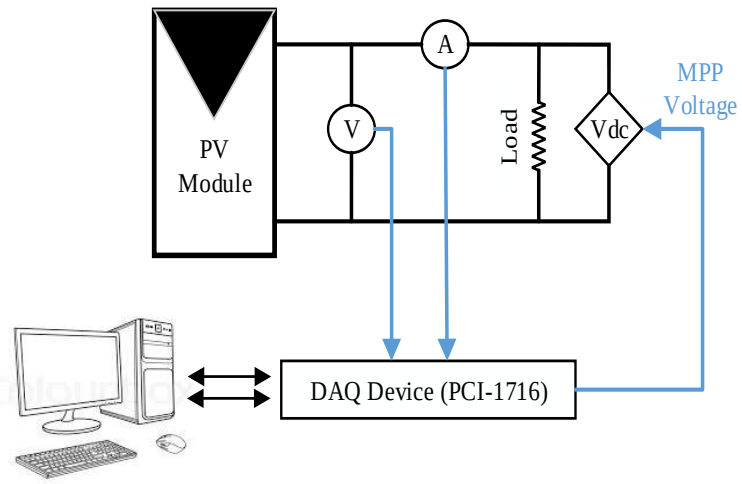

Figure 6-17: Schematic of the used experimental setup.

To quantify the improvement in the extracted energy for the proposed method, the energy of both methods were measured in the previous tests. The comparison between them is summarized in Table 6.4. As seen, the energy generated using the proposed method was 26.96 KJ while the energy generated using the model based MPPT was 25.12 KJ. This means that there is a 7.3% energy gain when the proposed MPPT is adopted compared to the model based MPPT. This can clearly show the superiority of the proposed method over the model based MPPT.

6.5. Discussion

This chapter proposed an enhanced MPPT method combining the heuristic P&O and model-based MPPT techniques. The main feature of the proposed method is it eliminates the need for temperature measurement, reducing the cost and complexity of the implementation. Moreover, it does not require an irradiance measurement.

The proposed method relies on a new set of equations capable of estimating the temperature by utilizing the current and voltage measurements. It uniquely adopts the polynomial based PV model, the

developed model in chapter 2 featuring reduced computational time, to reduce the computational complexity of the MPPT.

The chapter began by demonstrating the slow tracking speed of the heuristic methods and the inaccuracy of the model-based techniques. Then, it was shown that the proposed model combines both distinguished features of the heuristic and model-based methods and thus provides high accuracy and tracking speed. It was also shown that the proposed method is unaffected by the PV model inaccuracy. An experimental set up was built to verify the effectiveness of the proposed method.

The heuristic MPPT methods have been always preferred over the model-based MPPTs in industrial and practical applications, in spite of their slow tracking speed, because they do not require irradiance or temperature measurements, and they are not affected by the PV model accuracy which is influenced by PV system aging. However, the proposed method is expected to be chosen over the heuristic methods due to its improved tracking speed, while it does not require temperature or irradiance measurements and is not affected by the PV model inaccuracy.

Chapter 7 CONCLUSIONS

7.1. Summary

Although numerous PV systems have recently been built in locations around the world, the spread of PV systems has been limited due to the high costs arising from their inadequate efficiency. The primary goal of the work presented in this thesis was therefore to support and increase the global spread of photovoltaic (PV) power systems. The specific objectives for achieving this goal were 1) the development of a new PV circuit model and an enhanced modeling tool that would facilitate research into and the investigation of PV systems, and 2) the improvement of the efficiency of solar PV systems through the mitigation of their power losses. As indicated in the following paragraphs, the accomplishment of the first objective has been described in Chapter 2 and Chapter 3, while the work associated with realizing the second objective has been presented in the remaining chapters.

Chapter 2 details the challenges facing PV system designers and researchers with respect to the lengthy computational time required for the simulation of large PV systems. To address these issues, a new PV circuit model is proposed, which reduces computational time without scarifying the accuracy of existing models. Experimental measurements were obtained in order to validate the proposed model. For commercially available mono-crystalline, poly-crystalline, and thin-film PV technologies, the new model was proven to provide a high level of accuracy for both homogeneous and nonhomogeneous conditions at different temperatures and irradiance levels. A case study involving large, partially shaded PV systems showed that the percentage of the reduction in computational time increases exponentially with the size of the PV system, thus providing a clear advantage with respect to the simulation of large systems.

Chapter 3 explains how, in spite of the reduced computational time provided by the model proposed in Chapter 2, the time required is still large and unacceptable for some online applications for which the estimations of PV system power peaks must be in the range of a few seconds. Unfortunately, even when the proposed model is used, the estimation of the peaks requires the simulation of the entire power curve and consumes copious amounts of computational time: in the range of hours. A new, fast modeling tool has been developed, which is able to estimate the system power peaks directly without simulating the entire power peak. The proposed tool relies on developed rules that govern the formation of power peaks in a PV system. The accuracy of the proposed modeling tool was verified experimentally for a partially shaded PV system. The ability of the proposed tool to find the power peaks in only a few seconds was also validated, and the proposed method was thus found suitable for online applications. The proposed

tool was also utilized for the first-time development of a model-based MPPT for partially shaded PV systems.

Chapter 4 highlights the sources of misleading power losses in partially shaded PV systems and the inability of existing MPPT methods to eliminate them. It explains how these power losses are caused by the periodic curve scanning required in optimization-based MPPT methods during the tracking of the global power peak. A novel MPPT method is proposed that avoids the need for periodic curve scanning, thus eliminating misleading power losses. The proposed method utilizes the power peak estimator proposed in Chapter 3 for tracking the global maximum power point (GMPP), and innovatively employs an optical camera for estimating the irradiance levels received by the PV cells in the system. An experimental prototype was built for validating the effectiveness of the proposed method with respect to correctly tracking the GMPP without causing misleading power losses.

Chapter 5 reviews the failure of existing reconfiguration methods to minimize mismatch power losses of PV systems that are subject to rapidly moving shadows due to the time delay inherent in these methods. A proposed reconfiguration algorithm is presented. The new algorithm provides a reduced time delay that ensures the minimization of mismatch power losses. A case study was conducted with a large PV system. The results demonstrate the superiority of the proposed method over existing methods with respect to responding to rapidly changing shadows and confirm the ability of the proposed method to improve system energy gains.

Chapter 6 sets out the advantages of MPPT methods that combine both model-based and heuristic techniques for improving dynamic tracking performance and reducing tracking power losses in PV systems. However, as pointed out, the drawback of these MPPT methods is that they require accurate temperature measurements, which increases the complexity of commonly used heuristic MPPT methods and the cost of their implementation. A novel method for temperature estimation is then presented. The new model, which is based on the circuit model proposed in Chapter 2, was designed to estimate the temperature indirectly without the need for temperature measurements. The effectiveness of the method with respect to improving the speed and dynamic performance of the tracking was verified through both MATLAB and real-time OPAL-RT simulations. Validation of the proposed method also included the building of an experimental setup.

7.2. Contributions

The primary outcomes of the research presented in this thesis can be summarized as follows:

1- A reduction in the heavy computational time needed for simulating large, partially shaded PV systems has been provided by the proposed PV circuit model, which offers comparable accuracy but requires less computational time.
2- The estimation of power peaks for partially shaded PV systems is now possible in a few seconds as opposed to the few hours previously required with existing methods.
3- Misleading power losses have been eradicated for partially shaded PV systems through the development, for the first time, of a model-based MPPT method for use with partially shaded PV systems. The new method avoids the curve scanning required with existing MPPT methods.
4- Mismatch power losses in partially shaded PV systems have been minimized by the development of a new reconfiguration algorithm that reduces the time delay inherent in existing methods.
5- The use of MPPT methods that combine model-based and heuristic techniques, which feature reduced tracking power losses, has been facilitated by reducing their cost and complexity through the elimination of the previously required temperature measurements.

7.3. Direction of Future Work

Suggested areas for further investigation include the following:

1- Further improve the efficiency of PV systems by tackling other sources of power losses, such as power losses in micro-inverters.
2- Extend the developed image-based MPPT method in order to increase the number of covered PV modules that can be monitored by a camera.
3- Develop an improved reconfiguration method that can overcome the necessity for the voltage and current sensors required for estimating the levels of irradiance received by PV modules.

Appendix A TEMPERATURE AND IRRADIANCE EFFECT ON THE POLYNOMIAL COEFFICIENTS

This appendix shows that the temperature and irradiance effect on the polynomial coefficients of the proposed model is negligible. First, the PV module (mono-crystalline SM50-H) is parameterized at STC conditions and the resulted STC parameters are used to plot the *I-V* curves at different irradiance and temperature levels. Then the same PV module is parameterized again at each temperature and irradiance level using the measured *I-V* curves, and the resulted parameters at each temperature and irradiance level are used to plot the *I-V* curve at the corresponded temperature and irradiance. Finally, the resulted *I-V* curves from both methods are compared in the same figure to observe the deviation between them.

The characteristics *I-V* curves are compared in Figure A-1 at different temperature and irradiance with reference to the measured data. It is shown that the deviation between the *I-V* curves with and without considering the effect of the meteorological on polynomial coefficients are very small. Furthermore, the values of root mean square deviation between them are also quantified and compared in Table A.1.

Table A.1: The Percentage of Modeling Deviation at Different Temperature and Irradiance Levels with and without Considering Meteorological Effect on Polynomial Coefficients

Irradiance G and Temperature T	RMSD Without considering meteo. effect	RMSD with Considering meteo. effect	Percentage Difference
G = 1 kW/m^2 & T=25°C	0.5128	0.5128	0
G =0.8 kW/m^2 & T=25°C	1.1724	0.9318	0.2406
G =0.6 kW/m^2 & T=25°C	1.8789	0.5486	1.3303
G =0.4 kW/m^2 & T=25°C	1.2038	0.3629	0.8409
G =0.2 kW/m^2 & T=25°C	1.4100	0.3220	1.0880
G = 1 kW/m^2 & T=40°C	3.1049	2.2603	0.8446
G = 1 kW/m^2 & T=60°C	4.9584	4.1064	0.8520

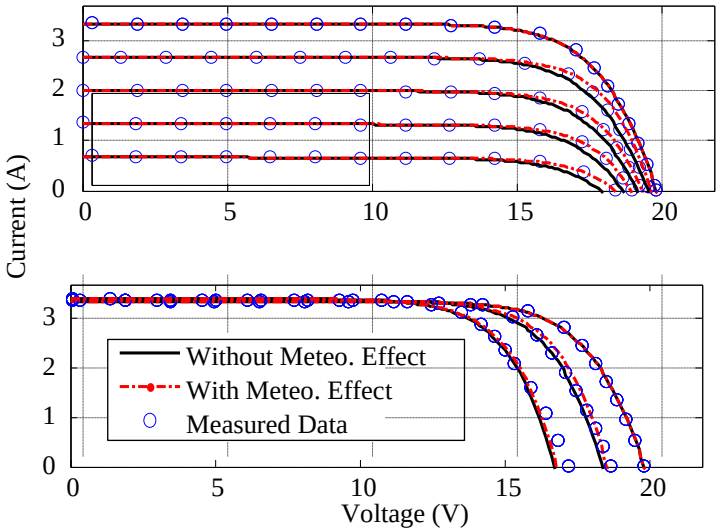

Figure A-1: *I-V* curves at different irradiance and temperature levels with and without considering the meteorological effect on the polynomial coefficients

Appendix B LIST OF PUBLICATIONS

The following is a list of IEEE journal publications by the author during doctoral studies.

[1] Y. Mahmoud, and E. F. El-Saadany, "Image-based Maximum Power Point Tracker for Partially Shaded PV Systems," in IEEE Transactions on Energy Conversion, under revision.

[2] Y. Mahmoud, and E. F. El-Saadany, "Enhanced PV Reconfiguration Method for Improving the Efficiency of Partially Shaded PV Systems," in IEEE Transactions on Industrial Informatics, under revision.

[3] Y. Mahmoud, M. Abdelwahed and E. F. El-Saadany, "An Enhanced MPPT Method Combining Model-Based and Heuristic Techniques," in IEEE Transactions on Sustainable Energy, vol. 7, no. 2, pp. 576-585, April 2016.

[4] Y. Mahmoud and E. F. El-Saadany, "Fast Power-Peaks Estimator for Partially Shaded PV Systems," in IEEE Transactions on Energy Conversion, vol. 31, no. 1, pp. 206-217, March 2016.

[5] Y. Mahmoud and E. El-Saadany, "Accuracy Improvement of the Ideal PV Model," in IEEE Transactions on Sustainable Energy, vol. 6, no. 3, pp. 909-911, July 2015.

[6] Y. Mahmoud and E. F. El-Saadany, "A Photovoltaic Model With Reduced Computational Time," in IEEE Transactions on Industrial Electronics, vol. 62, no. 6, pp. 3534-3544, June 2015.

References

[1] (2010-01-12). *U.S. EIA International Energy Statistics*. Available: http://www.eia.gov/cfapps/ipdbproject/IEDIndex3.cfm

[2] (2012-01-27). *World Proved Reserves of Oil and Natural Gas, Most Recent Estimates*. Available: http://www.eia.gov/beta/international/

[3] P. E. Hodgson. (10/22/08). *Nuclear Power and the Energy Crisis*. Available: http://www.firstprinciplesjournal.com/articles.aspx?article=1110&loc=qs

[4] J. D. Hamilton, "Historical Oil Shocks," *Routledge Handbook of Major Events in Economic History*, pp. 239-265, 2011.

[5] R. Angel, "Solar Energy as a Major Replacement for Fossil Fuel," ed, 2007.

[6] I. E. Agency, "Technology Roadmap: Solar Photovoltaic Energy," ed, 2014.

[7] P. Gevorkian, *Sustainable Energy System Engineering: The Complete Green Building Design Resource*: McGraw-Hill Education, 2007.

[8] S. B. Kjaer, J. K. Pedersen, and F. Blaabjerg, "A review of single-phase grid-connected inverters for photovoltaic modules," *IEEE Transactions on Industry Applications*, vol. 41, pp. 1292-1306, 2005.

[9] I. E. A. P. P. S. Programme, "Snapshot of Global PV 1992-2014," 30 March 2015.

[10] M. Sechilariu, W. Baochao, and F. Locment, "Building Integrated Photovoltaic System With Energy Storage and Smart Grid Communication," *IEEE Transactions on Industrial Electronics*, vol. 60, pp. 1607-1618, 2013.

[11] M. A. S. Masoum, H. Dehbonei, and E. F. Fuchs, "Theoretical and experimental analyses of photovoltaic systems with voltageand current-based maximum power-point tracking," *IEEE Transactions on Energy Conversion*, vol. 17, pp. 514-522, 2002.

[12] Y. Mahmoud, M. Abdelwahed, and E. F. El-Saadany, "An Enhanced MPPT Method Combining Model-Based and Heuristic Techniques," *Sustainable Energy, IEEE Transactions on*, vol. PP, pp. 1-10, 2016.

[13] L. V. Hartmann, M. A. Vitorino, M. B. R. Correa, and A. M. N. Lima, "Combining Model-Based and Heuristic Techniques for Fast Tracking the Maximum-Power Point of Photovoltaic Systems," *IEEE Transactions on Power Electronics*, vol. 28, pp. 2875-2885, 2013.

[14] A. Woyte, J. Nijs, and R. Belmans, "Partial shadowing of photovoltaic arrays with different system configurations: literature review and field test results," *Solar Energy*, vol. 74, pp. 217-233, 3// 2003.

[15] X. Weidong, N. Ozog, and W. G. Dunford, "Topology Study of Photovoltaic Interface for Maximum Power Point Tracking," *IEEE Transactions on Industrial Electronics, ,* vol. 54, pp. 1696-1704, 2007.

[16] E. Koutroulis and F. Blaabjerg, "A New Technique for Tracking the Global Maximum Power Point of PV Arrays Operating Under Partial-Shading Conditions," *IEEE Journal of Photovoltaics*, vol. 2, pp. 184-190, 2012.

[17] A. Maki and S. Valkealahti, "Effect of Photovoltaic Generator Components on the Number of MPPs Under Partial Shading Conditions," *IEEE Transactions on Energy Conversion*, vol. 28, pp. 1008-1017, 2013.

[18] K. Sundareswaran, P. Sankar, P. S. R. Nayak, S. P. Simon, and S. Palani, "Enhanced Energy Output From a PV System Under Partial Shaded Conditions Through Artificial Bee Colony," *IEEE Transactions on Sustainable Energy*, vol. 6, pp. 198-209, 2015.

[19] Y.-H. Liu, S.-C. Huang, J.-W. Huang, and W.-C. Liang, "A Particle Swarm Optimization-Based Maximum Power Point Tracking Algorithm for PV Systems Operating Under Partially Shaded

Conditions," *IEEE Transactions on Energy Conversion and Management*, vol. 27, pp. 1027-1035, 2012.
[20] W. Yanzhi, L. Xue, K. Younghyun, C. Naehyuck, and M. Pedram, "Architecture and Control Algorithms for Combating Partial Shading in Photovoltaic Systems," *Computer-Aided Design of Integrated Circuits and Systems, IEEE Transactions on*, vol. 33, pp. 917-930, 2014.
[21] M. Z. S. El-Dein, M. Kazerani, and M. M. A. Salama, "Optimal Photovoltaic Array Reconfiguration to Reduce Partial Shading Losses," *IEEE Transactions on Sustainable Energy*, vol. 4, pp. 145-153, 2013.
[22] Y. Mahmoud, W. Xiao, and H. H. Zeineldin, "A Simple Approach to Modeling and Simulation of Photovoltaic Modules," *IEEE Trans. on Sustainable Energy*, vol. 3, pp. 185-186, 2012.
[23] Y. Mahmoud and E. F. El-Saadany, "A Photovoltaic Model With Reduced Computational Time," *Industrial Electronics, IEEE Transactions on*, vol. 62, pp. 3534-3544, 2015.
[24] Y. Mahmoud and E. F. El-Saadany, "Fast Power-Peaks Estimator for Partially Shaded PV Systems," *Energy Conversion, IEEE Transactions on*, vol. PP, pp. 1-12, 2015.
[25] P. Maffezzoni, L. Codecasa, and D. D'Amore, "Modeling and Simulation of a Hybrid Photovoltaic Module Equipped With a Heat-Recovery System," *IEEE Trans. on Ind. Electron.*, vol. 56, pp. 4311-4318, 2009.
[26] A. Mellit, M. Benghanem, and S. A. Kalogirou, "Modeling and simulation of a stand-alone photovoltaic system using an adaptive artificial neural network: Proposition for a new sizing procedure," *Renewable Energy*, vol. 32, pp. 285-313, 2// 2007.
[27] P. E. Kakosimos, A. G. Kladas, and S. N. Manias, "Fast Photovoltaic-System Voltage- or Current-Oriented MPPT Employing a Predictive Digital Current-Controlled Converter," *IEEE Trans. on Ind. Electron.*, vol. 60, pp. 5673-5685, 2013.
[28] M. A. Vitorino, M. Beltrao de Rossiter Correa, C. B. Jacobina, and A. M. N. Lima, "An Effective Induction Motor Control for Photovoltaic Pumping," *IEEE Trans. on Ind. Electron.*, vol. 58, pp. 1162-1170, 2011.
[29] M. Amirabadi, A. Balakrishnan, H. A. Toliyat, and W. C. Alexander, "High-Frequency AC-Link PV Inverter," *IEEE Trans. on Ind. Electron.*, vol. 61, pp. 281-291, 2014.
[30] X. Weidong, M. G. J. Lind, W. G. Dunford, and A. Capel, "Real-Time Identification of Optimal Operating Points in Photovoltaic Power Systems," *IEEE Trans. on Ind. Electron.*, vol. 53, pp. 1017-1026, 2006.
[31] S. Jing Jun and L. Kay-Soon, "Photovoltaic Model Identification Using Particle Swarm Optimization With Inverse Barrier Constraint," *IEEE Trans. on Power Electron.*, vol. 27, pp. 3975-3983, 2012.
[32] O. C. Onar, M. Uzunoglu, and M. S. Alam, "Modeling, control and simulation of an autonomous wind turbine/photovoltaic/fuel cell/ultra-capacitor hybrid power system," *Journal of Power Sources*, vol. 185, pp. 1273-1283, 12/1/ 2008.
[33] A. I. Bratcu, I. Munteanu, S. Bacha, D. Picault, and B. Raison, "Cascaded DC–DC Converter Photovoltaic Systems: Power Optimization Issues," *Industrial Electronics, IEEE Transactions on*, vol. 58, pp. 403-411, 2011.
[34] P. Sang-Hoon, C. Gil-Ro, J. Yong-Chae, and W. Chung-Yuen, "Design and Application for PV Generation System Using a Soft-Switching Boost Converter With SARC," *Industrial Electronics, IEEE Transactions on*, vol. 57, pp. 515-522, 2010.
[35] R. Lanzafame, S. Nachtmann, M. Rosa-Clot, P. Rosa-Clot, P. F. Scandura, S. Taddei, *et al.*, "Field Experience With Performances Evaluation of a Single-Crystalline Photovoltaic Panel in an Underwater Environment," *IEEE Trans. on Ind. Electron.*, vol. 57, pp. 2492-2498, 2010.
[36] VeeracharyM, "PSIM circuit-oriented simulator model for the nonlinear photovoltaic sources," *IEEE Trans. on Aerospace and Electronic Systems*, vol. 42, pp. 735-740, 2006.

[37] Gonza, x, M. lez, x, C. n, P. Arboleya, *et al.*, "Improved model of photovoltaic sources considering ambient temperature and solar irradiation," in *Sustainable Alternative Energy (SAE), 2009 IEEE PES/IAS Conference on*, 2009, pp. 1-6.
[38] F. Adamo, F. Attivissimo, A. Di Nisio, and M. Spadavecchia, "Characterization and Testing of a Tool for Photovoltaic Panel Modeling," *IEEE Transactions on Instrumentation and Measurement*, vol. 60, pp. 1613-1622, 2011.
[39] K. Nishioka, N. Sakitani, Y. Uraoka, and T. Fuyuki, "Analysis of multicrystalline silicon solar cells by modified 3-diode equivalent circuit model taking leakage current through periphery into consideration," *Solar Energy Materials and Solar Cells*, vol. 91, pp. 1222-1227, 8/15/ 2007.
[40] M. G. Villalva, J. R. Gazoli, and E. R. Filho, "Comprehensive Approach to Modeling and Simulation of Photovoltaic Arrays," *IEEE Trans. on Power Electron.*, vol. 24, pp. 1198-1208, 2009.
[41] Y. A. Mahmoud, X. Weidong, and H. H. Zeineldin, "A Parameterization Approach for Enhancing PV Model Accuracy," *IEEE Trans. on Ind. Electron.*, vol. 60, pp. 5708-5716, 2013.
[42] K. Ishaque and Z. Salam, "An improved modeling method to determine the model parameters of photovoltaic (PV) modules using differential evolution (DE)," *Solar Energy*, vol. 85, pp. 2349-2359, 9// 2011.
[43] E. I. Batzelis, I. A. Routsolias, and S. A. Papathanassiou, "An Explicit PV String Model Based on the Lambert W Function and Simplified MPP Expressions for Operation Under Partial Shading," *IEEE Trans. on Sustainable Energy*, vol. 5, pp. 301-312, 2014.
[44] H. Tian, F. Mancilla-David, K. Ellis, E. Muljadi, and P. Jenkins, "A cell-to-module-to-array detailed model for photovoltaic panels," *Solar Energy*, vol. 86, pp. 2695-2706, 9// 2012.
[45] E. V. Paraskevadaki and S. A. Papathanassiou, "Evaluation of MPP Voltage and Power of mc-Si PV Modules in Partial Shading Conditions," *IEEE Trans. on Energy Convers.*, vol. 26, pp. 923-932, 2011.
[46] S. Jing Jun and L. Kay-Soon, "Optimizing photovoltaic model parameters for simulation," in *Industrial Electronics (ISIE), 2012 IEEE International Symposium on*, 2012, pp. 1813-1818.
[47] E. M. Natsheh and A. Albarbar, "Photovoltaic model with MPP tracker for standalone / grid connected applications," in *Renewable Power Generation (RPG 2011), IET Conference on*, 2011, pp. 1-6.
[48] K. Rouzbehi, A. Miranian, A. Luna, and P. Rodriguez, "Identification and maximum power point tracking of photovoltaic generation by a local neuro-fuzzy model," in *IECON 2012 - 38th Annual Conference on IEEE Industrial Electronics Society*, 2012, pp. 1019-1024.
[49] S. Lineykin, M. Averbukh, and A. Kuperman, "Issues in Modeling Amorphous Silicon Photovoltaic Modules by Single-diode Equivalent Circuit," *IEEE Trans. on Ind. Electron.*, vol. PP, pp. 1-1, 2014.
[50] A. Chatterjee, A. Keyhani, and D. Kapoor, "Identification of Photovoltaic Source Models," *IEEE Trans. on Energy Convers.*, vol. 26, pp. 883-889, 2011.
[51] G. Petrone, G. Spagnuolo, and M. Vitelli, "Analytical model of mismatched photovoltaic fields by means of Lambert W-function," *Solar Energy Materials and Solar Cells*, vol. 91, pp. 1652-1657, 11/6/ 2007.
[52] J. D. Bastidas, E. Franco, G. Petrone, C. A. Ramos-Paja, and G. Spagnuolo, "A model of photovoltaic fields in mismatching conditions featuring an improved calculation speed," *Electric Power Systems Research*, vol. 96, pp. 81-90, 3// 2013.
[53] Y. J. Wang and P. C. Hsu, "Analytical modelling of partial shading and different orientation of photovoltaic modules," *IET Renewable Power Generation*, vol. 4, pp. 272-282, 2010.

[54] K. Sundareswaran, S. Peddapati, and S. Palani, "MPPT of PV Systems Under Partial Shaded Conditions Through a Colony of Flashing Fireflies," *IEEE Trans. on Energy Convers.*, vol. 29, pp. 463-472, 2014.
[55] M. L. Orozco-Gutierrez, J. M. Ramirez-Scarpetta, G. Spagnuolo, and C. A. Ramos-Paja, "A technique for mismatched PV array simulation," *Renewable Energy*, vol. 55, pp. 417-427, 7// 2013.
[56] H. Patel and V. Agarwal, "MATLAB-Based Modeling to Study the Effects of Partial Shading on PV Array Characteristics," *IEEE Trans. on Energy Convers.*, vol. 23, pp. 302-310, 2008.
[57] H. Zheng, S. Li, R. Challoo, and J. Proano, "Shading and bypass diode impacts to energy extraction of PV arrays under different converter configurations," *Renewable Energy*, vol. 68, pp. 58-66, 8// 2014.
[58] R. M. Corless, G. H. Gonnet, D. E. G. Hare, D. J. Jeffrey, and D. E. Knuth, "On the LambertW function," *Advances in Computational Mathematics*, vol. 5, pp. 329-359, 1996/12/01 1996.
[59] S. Moballegh and J. Jiang, "Modeling, Prediction, and Experimental Validations of Power Peaks of PV Arrays Under Partial Shading Conditions," *IEEE Transactions on Sustainable Energy*, vol. 5, pp. 293-300, 2014.
[60] G. N. Psarros, E. I. Batzelis, and S. A. Papathanassiou, "Partial Shading Analysis of Multistring PV Arrays and Derivation of Simplified MPP Expressions," *IEEE Transactions on Sustainable Energy*, vol. 6, pp. 499-508, 2015.
[61] B. N. Alajmi, K. H. Ahmed, S. J. Finney, and B. W. Williams, "A Maximum Power Point Tracking Technique for Partially Shaded Photovoltaic Systems in Microgrids," *IEEE Transactions on Industrial Electronics*, vol. 60, pp. 1596-1606, 2013.
[62] T. Noguchi, S. Togashi, and R. Nakamoto, "Short-current pulse-based maximum-power-point tracking method for multiple photovoltaic-and-converter module system," *IEEE Transactions on Industrial Electronics*, vol. 49, pp. 217-223, 2002.
[63] Y. Chih-Yu, H. Chun-Yu, F. Fu-Kuei, and C. Ke-Horng, "Highly Efficient Analog Maximum Power Point Tracking (AMPPT) in a Photovoltaic System," *IEEE Transactions on Circuits and Systems I: Regular Papers*, vol. 59, pp. 1546-1556, 2012.
[64] M. Miyatake, T. Inada, I. Hiratsuka, Z. Hongyan, H. Otsuka, and M. Nakano, "Control characteristics of a fibonacci-search-based maximum power point tracker when a photovoltaic array is partially shaded," in *Power Electronics and Motion Control Conference, 2004. IPEMC 2004. The 4th International*, 2004, pp. 816-821 Vol.2.
[65] M. Miyatake, M. Veerachary, F. Toriumi, N. Fujii, and H. Ko, "Maximum Power Point Tracking of Multiple Photovoltaic Arrays: A PSO Approach," *IEEE Transactions on Aerospace and Electronic Systems*, vol. 47, pp. 367-380, 2011.
[66] K. Kobayashi, I. Takano, and Y. Sawada, "A study of a two stage maximum power point tracking control of a photovoltaic system under partially shaded insolation conditions," *Solar Energy Materials and Solar Cells*, vol. 90, pp. 2975-2988, 11/23/ 2006.
[67] G. Carannante, C. Fraddanno, M. Pagano, and L. Piegari, "Experimental Performance of MPPT Algorithm for Photovoltaic Sources Subject to Inhomogeneous Insolation," *IEEE Transactions on Industrial Electronics*, vol. 56, pp. 4374-4380, 2009.
[68] H. Patel and V. Agarwal, "Maximum Power Point Tracking Scheme for PV Systems Operating Under Partially Shaded Conditions," *IEEE Transactions on Industrial Electronics*, vol. 55, pp. 1689-1698, 2008.
[69] Y. Liu, "Advance control of photovoltaic converters," Ph.D., Dept. Eng., Univ. Leicester, 2009.
[70] T. L. Nguyen and K.-S. Low, "A Global Maximum Power Point Tracking Scheme Employing DIRECT Search Algorithm for Photovoltaic Systems," *IEEE Transactions on Industrial Electronics*, vol. 57, pp. 3456-3467, 2010.

[71] M. Boztepe, F. Guinjoan, G. Velasco-Quesada, S. Silvestre, A. Chouder, and E. Karatepe, "Global MPPT Scheme for Photovoltaic String Inverters Based on Restricted Voltage Window Search Algorithm," *IEEE Transactions on Industrial Electronics,* vol. 61, pp. 3302-3312, 2014.
[72] K. Ishaque and Z. Salam, "A Deterministic Particle Swarm Optimization Maximum Power Point Tracker for Photovoltaic System Under Partial Shading Condition," *IEEE Transactions on Industrial Electronics,* vol. 60, pp. 3195-3206, 2013.
[73] S. Roy Chowdhury and H. Saha, "Maximum power point tracking of partially shaded solar photovoltaic arrays," *Solar Energy Materials and Solar Cells,* vol. 94, pp. 1441-1447, 9// 2010.
[74] T. Kok Soon and S. Mekhilef, "Modified Incremental Conductance Algorithm for Photovoltaic System Under Partial Shading Conditions and Load Variation," *IEEE Transactions on Industrial Electronics,* vol. 61, pp. 5384-5392, 2014.
[75] Y. Hu, W. Cao, J. Wu, B. Ji, and D. Holliday, "Thermography-Based Virtual MPPT Scheme for Improving PV Energy Efficiency Under Partial Shading Conditions," *IEEE Transactions on Power Electronics,* vol. 29, pp. 5667-5672, 2014.
[76] E. Trucco and A. Verri, *Introductory Techniques for 3-D Computer Vision*: Prentice Hall PTR, 1998.
[77] D. Paul E. and M. Jitendra, "Recovering High Dynamic Range Radiance Maps from Photographs," *SIGGRAPH,* 1997.
[78] Available: http://www.iesmith.net/tools/solarcalc.html
[79] K. Jazayeri, S. Uysal, and M. Jazayeri, "MATLAB/simulink based simulation of solar incidence angle and the sun's position in the sky with respect to observation points on the Earth," in *Renewable Energy Research and Applications (ICRERA), 2013 International Conference on*, 2013, pp. 173-177.
[80] L. Cristaldi, M. Faifer, M. Rossi, and S. Toscani, "An Improved Model-Based Maximum Power Point Tracker for Photovoltaic Panels," *IEEE Transactions on Instrumentation and Measurement,* vol. 63, pp. 63-71, 2014.
[81] G. Velasco-Quesada, F. Guinjoan-Gispert, R. Pique-Lopez, M. Roman-Lumbreras, and A. Conesa-Roca, "Electrical PV Array Reconfiguration Strategy for Energy Extraction Improvement in Grid-Connected PV Systems," *IEEE Transactions on Industrial Electronics,* vol. 56, pp. 4319-4331, 2009.
[82] N. Dzung and B. Lehman, "An Adaptive Solar Photovoltaic Array Using Model-Based Reconfiguration Algorithm," *IEEE Transactions on Industrial Electronics,* vol. 55, pp. 2644-2654, 2008.
[83] J. P. Storey, P. R. Wilson, and D. Bagnall, "Improved Optimization Strategy for Irradiance Equalization in Dynamic Photovoltaic Arrays," *IEEE Transactions on Power Electronics,* vol. 28, pp. 2946-2956, 2013.
[84] H. Al-Atrash, I. Batarseh, and K. Rustom, "Effect of Measurement Noise and Bias on Hill-Climbing MPPT Algorithms," *IEEE Transactions on Aerospace and Electronic Systems,,* vol. 46, pp. 745-760, 2010.
[85] E. Koutroulis, K. Kalaitzakis, and N. C. Voulgaris, "Development of a microcontroller-based, photovoltaic maximum power point tracking control system," *IEEE Transactions on Power Electronics,* vol. 16, pp. 46-54, 2001.
[86] H. Chihchiang, L. Jongrong, and S. Chihming, "Implementation of a DSP-controlled photovoltaic system with peak power tracking," *IEEE Transactions on Industrial Electronics,* vol. 45, pp. 99-107, 1998.
[87] A. Pandey, N. Dasgupta, and A. K. Mukerjee, "High-Performance Algorithms for Drift Avoidance and Fast Tracking in Solar MPPT System," *IEEE Transactions on Energy Conversion,* vol. 23, pp. 681-689, 2008.

[88] S. Jain and V. Agarwal, "A new algorithm for rapid tracking of approximate maximum power point in photovoltaic systems," *IEEE Power Electronics Letters*, vol. 2, pp. 16-19, 2004.
[89] A. Safari and S. Mekhilef, "Simulation and Hardware Implementation of Incremental Conductance MPPT With Direct Control Method Using Cuk Converter," *IEEE Transactions on Industrial Electronics*, vol. 58, pp. 1154-1161, 2011.
[90] K. S. Tey and S. Mekhilef, "Modified incremental conductance MPPT algorithm to mitigate inaccurate responses under fast-changing solar irradiation level," *Solar Energy*, vol. 101, pp. 333-342, 3// 2014.
[91] M. Veerachary, T. Senjyu, and K. Uezato, "Feedforward maximum power point tracking of PV systems using fuzzy controller," *IEEE Transactions on Aerospace and Electronic Systems*, vol. 38, pp. 969-981, 2002.
[92] T. Hiyama, S. Kouzuma, and T. Imakubo, "Identification of optimal operating point of PV modules using neural network for real time maximum power tracking control," *IEEE Transactions on Energy Conversion*, vol. 10, pp. 360-367, 1995.
[93] L. Whei-Min, H. Chih-Ming, and C. Chiung-Hsing, "Neural-Network-Based MPPT Control of a Stand-Alone Hybrid Power Generation System," *IEEE Transactions on Power Electronics*, vol. 26, pp. 3571-3581, 2011.
[94] D. Casadei, G. Grandi, and C. Rossi, "Single-phase single-stage photovoltaic generation system based on a ripple correlation control maximum power point tracking," *IEEE Transactions on Energy Conversion*, vol. 21, pp. 562-568, 2006.
[95] T. Esram, J. W. Kimball, P. T. Krein, P. L. Chapman, and P. Midya, "Dynamic Maximum Power Point Tracking of Photovoltaic Arrays Using Ripple Correlation Control," *IEEE Transactions on Power Electronics*, vol. 21, pp. 1282-1291, 2006.
[96] K. K. Tse, M. T. Ho, H. S. H. Chung, and S. Y. R. Hui, "A novel maximum power point tracker for PV panels using switching frequency modulation," *IEEE Transactions on Power Electronics*, vol. 17, pp. 980-989, 2002.
[97] H. S. H. Chung, K. K. Tse, S. Y. R. Hui, C. M. Mok, and M. T. Ho, "A novel maximum power point tracking technique for solar panels using a SEPIC or Cuk converter," *IEEE Transactions on Power Electronics*, vol. 18, pp. 717-724, 2003.
[98] L. Xiao, L. Yaoyu, and J. E. Seem, "Maximum Power Point Tracking for Photovoltaic System Using Adaptive Extremum Seeking Control," *IEEE Transactions on Control Systems Technology*, vol. 21, pp. 2315-2322, 2013.
[99] K. Ishaque, Z. Salam, M. Amjad, and S. Mekhilef, "An Improved Particle Swarm Optimization (PSO) Based MPPT for PV With Reduced Steady-State Oscillation," *IEEE Transactions on Power Electronics*, vol. 27, pp. 3627-3638, 2012.
[100] C. Liang-Rui, T. Chih-Hui, L. Yuan-Li, and L. Yen-Shin, "A Biological Swarm Chasing Algorithm for Tracking the PV Maximum Power Point," *IEEE Transactions on Energy Conversion*, vol. 25, pp. 484-493, 2010.
[101] L. V. Hartmann, M. A. Vitorino, M. B. R. Correa, and A. M. N. Lima, "Combining Model-Based and Heuristic Techniques for Fast Tracking the Maximum-Power Point of Photovoltaic Systems," *IEEE Trans. on Power Electron.*, vol. 28, pp. 2875-2885, 2013.
[102] L. Cristaldi, M. Faifer, M. Rossi, and S. Toscani, "An Improved Model-Based Maximum Power Point Tracker for Photovoltaic Panels," *IEEE Trans. on Instrument. and Measur.*, vol. 63, pp. 63-71, 2014.
[103] L. Zhang, A. Al-Amoudi, and B. Yunfei, "Real-time maximum power point tracking for grid-connected photovoltaic systems," in *Power Electronics and Variable Speed Drives, 2000. Eighth International Conference on (IEE Conf. Publ. No. 475)*, 2000, pp. 124-129.

[104] K. M. Tsang and W. L. Chan, "Model based rapid maximum power point tracking for photovoltaic systems," *Energy Conversion and Management*, vol. 70, pp. 83-89, 6// 2013.
[105] M. A. Vitorino, L. V. Hartmann, A. M. N. Lima, Corre, x, and M. B. R. a, "Using the model of the solar cell for determining the maximum power point of photovoltaic systems," in *Power Electronics and Applications, 2007 European Conference on*, 2007, pp. 1-10.
[106] M. Veerachary, "Power tracking for nonlinear PV sources with coupled inductor SEPIC converter," *IEEE Transactions on Aerospace and Electronic Systems*, vol. 41, pp. 1019-1029, 2005.
[107] M. Veerachary, T. Senjyu, and K. Uezato, "Maximum power point tracking control of IDB converter supplied PV system," *IEE Proceedings -Electric Power Applications*, vol. 148, pp. 494-502, 2001.
[108] S. K. Kollimalla and M. K. Mishra, "A Novel Adaptive P&O MPPT Algorithm Considering Sudden Changes in the Irradiance," *IEEE Transactions on Energy Conversion*, vol. 29, pp. 602-610, 2014.